HETEROGENEOUS CATALYSIS BY GOLD: THE EFFECT OF OXIDE SUPPORT, EXTERNAL CONDITIONS, AND THE METAL/OXIDE INTERFACE

by

Siris Ödin Laursen

A dissertation submitted in partial fulfillment
of the requirements for the degree of
Doctor of Philosophy
(Chemical Engineering)
in The University of Michigan
2009

Doctoral Committee:

Assistant Professor Suljo Linic, Chair
Professor Rachel S. Goldman
Professor Erdogan Gulari
Professor Levi T. Thompson Jr.
Adjunct Professor Galen Fisher

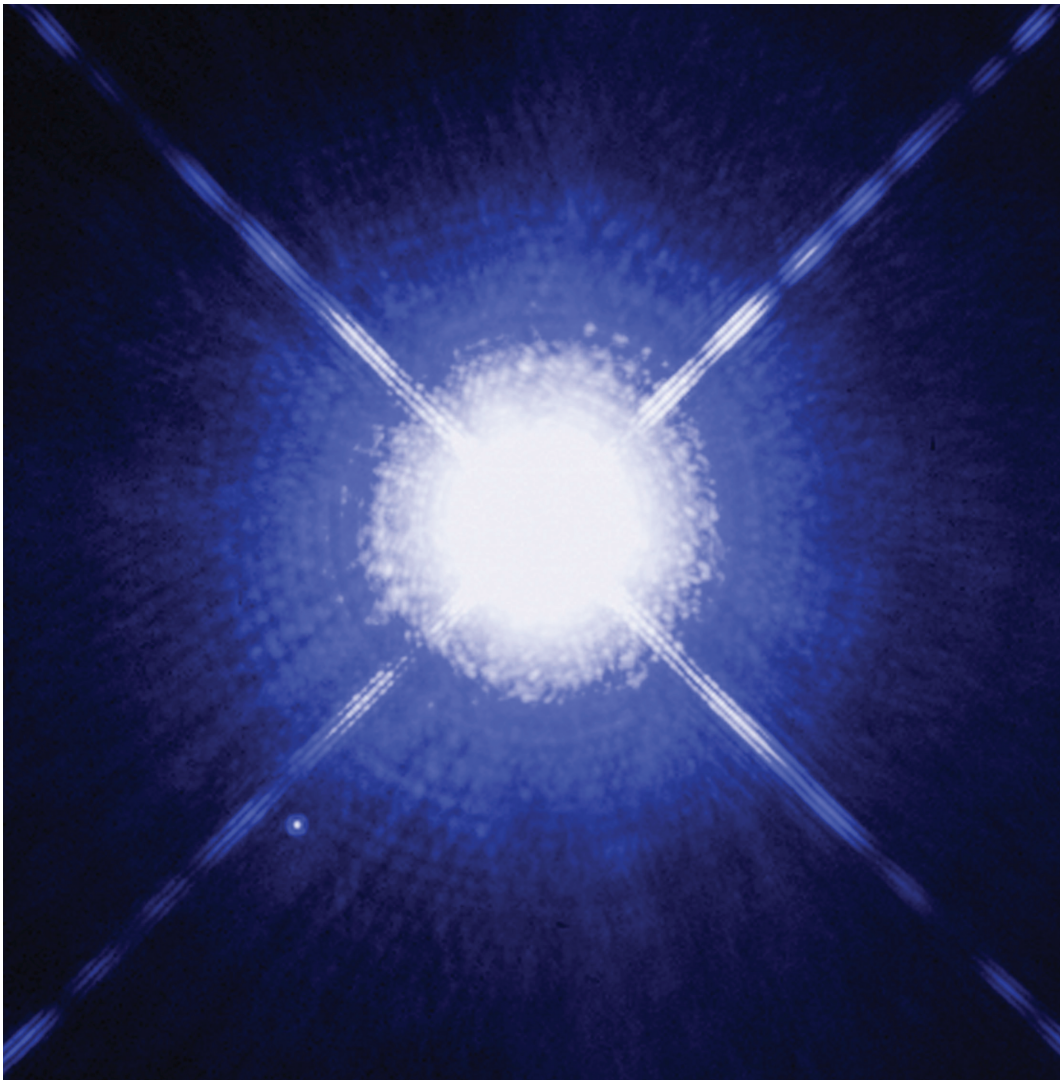

Sirius A and B

This dissertation is dedicated to all that bring order to chaos, understanding to the obscure, and light into the darkness. May all of your paths stay brightly lit, populated by excellent people, and full of bountiful spoils.

ACKNOWLEDGEMENTS

Many people have contributed in various ways to the completion of this dissertation. To acknowledge you all individually, and with proper measure, would dwarf the scientific contents of this document. Instead, I thank you all in concert, everyone who is close, far, and no longer with us. Thank you. Your indelible mark has been made.

TABLE OF CONTENTS

LIST OF FIGURES

Figure

LIST OF TABLES

Table

ABSTRACT

HETEROGENEOUS CATALYSIS BY GOLD: THE EFFECT OF OXIDE SUPPORT, EXTERNAL CONDITIONS, AND THE METAL/OXIDE INTERFACE

by

Siris Ödin Laursen

Chair: Suljo Linic

Bulk Au is inert. However, when dispersed as small particles on an oxide support its chemistry changes dramatically, and can become active in many catalytic reactions. This unprecedented change in Au chemistry is still not well understood, and is the focus of this dissertation. A combined theoretical/experimental approach was used to investigate the active form of Au in low–temperature CO oxidation, how external conditions affect Au, and the role the oxide support.

From literature, many forms of Au ($Au^{\delta-}$, Au^0, and $Au^{\delta+}$) have been proposed as the catalytically active form of Au in low–temperature CO oxidization. We found that experimental conditions directly affected the form of Au present, and, to some degree, all forms of Au could perform catalytically. Moreover, that Au/oxide interface played a critical role in producing charged Au species, which exhibited superior catalytic activity over metallic Au.

Another key issue is the role of different forms of cationic Au. In literature it was argued that $Au^{\delta+}$ was both highly active and catalytically dead. We found that not all forms of cationic Au perform the same chemistry, and that only specific

$Au^{\delta+}$ species could perform oxidation. Furthermore, we determined that common catalyst preparation procedures result in the deposition of $AuCl_x$ or AuO_x species, both cationic in nature, yet only AuO_x is able to catalyze CO oxidation. Our results were further corroborated by experimental studies that directly tested the activity of $AuCl_x$ and AuO_x.

Lastly we investigated the effect of the oxide support. We tested the effect of four oxides of different electronic character (SiO_2, TiO_2, SnO_2, and IrO_2), and found that the Au/oxide interface site was directly affected by the type of oxide present. Moreover, that the activity of the Au/oxide interface towards binding and dissociating O_2 followed a volcano shaped curve with a maximum situated at the semi–conductor supported Au systems, i.e, TiO_2 and SnO_2. These results were found to be directly inline with the experimentally measured support effect, and indicated that the surface chemistry of Au/oxide may be rationally tuned.

CHAPTER I

Introduction

1.1 Overview

As an introduction to this dissertation, we define catalysis, present a short motivation indicating how catalysis directly affects the workings of every day life, how catalysis affects chemical reactions, and the tools that are commonly used to study it. We then delve into the main topic of discussion, gold (Au) catalysis. We discuss the procedure discovered to produce highly catalytically active Au, and the efforts, to date, to explain its unprecedented activity in low–temperature CO oxidation. Then, for the benefit of the reader, a brief summary of the material covered in each of the chapters is presented.

1.2 Motivation

The world is driven by the catalytic production of chemicals. It is estimated that 35% of the world Gross Domestic Product (GDP) (54.3 trillion US dollars 2008) is linked to chemicals and high energy fuels produced by catalytic reactions [1, 2]. Approximately 40% of the world population is nourished by crops fertilized by chemicals produced by the catalytic Haber–Bosch process. The Haber–Bosch process utilizes a form of iron oxide to combine hydrogen and nitrogen into ammonia, a process that would be almost impossible without the catalyst. This process is postulated to be responsible for feeding ∼50% of the world population today [3]. One out of every six people on earth drives an automobile, with most equipped with catalytic technology that continuously cleans the engine exhaust, helping to keeping our environment healthy. Most if not all of the 85 million barrels of oil consumed per day touches a catalyst after it leaves the ground [4]. This oil not only fuels our cars, trains, and airplanes, but also provides a critical source of carbon–based compounds which are used to produce many consumer products. Aside from the present applications of catalysis, the successful implementation of alternative energy technologies in the future will directly rely on on developing new highly efficient catalytic materials. For example, fuel cell, biologically based fuel, hydrogen generation, and other technologies all depend critically on discovering and optimization highly active, selective, and stable catalytic materials. Clearly, a large portion of daily life is directly and continuously affected by catalytic materials, therefore, the motivation for its research and development is obvious.

1.3 Catalytic Phenomena and Materials

Catalysis is the acceleration of a chemical reaction by a material that remains unchanged by the chemical reaction. The unchanged material is called a catalyst.

The physical form of catalytic materials can vary widely, from the a simple proton to structurally and chemically complex biological enzymes. Even though these materials are structurally and chemically very different, their role in a catalytic reactions are similar. A catalyst functions by directly participating in the chemical reaction modifying the energy pathway between reactants and products by reducing the energy barriers along the path. These energy barriers determine the rate at which the chemical reaction takes place. By lowering the energy barriers between reactant and products a chemical reaction may proceed at a higher rate, or the temperature required to achieve an appreciable rate can be lowered. In some cases the presence of a catalyst can enable reactions that would otherwise be impractical to perform. The phenomena of catalytic reactions results from the interactions present between the species in a chemical reaction and the catalytic material. Therefore, discovering and optimizing catalysts hinges upon an understanding of not just chemical reactions but how the presence of a catalyst affects the chemical reaction at every step along the reaction pathway.

In this dissertation we focus on a specific catalyst that consist of gold (Au) metal finely dispersed on an oxide support. This material catalyzes the reaction between gas phase molecules thus is an example of a heterogeneous catalyst. In the following sections we discuss the approaches used to discover and optimize heterogeneous catalysts and then discuss in greater detail the state–of–the–art knowledge concerning catalyst of interest.

1.4 The Study of Heterogeneous Catalysis

The classical methods for discovering and optimizing catalysts have proven useful in roughly quantifying the catalytic activity of the elements in the periodic table, however, they have been slow to produce fundamental predictive theoretical frameworks that may be used to rationally design catalytic materials. The classical procedure for

testing catalysts consists of heuristic approaches where many materials are tested for catalytic activity in a trial–and–error fashion. This approach allows many materials to be tested quickly and has helped produce rough trends in catalytic activity across the periodic table. A further benefit is that the same technique can be used to optimize catalyst performance determining the variables that affect catalytic activity. Even more importantly, using this type of technique ultimately results in an operational material, one that may be employed scientifically or industrially. Undoubtedly, there are many benefits of employing the heuristic approach, however, from the stand–point of developing predictive theories based on fundamental physical mechanisms the approach is lacking. For example, the reaction rates measured in bench–top reactors are average rates for all of the catalytically active sites on the catalyst surface thus it is impossible to isolate the active site on the catalyst surface. This hinders the fundamental understanding of how the local chemical environment and physical geometry of the active site affects its activity. Furthermore, when optimizing metal loading and catalyst preparation conditions the optimal conditions found are commonly not transferable to other reaction conditions or materials. Also determining how these preparation variables directly affect the atomic structure and activity of the catalyst surface is ultimately speculative. Therefore, the heuristic method is excellent for roughly outlining trends in catalytic activity and optimizing catalyst performance, but is not well suited to produce clear connections between fundamental variables and catalyst performance.

1.5 Towards a Fundamental Understanding

A more fundamental approach may be used to directly test the chemical activity of well–defined material surfaces such that clear connections may be made between atomic and electronic structure and surface reactivity. This approach utilizes well defined atomically flat single crystal surfaces and ultra–pure gas phase environments

to investigate surface reactions. The definition of the experiment is further increased by using atomically clean reaction vessels evacuated to ultra–high vacuum (10^{-13} atmospheres of pressure) and well–defined ultra–pure compositions of gases. Furthermore, many techniques have been developed to characterize the geometry and chemical environment of the surface thus direct connections can be made between the atomic structure and local chemical environment of the surface and its surface chemistry. Studies such as these are also instrumental in investigating the effects of catalyst promoters or poisons which are present in extremely low concentrations, yet can drastically affect catalyst performance. For example, one important discovery enabled by such studies proved that different crystal facets exhibit different chemical activity. For example, it was found that the close packed surface of a face–centered–cubic metal was much less active in binding adsorbates than surfaces that contained steps or a less closely packed array of atoms. This discovery was paramount in understanding that the chemical reactivity of a surface does not just depend on the material of the surface, but is also dependent upon local atomic structure. The Nobel prize in chemistry was awarded in 2007 for these discoveries, and others related to the chemistry of surfaces. Undeniably, this approach is crucial to understanding the fundamental physical mechanisms that govern surface chemistry, however, as with the heuristic method, this approach has shortcomings in some respects. For example, in order to produce atomically ordered sample surfaces extreme cleaning techniques must be employed such as high energy ion bombardment (500–1000 eV Ar^+ ions) and high temperature annealing (700–1200 K), commonly performed together as a sequence of sputter/anneal cycles. This cleaning procedure works well for metal surfaces; however, when used to clean oxide surfaces or fragile surface structures, unnatural surface terminations and configurations may be produced. Additionally, the ultra–high vacuum environment required for definition, chemical detection, and surface characterization can directly affect the chemical composition of a surface. For

example, the ultra–high vacuum environment can easily remove adsorbates from a surface or reduce weak oxides back the pure metal constituent. These extreme environments contribute significantly to these types of experiments being perceived as disconnected from real system or subject to the "pressure–gap".

1.6 First Principles Calculation

With the advent of fast computing, and the clustering of computers, calculations based on the principles of quantum mechanics can be performed on atomically defined systems that mimic model and non–model catalyst surfaces. These calculations can aid in gaining a clear understanding of how the atomic and electronic structure of a surface dictates its chemical and catalytic activity. The quantum calculations, in their purest form, involve no adjustable parameters and are based solely on fundamental physical constants. Quantum theory is used to calculate the internal structure of the atoms, molecules, and surfaces giving the energy associated with the steps in a reaction. Whereas, the theoretical stability of model systems and adsorbate over layers with respect to temperature and pressure may be investigated by the thermodynamics calculations. These calculations can capture all of the pertinent reaction steps that occur on a catalyst surface, and allow a connection to be made between the fundamental structure of the surface and its reactivity.

The benefit of *ab initio* calculation is that it may be used to investigate aspects of a system that are difficult or impossible to measure experimentally; however, the calculations must be employed methodically and continually compared to experimental findings. For example, each of the reaction steps in a reaction pathway are of interest when attempting to tune the catalytic properties of a surface. However, experimentally measuring each individually is impossible, even when using well–defined single crystal UHV studies. Using *ab initio* calculation, each of these steps can be directly calculated, and directly linked to the electronic structure of the surface. The

calculations also allow direct access to the electronic structure of all chemical species along the reaction pathway and of the surface, facilitating a fundamental understanding of the connection between electronic structure and chemical reactions. Possibly the only major drawback to *ab initio* calculation is that the systems calculated are closely motivated by experimental results; therefore, misconceptions, assumptions, or errors in experiment can propagate to calculation. Some example model systems are presented in Figure 1.1. Because of experimental error and misconception, many different systems must be calculated, and their energetic feasibility tested to ensure assumptions made in experiments do not propagate to calculation. Theoretically if the exact geometry of a surface is calculated the result should be directly in line with what is seen experimentally.

Each of the approaches outlined above can produce valuable information depending on the aim, however, in order to develop a fundamental understanding of catalytic phenomena we think all must be used in unison. With each benefit and drawback enhanced and supplemented respectively to weave a complete picture from the atomic scale to the reaction rate measured in a bench–top reactor.

1.7 Gold Catalysis

The major focus of this dissertation is to understand the fundamental physical mechanisms that govern the chemistry and catalytic activity of oxide supported gold (Au). Interest has drawn to Au because of the strange and interesting chemistry that takes place as Au is constrained to the nano–scale. For example, bulk Au is inert; however, when dispersed on an oxide as very small nano–particles it can exhibit extremely high catalytic activity below room temperature. Furthermore, Au catalysts have exhibited many other unusual phenomena unseen before the discovery of catalytically active Au. Here we give an account of the discovery of catalytically active Au and a short summary of the physical mechanisms proposed to be responsible

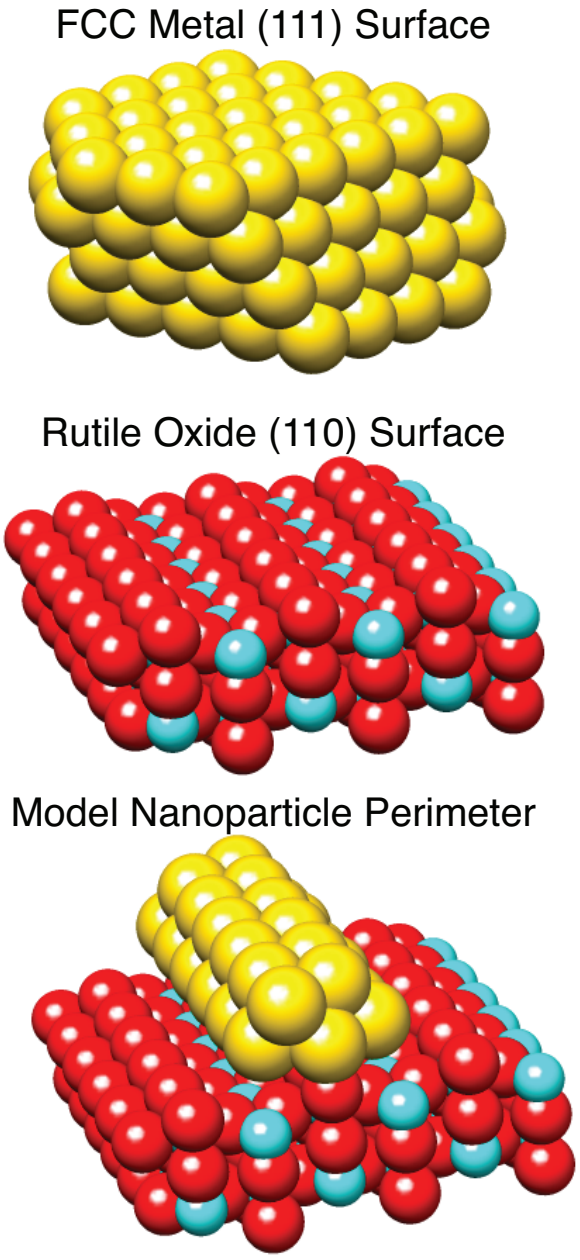

Figure 1.1: Common model surfaces for quantum chemical calculations. In practice the most thermodynamically stable crystal facet is chosen to model the metal or oxide surface as this is the surface that will dominate a significant portion of the crystallite surface area. It is also common to model other low Miller index facets, such as the (211) or (110) or (100) surfaces of an FCC metal, because they tend to be more chemically active towards binding and dissociating reactants thus are thought to contribute significantly to the overall catalytic activity of a particle. Gold, red, and blue spheres represent the elements: gold, oxygen, and titanium respectively.

for the unprecedented activity of the most noble metal.

1.7.1 Pre–Haruta

Prior to Haruta's discovery in the late 80's, Au found few applications in heterogeneous catalysis. It was researched primarily in conjunction with Pt–group metals as an alloy for hydrogenation or oxidation of alkanes or alkenes [5–11]. The catalysts in these studies were prepared by impregnation of an Au chloride salt with subsequent decomposition. This procedure yielded large Au nano–particles on the order of 50 nm. These particles had much the same chemistry as bulk Au, therefore, Au gained little traction in heterogeneous catalysis research. The story changed markedly at the end of the 1980's.

1.7.2 Haruta's Discovery

In the 1987 and 1989, seminal papers by Haruta and co–workers were published showing that Au could be an incredibly active in catalytic CO oxidation "at temperatures far below 0 C" [12, 13]. Haruta presented a catalyst preparation procedure that resulted in very small Au nano–particles, on the order of 2–3 nm, and showed that Au could catalyze both CO and H_2 oxidation at temperatures as low as –70 °C, see Eqn. 1.1 and 1.2. The catalyst preparation procedure employed by Haruta was fairly simple, mix Au and support precursors together in an aqueous solution, and increase the pH. With subsequent high temperature calcination, the catalysts became extremely active at low temperatures. Aside from the unprecedented low–temperature activity, Haruta showed that the oxide support played a critical role in the overall Au catalytic activity. The magnitude of the support effect was unprecedented and could not be understood in the framework of the spill–over effect [12–15]. Haruta's discovery has effectively produced a fervent subfield of heterogeneous catalysis that is still highly active.

$$CO + \frac{1}{2}O_2 \rightleftharpoons CO_2 \tag{1.1}$$

$$H_2 + \frac{1}{2}O_2 \rightleftharpoons H_2O \tag{1.2}$$

1.7.3 The Surface Chemistry of Au

To develop an appreciation for the large change in Au chemical activity as the atomic scale is approached, we first discuss the surface chemistry of bulk–like Au. As discussed previously, the activity of catalytic metal particles may be understood by studying the interaction between the reactant species and well–defined single crystal surfaces. Interestingly, the surface chemistry of Au nano–particles and their bulk analog appear to exhibit greatly dissimilar surface chemical properties. For example, in reactions involving reactions with diatomic molecules (O_2) the rate determining step, i.e., the reaction step with the highest reaction barrier, is commonly found to be the dissociation of the diatomic molecule. In CO and H_2 oxidation this is also believed to be the case. Interestingly, bulk Au cannot chemisorb or dissociate O_2. In single crystal UHV studies it was found that even at temperatures, as low as 100 K, molecular oxygen does not adsorb on a crystal of Au. It was also found that in order to dissociate O_2 to form adsorbed atomic oxygen temperatures above 800 K were required [16–18]. These results indicate minimal interaction between O_2 and bulk Au, a stark contrast to the activity found for oxide supported nano–structure Au. For instance, activation barriers measured in low–temperature CO oxidation are on the order of zero to 30 kJ/mole indicating all steps in the reaction mechanism have exceedingly low activation barriers, or no activation barriers at all [14]. Equally intriguing, it was found that the associative desorption of atomic oxygen from an extended Au surface was activated, with barriers of 80–130 kJ/mol indicating that kinetic barriers existed for breaking and forming O—O bonds [16–18]. These results may be viewed in a different light, if oxygen dissociation does occur on the

Au surface, the adsorbed atomic oxygens would be stable. In a different study, the reaction between pre-adsorbed atomic oxygen and CO was investigated [19]. Madix and co–workers found that atomic oxygen could be removed from the Au surface by CO at very low temperatures with an activation barrier of ∼8 kJ/mol. This result indicates that atomic oxygen may be stable on Au surfaces, but because such a large thermodynamic driving force exists for CO oxidation (∼2.9 eV/CO_2), oxygen is easily reacted away. From these single crystal studies it can be concluded that the chemistry occurring on oxide supported Au catalysts is quite different than the chemistry that takes place on bulk Au crystals. Because the chemistry of nano–Au appears to be drastically different than bulk Au, many unorthodox mechanisms have been proposed.

1.7.4 Geometric (Particle Size) and Electronic Effects

The difference in chemical activity of bulk and nano–sized Au has been, in part, connected to purely geometric effects [20–24]. For example, as the nano– and sub–nano–scale is approached the surface to volume ratio of a particle increases rapidly, roughly as the reciprocal of the particle radius. This effectively places more metal atoms at the surface of the particle with fewer surrounding metal atoms bound to them. This effect leads to an increase in chemical activity of these under coordinated sites increasing their ability to bind adsorbates [20, 21, 23]. Single crystal UHV experiments have shown that higher index crystal facets with lower metal–metal coordination are more chemically active than densely packed low index facets [25–27]. However, with respect to oxygen binding on Au crystal surfaces, never has O_2 adsorption and dissociation been encountered, even over highly stepped (211) surfaces [28]. Even in the extreme case of atomic clusters, which approach the of Au—Au under coordination, molecular oxygen adsorption and dissociation was never found. Only when Au is negatively charged does O_2 adsorb favorably [29, 30]. Similar results were found in an extensive quantum chemical study, where O_2 adsorption was tested

on Au^-, Au^0, and Au^+ [31]. In this work, it was found that, out of the three types of Au_n clusters tested, only the negatively charged cluster bound molecular oxygen with appreciable energy [31]. It was also found that any exothermic binding found in cationic and metallic Au clusters was lost quickly as larger particles were tested (n > 5 in Au_n).

The role of under coordination in Au catalysis was further brought into question when comparing the catalytic activity of identical Au particles supported by different oxides. For example, Rousset and co–workers prepared catalysts by size–selected Au particle deposition on different oxides, and found that almost identical Au particle sizes on different oxide supports could produce very different catalytic activity [32]. Furthermore, in comparing 2-3 nm Au particles supported by TiO_2 or SiO_2 exhibit catalytic rates that differ by an order of magnitude or more [14, 33]. These results directly contradict the proposed role of under–coordinated sites since similar sized Au nano–particles can exhibit drastically different catalytic activity when supported on different oxides. Considering these results, it is fairly clear that alternate effects exist that govern the catalytic activity of nano–Au.

1.7.5 Evoking Non–Metallic Au

A decade after Haruta's discovery it was found that the presence of oxide surface defects promoted the catalytic oxidation of CO over MgO supported size–selected Au nano–particles at low temperature <300 K [34, 35]. This result indicated that the oxide surface could play a direct role in enhancing the chemistry of oxide supported Au nano–particles. Further studies by Besenbacher and co–workers showed that these oxide surface defects were most likely oxygen vacancies and that the defects were nucleation sites for Au nano–particle growth on TiO_2 [36]. The interaction between Au and the oxygen vacancies was understood through further UHV STM studies and ultra-violet photoelectron spectroscopy (UPS) [37, 38]. Where it was found via UPS

that oxygen vacancy rich TiO_2 exhibited electronic states directly below the Fermi level indicating activated electron density at the oxygen vacancies. Upon dosing Au these states diminished indicating electronic charge transfer to the supported Au nano–particles producing anionic Au. These results fell directly in line with the gas phase cluster results of Whetten and co–workers showing only unsupported anionic Au bound O_2, and the calculations of Zhu and co–workers [31]. Further quantum chemical calculations showed that oxygen vacancy laden oxide supported Au could bind molecular and atomic oxygen with appreciable energies and catalyze CO oxidation with low activation barriers [34, 39–46]. In light of these results, a seemingly clear connection was made between anionic Au, the Au species present in oxide supported Au, and the catalytically active form of Au in Au catalysis. However, with the totality of experimental evidence supporting anionic Au being derived from UHV conditions on model catalyst systems the applicability of this mechanism in non–model systems is questioned.

Despite the data and the intuitive nature of O_2 activation by anionic Au, this concept is in direct contradiction to what is found in non–model catalysts. In catalysts exhibiting the highest reported activity in low–temperature CO oxidation strong cationic Au signal is measured [47]. Similarly, in many other studies the presence of cationic Au or oxidized Au has been correlated with highly active catalysts [47–53]. This indicates that cationic or oxidized Au is the catalytically active Au species, the opposite of what is found under UHV conditions. Insight into the catalytic activity of oxidized Au may be drawn from single crystal UHV studies that show atomic oxygen pre–covered Au surfaces can further dissociate O_2 and readily oxidize CO with a low apparent activation barrier ($\sim$8 kJ/mole) [19, 54]. These results indicate that if Au was in an oxidized form i.e., oxygen pre–covered Au, it could theoretically perform catalytic CO oxidation. These results help to understand the non–intuitive nature of O_2 activation by a cationic metal. Interestingly, just as with oxygen vacancies, it has

been shown in a UHV STM study that extra oxygen atoms on a TiO_2 surface serve as nucleation sites for Au particle growth and may stabilize Au against sintering to a greater degree than oxygen vacancies [55]. Quantum chemical calculations have been used to investigate the feasibility of oxidized Au as a oxidation catalyst and it was found that oxygen laden Au particles could in deed dissociate O_2 and oxidize CO with activation barriers surmountable at low temperatures [44, 46, 56–59]. Lastly, recent gas phase cluster experiments have confirmed that cationic Au clusters can be highly active in CO oxidation [60]. Just as with anionic Au, the case for cationic Au as the active species in low–temperature CO oxidation is strong. Moreover, the fact that the experimental observations were from non–model catalysts further validates the claim that these species may be present under operating conditions.

Interestingly, albeit not surprising, there is also a body of literature which supports metallic Au as the active species of Au in CO oxidation [49, 61–67]. Where non–model powdered catalysts were reduced in H_2 at high temperatures and still exhibited activity for low–temperature CO oxidation. In these experiments the high whiteline intensity in x–ray absorption (XAS) was reduced to that of metallic Au indicating the complete decomposition of $AuCl_x$, AuO_x, or $Au(OH)_x$, however, the catalysts still exhibited catalytic activity in low–temperature CO oxidation. The argument presented in favor of metallic Au is that electron density may be transfered from metallic Au to O_2 to activate the O—O bond for dissociation. This view effectively places cationic Au or the $Au^{\delta+}$—$O_2^{\delta-}$ species as an intermediate in the reaction mechanism. These results are valuable in indicating that there may be a mechanism present on a catalyst surface that is not directly associated with the presence of high concentrations of oxidized Au. From a recent publication by Behm and co–workers it was found that the overall measured rate tracked well with the Au particle perimeter and not the Au surface area exposed indicating that the Au/oxide interface perimeter is a likely location for the active site in low–temperatures CO oxidation [68]. Attempt-

ing to decipher these seemingly contradictory reports on $Au^{\delta-}$, Au^0, and $Au^{\delta+}$ will be one of the issues we focus upon in this dissertation.

1.7.6 The Support Effect

The catalytic activity of Au appears to be affected by many factors, however, none so much as the oxide support used to disperse the metal. The effect of the oxide on Au catalytic activity been clearly shown by a number of experimental studies [14, 32, 69–81]. Possibly the most interestingly of these studies is the well defined study of Rousset and co–workers. In their study they clearly showed that similar Au nano–particles could be deposited on various oxides and that these almost identical Au clusters exhibited drastically different catalytic activity towards CO oxidation. The fact that the same Au geometries could yield different surface chemistry indicates that the oxide support plays a direct role in the catalytic activity. The existence of this phenomena indicates that undiscovered metal/oxide interactions may be present at the Au/oxide interface and may be key to developing highly active low–temperature catalysts. Very little work has been presented on this issue thus a major focus of this dissertation is to understand how the oxide support type and surface composition can directly affect the catalytic activity of Au.

1.8 Scope of the Dissertation

The focus of this dissertation is to investigate the fundamental physical mechanisms which govern oxide supported Au catalysis. The two primary aims are: *i*) to understand the catalytically active Au species in low–temperature oxidation reactions and *ii*) to determine the role of the oxide support in the overall chemistry and catalytic activity of Au. Our approach is to combine experimental and theoretical insights in an iterative fashion. Here we present a brief summary of the material in each of the chapters as a guide to the reader.

1.8.1 Chapter 2: Theoretical Development and Background

In this chapter we present the theoretical framework on which all theoretical calculations used herein are based. A broad introduction to quantum mechanics and Schrödinger's wave equation are given. To solve these equations for multiple particles (i.e., electrons) we employ the Density–Functional Theory (DFT) method. The fundamental basis and mathematical formalism for DFT is presented and explained. This is followed by a development of *ab initio* thermodynamics, which connects the total internal energy electronic calculations of DFT to external conditions such as gas phase temperature and pressure of reactants. Then a broad overview of electronic structure is presented focusing specifically on the structure of molecules and extended structures. The electronic structure of metals and oxides will be explained in detail as the dynamics of these materials' electronic structure drives many of the conclusions drawn in the body of the dissertation. Lastly, the model systems used for calculation will be presented and connected back to what is measured experimentally with respect to catalyst surface geometry.

1.8.2 Chapter 3: Experimental Methods

In this chapter we discuss the experimental methods used to prepare and characterize non–model powdered catalysts. We describe the spectroscopic and microscopic techniques used and the underlying physical mechanisms that govern the techniques. We also discuss how the experimental data was processed and what information could be extracted.

1.8.3 Chapter 4: Oxide Specific Effects in Au Catalysis: promotion of oxygen adsorption

In this chapter, we present our first results pertaining to Au catalysis. Here, we focus on understanding how the type of oxide support (reducible vs. irreducible) can

affect the chemistry of Au. Specifically, we investigate the interaction between atomic oxygen and the surface of an Au layer supported by two oxides. The oxides considered are TiO_2 and SiO_2, the former being a semi–conductor reducible oxide and the latter being an insulating irreducible oxide. The promoting effect of oxide surface oxygen vacancies on oxygen adsorption on Au was calculated and a physical mechanism proposed. In short, it was found that electronic charge transfer from the oxide to the supported Au nano–structure promoted atomic oxygen adsorption. The degree of charge transfer to Au was found to be oxide specific, with the transfer being greater for the reducible oxide (TiO_2) and less for the irreducible oxide (SiO_2). Investigating the electronic structure of the oxide indicated that the electronic response to surface reduction dictated the magnitude of the charge transfered from the oxide to Au.

1.8.4 Chapter 5: Insight into the General Effect of Oxide Surface Off–stoichiometric Defect Promoted Au Surface Chemistry

In this chapter, we broaden our approach to investigating how the oxide surface can impart additional chemistry within the Au nano–structure. Driven by experimental results which showed a strong correlation between catalyst activity and the presence of cationic Au (i.e., oxidized Au) and well–defined surface science reports that indicated extra oxygen at the Au/oxide interface enhanced the stability of Au, we investigated the effect of oxide surface defects in general. Specifically, we investigated how reduced (oxygen vacancy rich), stoichiometric (pristine), and over oxidized (oxygen atom rich) surfaces interacted with Au nano–structures and how this interaction may promote Au–oxygen chemistry. We found that oxide surface defects destabilized the Au–Au internal structure by binding strongly to the Au nano–structure. This destabilization lead to an increase in Au surface chemical reactivity towards binding adsorbates in general (molecular and atomic oxygen and CO). To explain this phenomena, grounded in bond conservation and charge transfer to and from Au is presented to explain this

phenomena and is supported by calculations.

1.8.5 Chapter 6: The Chemistry and Electronic Structure of Oxide Supported Cationic Au Species

In this chapter we focused on a literature controversy regarding the active Au species for CO oxidation, either cationic or metallic Au. To clarify what may be the active form of Au, we again employed *ab initio* calculations. We found that the discrepancy between published results in literature most likely stemmed from the preparation procedure and incomplete removal of precursor chlorine. In the framework of this view we also found that the Au/oxide interface was highly active binding and possibly dissociating di–oxygen with energies conducive to a room–temperature catalytic process. Interestingly, these interface sites were also very active in binding chlorine, so much so that if chlorine was present, these sites would be poisoned and could not facilitate oxygen reduction. These findings were corroborated by experiments presented in Chapter 8.

1.8.6 Chapter 7: Connection Between the Oxides Electronic Structure and the Chemistry of Oxide Supported Au

In this chapter, we focus on the chemistry at the Au/oxide interface site and how this chemistry is affected by different oxide supports. We investigate four oxides with a range of electronic properties. Namely, SiO_2, TiO_2, SnO_2, IrO_2, an insulator, two semi–conductors, and a metallic oxide respectively. Surprisingly, we found that the activity of the Au/oxide interface site varied almost linearly with the electronic character of the oxide, with the Au/SiO_2 interface being relatively inert and the Au/IrO_2 binding O and O_2 strongly. The trends calculated for the Au/oxide interface site were found to be in line with the activity measured experimentally for Au/oxide powdered catalysts. To investigate the uniqueness of the Au/oxide system, we reproduced the

oxygen adsorption calculations using a Pt nano–rod in place of the Au nano–rod. We found that Au was special in that the oxygen adsorption depended highly on the type of oxide present, whereas oxygen adsorption at the Pt/oxide interface was promoted in general for all oxides tested. These results indicate that the Au/oxide interface is directly affected by the type of oxide present and may help to understand the measured oxide support effect in Au catalysis.

1.8.7 Chapter 8: Rational Design of Highly Active Au CO Oxidation Catalysts Driven by Insights from *ab initio* Calculations

In this chapter, we further isolate the active form of Au coupling theoretical and experimental approaches. Calculations indicate that the Au/oxide region can stabilize cationic forms of Au, namely, AuO_x and $AuCl_x$. The relative stability of the oxide and chloride species indicates that latter cannot participate in a catalytic oxidation reaction mechanism, i.e., chlorine poisons the Au/TiO_2 surface. From these insights we formulated specific catalyst preparation procedures that result in AuO_x and $AuCl_x$ deposition, verified by XPS, UV–vis, and Raman spectroscopy. The measured catalytic activity of the samples was directly inline with the theoretical calculations. We postulate, from the calculations and experimental results, that most catalytically active form of Au is an oxygen rich Au, not specifically Au_2O_3, and inactive cationic Au is caused by chlorine rich Au.

1.8.8 Chapter 9: Conclusions and Future Work

In this chapter we present the major conclusions drawn in this dissertation, and attempt to compile a larger picture of how various Au/oxide systems can exhibit vastly different surface chemistry. We follow the conclusions by presenting future directions which this work has motivated. In the future work we focus mainly on fundamental questions concerning low temperature catalytic chemistry, highly tun-

able surface sites, and connecting the electronic structure of materials to their surface chemistry.

CHAPTER II

Theoretical Development and Background

2.1 Overview

The aim of all experimentation is to develop a theoretical framework in which we can explain and, more importantly, predict physical nature. In this section, we describe the theoretical background and framework used in this dissertation. First, we describe the basis for atomic electronic structure and how this applies to chemical systems. We then describe Density–Functional theory, the engine for calculating the electronic structure and energy of atomic, molecular, and solid systems. Then, the fundamental framework for *ab initio* thermodynamics is developed, which is used to connect total energy electronic calculations to external conditions such as temperature and pressure. Finally, a general background on electronic structure of atoms, molecules, and extended surfaces, specifically oxides and metals is presented.

2.2 Electronic Structure

The dynamics of the macroscopic world can be accurately modeled and predicted by Newtonian mechanics, however, this theory fails when attempting to describe atomic and molecular structure or the interaction between electromagnetic radiation and matter. On the foundation set by many great scientists, Erwin Schrödinger developed a mathematical formalism describing the experimentally observed atomic phenomena. His theory adhered to all predetermined laws of classical Newtonian dynamics in the limit of the macroscopic scale and captured the dynamics of the internal structure of atoms and molecules [82]. The primary equation presented in Schrödinger's theoretical development:

$$H\Psi = E\Psi \tag{2.1}$$

'H' is a hermitian Hamiltonian operator which contains terms that operate upon the wave–function 'Ψ' returning the energy 'E' associated with each interaction contained within the Hamiltonian.

Schrödinger's equation (Eqn. 2.1) describes the many complex interactions between the charged particles within an atomic system. The atomic system consists of heavy positively charged particles (protons), heavy neutral particles (neutrons), and light negatively charged particles (electrons). The interaction between charged particles in an atom largely obeys Coulombs laws of charge–charge interaction with positive repelling positive and attracting negative. The structure of atoms, as we currently understand it, consists of a dense collection of protons at the center of an atom with lighter negatively charged electrons orbiting the positive center. It has been found that much of the dynamics of atoms, molecules, and solids are dictated by the energy and structure of the orbiting electrons. In Schrödinger's equation, the interaction between subatomic particles are contained within the hermitian Hamilto-

nian operator (H). The Hamiltonian operator (Eqn. 2.2) operates on the electronic wave function (Ψ), which contains information about the position or density of electrons within the potential presented by the positively charged atom nuclei. When the total energy Hamiltonian operator (Eqn. 2.2 in atomic units) is applied to the wave function the resultant energy (E) is the total energy of the atomic system.

$$H = -\frac{1}{2}\nabla_i^2 + V_{pot} \tag{2.2}$$

The exact solution of the Schrödinger equation can only be performed on a one electron system. When multiple electrons are present the solution must be performed numerically. As the number of electrons is increased the number of interactions increases approximately as N^2. To apply quantum theory to systems of practical importance such as a molecule of methane (10 electrons) or a model catalyst surface (100's of electrons), theories which approximate the electron–electron interaction must be employed. The first to treat this problem was Hartree and Fock, which approximated the electron–electron interaction by an average repulsive term in the Hamiltonian Eqn. 2.3.

$$H = -\frac{1}{2}\Delta_i^2 - \sum_A \frac{Z_A}{r_{iA}} + \sum_{i=1}^{2N-1}\sum_{j=i+1}^{2N}\frac{1}{r_{ij}} \tag{2.3}$$

However, many aspects of quantum dynamics were not present in the model, specifically non–classical electrostatic electron–electron interactions.

In 1963, Hohenberg and Kohn developed density functional theory (DFT) and applied this theory to atomic electrodynamics. DFT transformed the difficult many electron problem to a tractable problem dealing with many one–electron wave–functions. This is achieved by utilizing the electron density as the independent variable. The formulation of a more applicable mathematical model was presented by Kohn and Sham (Eqn. 2.4). In contrast to the Hartree–Fock method, DFT directly treats electron–electron interactions (Eqn. 2.7 and 2.8) including non–classical Exchange

and Correlation (XC) effects (Eqn. 2.8).

$$E[\rho(r)] = T_s[\rho(r)] + V_{e-nuc}[\rho(r)] + V_{e-e}[\rho(r)] + E_{xc}[\rho(r)] \tag{2.4}$$

$$T_s[\rho(r)] = \sum_i \int \Psi_i^*(r)(-\frac{1}{2}\nabla^2\Psi_i(r))dr \tag{2.5}$$

$$V_{e-nuc}[\rho(r)] = \int \nu_{nuc}(r)\rho(r)dr \tag{2.6}$$

$$V_{e-e}[\rho(r)] = \frac{1}{2}\int \phi(r)\rho(r)dr \tag{2.7}$$

$$E_{xc}[\rho(r)] = \int f_{xc}(\rho(r))dr \tag{2.8}$$

The terms in Eqn. 2.4 correspond physically to the kinetic energy (T_s), the electrostatic electron–nucleus interaction (V_{e-nuc}), the electrostatic electron–electron interaction (V_{e-e}), and electron exchange and correlation effects (E_{xc}). The electrostatic interactions are well quantified. The physical significance of exchange is the energy associated with exchanging electrons in orbitals and correlation is the energy associated with electrons interacting with all the other electrons around it. The energy associated with electron exchange and correlation is still a topic of active investigation [83].

The current theoretical description of exchange and correlation utilizes either the local electron density or the local electron density combined with it's derivative. The former method is coined the Local Density Approximation (Eqn. 2.9) and has roots in original theories developed by Thomas Fermi in approximating the kinetic energy of a free electron gas.

$$E_{xc}^{LDA} = \int \rho(r)\epsilon_{xc}[\rho_\uparrow(r)\rho_\downarrow(r)]dr \tag{2.9}$$

This method had surprising accuracy in representing the electron–electron exchange correlation energy of multi electron systems. The latter method employing density gradients (Generalized Gradient Approximation (GGA)) was a further improvement

(Eqn. 2.10).

$$E_{xc}^{GGA} = \int f(\rho(r), \nabla\rho(r))dr^3 \tag{2.10}$$

Many of the large DFT calculations performed today utilize some form of LDA or GGA description of exchange correlation energy. The approaches have varying accuracy. For our studies we have utilized the Perdew–Wang 91 GGA functional [84].

In this theoretical framework we calculate the total energy of quantum chemical model systems. The calculations were performed using DACAPO and the Atomic Simulation Environment (ASE) code [85]. DACAPO was used to calculate the wave function and electronic structure and ASE was used to optimize the model system geometry and calculate reaction activation barriers.

2.3 *Ab Initio* Thermodynamics

To investigate the stability of model systems in contact with an external chemical potential, total electronic energy calculations may be coupled with *ab initio* thermodynamics. Total electronic energy calculations are performed with a constant number of particles, temperature, and volume corresponding to the Helmholtz free energy thermodynamic potential (Eqn. 2.11).

$$F(N, V, T) = E^{elec}(N, V) + E^{vib}(N, V, T) - TS^{vib}(N, V, T) \tag{2.11}$$

The Helmholtz free energy may be connected to the more physically transparent Gibb's free energy by Eqn. 2.12.

$$G(N, P, T) = F(N, V, T) + PV(N, P, T) \tag{2.12}$$

Upon an order of magnitude estimation the pressure–volume term contributes $\sim$0.03 eV to formation energies (ΔG_f) and $\sim 10^{-3}$ eV/A^2 to surface energies (γ_f). There-

fore, G(N,P,T)≈F(N,V,T) allowing the connection between DFT calculations and thermodynamics.

Thermodynamics are used to investigate the relative stability of model systems and adsorbate over layers. Thus, the change in Gibb's free energy is the quantity of interest Eqn. 2.13.

$$\Delta G_f(T,P) = G_{final}(T,P) - G_{initial}(T,P) \tag{2.13}$$

External chemical potentials may be included in this formulation via Eqn. 2.14.

$$G_i(T,P) = N_i \mu_i(T,P) \tag{2.14}$$

Combining Eqn. 2.13 and 2.14.

$$\Delta G_f(T,P) = G_{final}(T,P) - G_{initial}(T,P) - \sum_i N_i \mu_i(T,P) \tag{2.15}$$

The Gibb's free energy may be decomposed into its electronic, vibrational, rotational, and translational contributions (Eqn. 2.16).

$$G(T,P) = E^{elec}(T,P) + F^{vib,rot,trans}(T,P) \tag{2.16}$$

For a solid surface and atomic adsorbates, the rotational and translational energy may be assumed to be a minor contribution to the total system Gibb's free energy. The vibrational contributions of surface phonons and adsorbates may be estimated by Einstein's equation and one characteristic vibrational frequency. The gas phase chemical potential may also be decomposed into it's electronic, vibrational, rotational, and translational contributions (Eqn. 2.17).

$$\mu = \mu_{gas}^{vib,rot,trans} + \frac{E_{gas}^{elec}}{N} \tag{2.17}$$

Calculating the energetic contributions to the gas phase chemical potentials may be done utilizing statistical mechanics or experimentally determined thermochemical data [86]. Combining Eqn. 2.15, 2.16, 2.17:

$$\begin{aligned}\Delta G_f(T,P) = G^{elec}_{final}(T,P) - G^{elec}_{initial}(T,P) - E^{elec}_{i}(T,P) \\ - \sum_i N_i \mu^{vib,rot,trans}_i(T,P) + \Delta F^{vib}_{surf}(T,P)\end{aligned} \tag{2.18}$$

Combining electronic terms Eqn. 2.18 may be approximated as:

$$\Delta G_f(T,P) \approx \Delta E^{elec}_{ads}(T,P) - \sum_i N_i \Delta\mu^{vib,rot,trans}_{i,gas}(T,P) + \Delta F^{vib}_{surf}(T,P) \tag{2.19}$$

Where ΔE^{elec}_{ads} is the DFT calculated adsorption energy or electronic energy of model formation (i.e., oxide surface termination). Eqn. 4.1 is the working equation in our treatment of *ab initio* thermodynamics. When calculated with a single gas phase chemical potential ($\Delta\mu_i$), the data is presented in a two dimensional plot consisting of straight lines. The $\Delta G_f = 0$ ordinate intercept and the slope of the line are determined by the change in system energy ΔE^{elec}_{ads} and the concentration of surface perturbations (adsorbates or model surface changes) respectively (N_i). The most favorable model system or adsorbate over layer is the system which minimizes the change in Gibb's free energy. Therefore the line (single μ case) or surface (multiple μ case) which is lowest in energy (most negative) for a given external chemical potential is the theoretically most favorable surface structure.

2.4 Molecular and Extended Electronic Structure

Electronic structure of molecular and extended solid state systems are utilized in this dissertation extensively to understand the fundamental physical mechanisms which govern adsorbate, oxide, and metal systems. In this subsection, we present

a short primer on molecular orbital theory and the electronic structure of extended systems.

2.4.1 Hydrogen Atomic and Molecular Orbitals

All atomic, molecular, and extended solid state chemistry is dictated by electronic structure. The fundamental understanding of how the electronic structure dictates chemistry stems from an understanding of atomic orbitals. Atomic orbitals are designated by letters s, p, d, and f. The orbitals increase in energy and number of nodes (locations of zero electron density) going from s to d, with s–orbitals having zero nodes and d–orbitals having two nodes. Within a molecule, these atomic orbitals interact depending on their phase, to form bonding or anti–bonding orbitals, which either attract or repel the atomic nuclei. When atomic orbitals combine to form molecular orbitals, first, the electrons rearrange to fill the lowest energy molecular orbitals, then fill higher energy molecular orbitals. The atomic and molecular orbitals of a hydrogen molecule are presented in Figure 2.1 (b). Utilizing group theory and symmetry operations the simple case of H_2 may be extended to more complex molecules and structures. In this dissertation, we focus on the interaction between atomic and molecular oxygen and oxide supported Au nano–structures. Therefore, we shall review each of their respective electronic structures to form a basis for our discussions.

2.4.2 Oxygen Atomic and Molecular Orbitals

The oxygen atom has the electronic structure $1s^2 2s^2 2p^4$ (see Figure 2.2). When two oxygen atoms interact they form several bonding and anti–bonding orbitals both through the s–orbitals and the p–orbitals. The Highest Occupied Molecular Orbital (HOMO) in O_2 is the p–type or π^* anti-bonding orbital (see Figure 2.2). Upon summing the favorable (bonding) and unfavorable (anti–bonding) interactions the

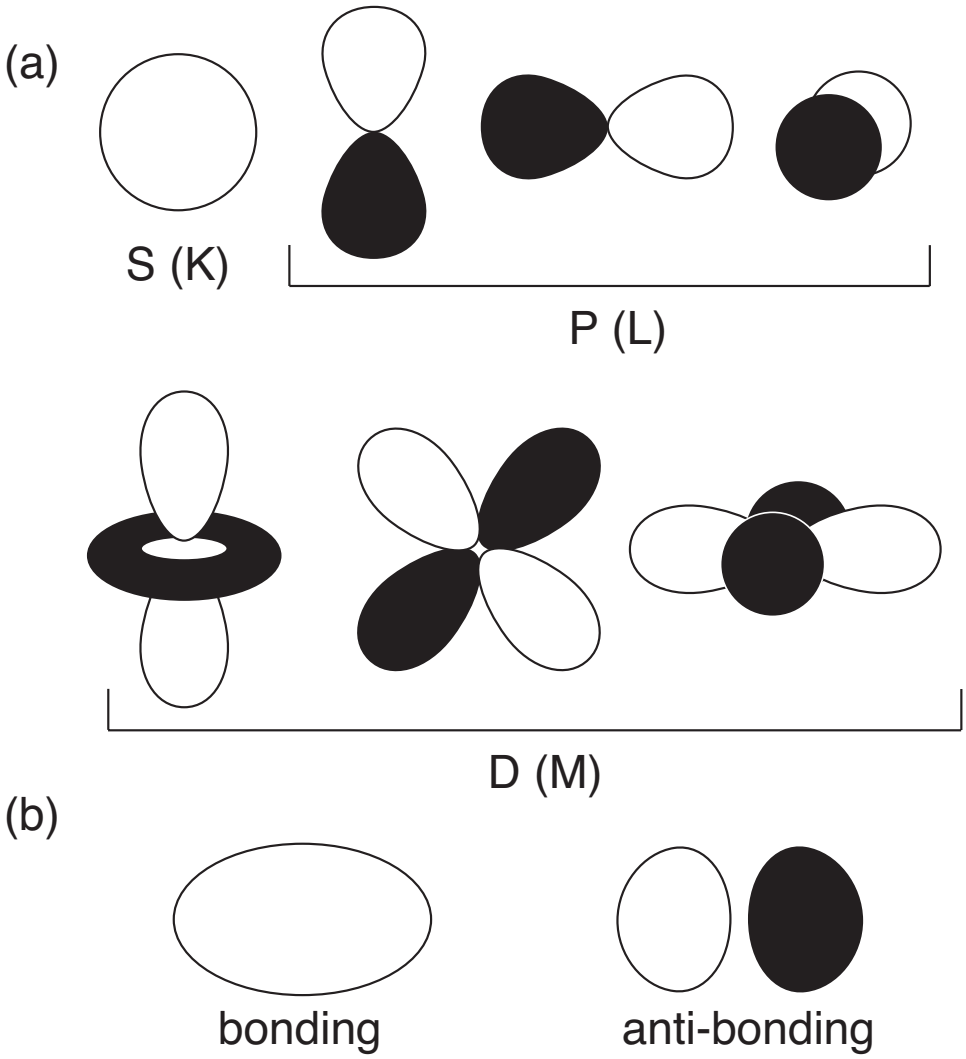

Figure 2.1: Geometries of electronic wave–function solutions of a hydrogen atom. The electronic shells are S, P, D, and above increasing in energy. As the energy increases the number of nodes and lobes increases. The understanding of bonding is based on the geometries and energies of these electronic wave–functions.

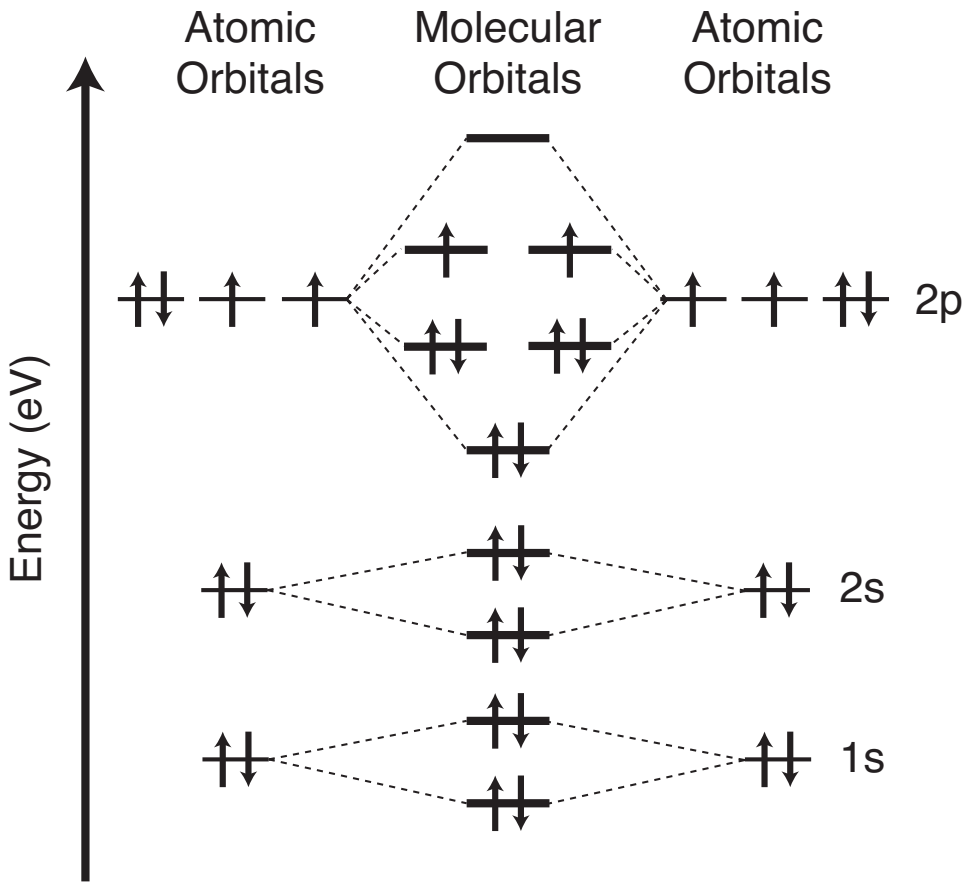

Figure 2.2: Depiction of atomic and molecular oxygen electronic orbitals. Upon interaction the atomic orbitals of a molecule mix and split into bonding and anti–bonding molecular orbitals depending on atomic orbital symmetry and energy. The oxygen molecule valence consists of half populated π^* anti–bonding orbitals. The bonding character may be approximated at two total covalent bonds present between the oxygen atoms. Further population of the π^* orbitals leads to a reduction in the overall bonding facilitating molecular dissociation.

number of chemical bonds equals two. To dissociate O_2, both of these bonds must be broken. This may be accomplished by populating the anti–bonding molecular orbitals via charge transfer, forming O_2^- or O_2^{-2}, both of which are more easily dissociated. Dissociation may also be facilitate by strong electronic interactions with another atom, molecule, or surface which results in a significant change in the electronic structure of the O_2 molecule. Both of these effects will be discussed in greater detail in the following chapters.

2.4.3 From Molecular Orbitals to the Solid State

Due to the wide range of atomic interactions present in a solid crystal, the electronic structure becomes continuous. The most simple case to illustrate the connection between molecular orbital theory and the solid state is a chain of hydrogen atoms. The molecular orbital structure of H_2 is intuitively simple (see Figure 2.1) with one set of in phase orbitals forming the bonding orbital and one set of out–of–phase orbitals forming the anti–bonding orbital. When there are an infinite number of hydrogen atoms in a chain the combinations of in–phase and out–of–phase orbitals is infinite. The resultant molecular orbitals of the chain span an energy range depending on their degree of interaction. These periodic wave functions may be represented by Bloch functions (Eqn. 2.20).

$$\psi_{n,i}(\mathbf{r}) = e^{i\mathbf{k}\cdot\mathbf{r}} f_i(\mathbf{r}) \tag{2.20}$$

With ψ_i, the ith orbital, equal to a periodic function with the periodicity of the unit cell reflected multiplied by a basis set of wave functions. The periodicity of the crystal depends upon the reciprocal wave vector ($\mathbf{k}$). When the orbitals in a solid interact, they form an infinite collection of orbitals that span an energy range, called a band. The energy bands for a hydrogen molecule and chain of hydrogens are presented in Figure 2.3. The bands or electronic structure in k–space can be more easily interpreted by viewing the lowest energy portion of the band as mostly

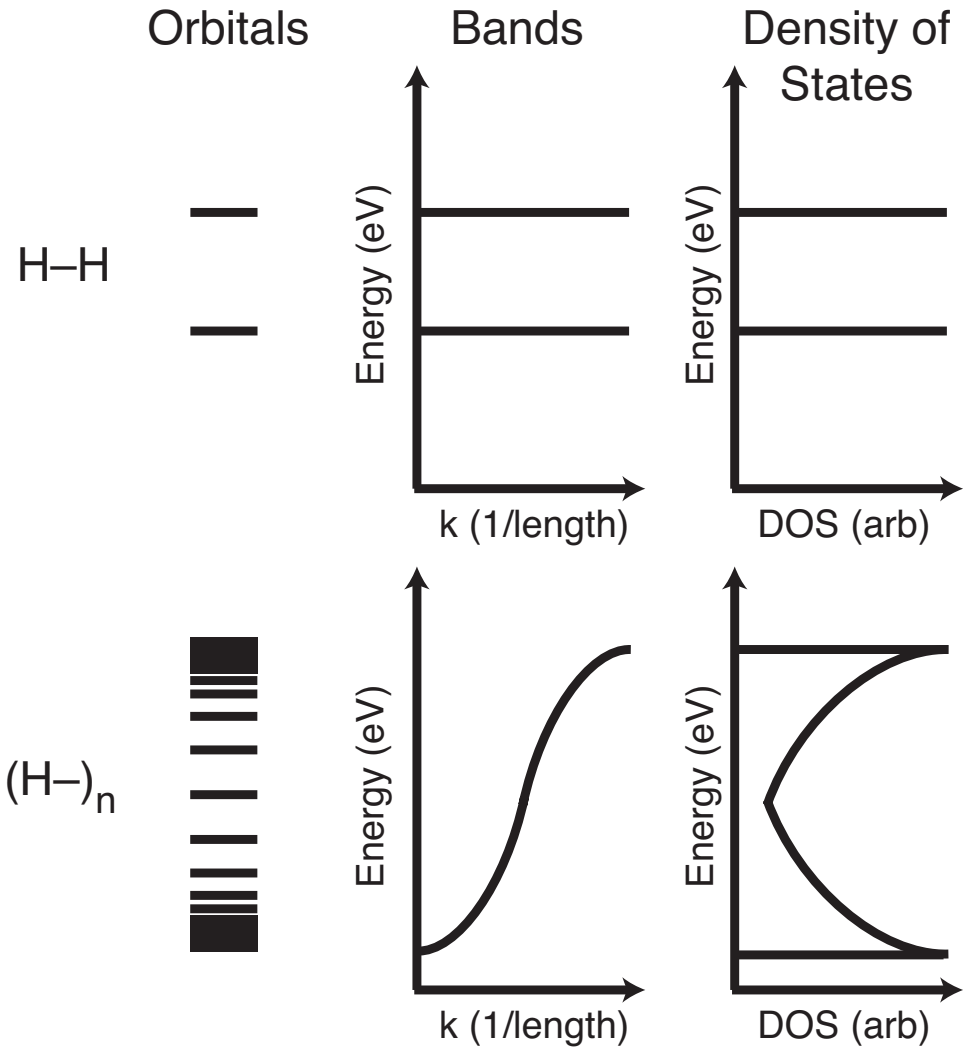

Figure 2.3: A pictorial depiction of the formation of electronic bands from a view of molecular orbital theory. The electronic structure of molecules consists of distinct electronic energy levels as only select orbitals interact producing bonding and anti–bonding orbitals. Whereas, in an extended structure many orbital interactions of varying degree are present, therefore, a range of electronic states exists. The "bands" or continuum of electronic states are more easily visualized by converting them into the density of states, which clearly shows the density of electronic states at specific energy levels.

bonding, the highest energy portion as mostly anti–bonding, and the middle portion as a mixture of bonding and anti–bonding. When dealing with complex many electron systems, the electronic structure is typically visualized by plotting the Density of States (DOS), which is the density of electronic states at a given energy level (see Eqn. 2.21).

$$DOS(E) = \frac{1}{dE/d\mathbf{k}} \tag{2.21}$$

The DOS of the hydrogen chain clearly shows the approximate segmentation of low energy bonding orbitals and high energy anti–bonding orbitals (see Figure 2.3. Armed with this conceptual understanding, we now move to more complex systems such as an extended metal structure and oxide structure.

2.4.4 Electronic Structure of Metals

The atomic packing in metals is dense, yet the electronic interactions between atom centers is not as directional as in organic molecules (strong localized bonds between atoms). On the other hand, the bonding within a metal is of a more non–local periodic nature. When dealing with the d–block metals, which are commonly utilized in heterogeneous catalysis, the electronic structure consists of a wide s– and p–state DOS plus a more localized d–state DOS. An example of a metallic electronic structure is presented in Figure 2.4. The electronic states of a metal are distributed in energy ranging from tightly bound electrons (large negative energy) to electrons at the Fermi level (zero energy), which move freely through the solid.

2.4.5 Electronic Structure of Oxides

Conceptually, the electronic structure of oxides lies between the electronic structure of molecules and metals. The atomic interactions between the metal centers and oxygen range in chemical character from highly localized orbitals (insulator oxide) to moderately delocalized orbitals (semi–conducting to metallic oxides). This in-

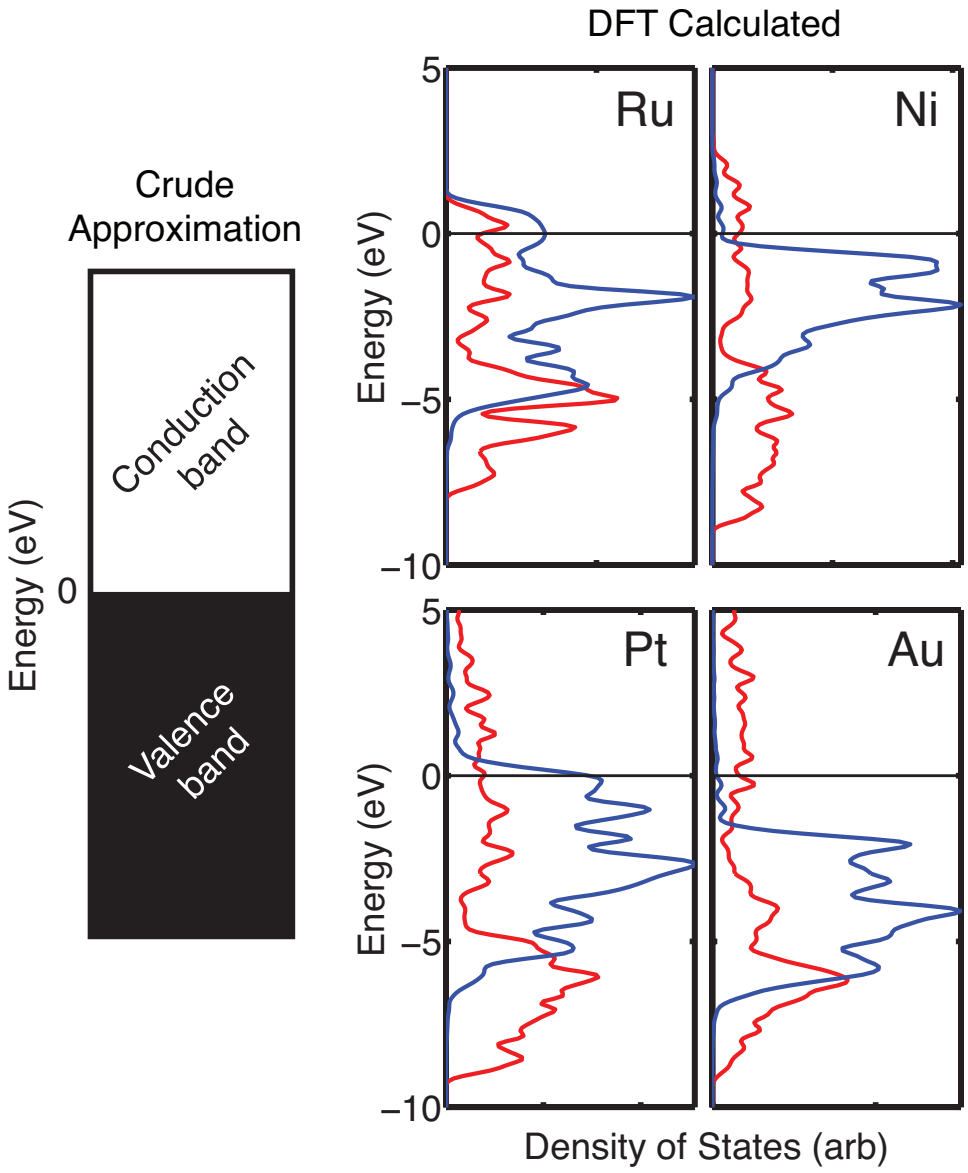

Figure 2.4: The electronic structure of metals is commonly perceived as unstructured and depicted as a "crude approximation". In many cases where bulk properties are sought this approximation is sufficient. On the other hand, to fully understand the surface chemistry of metals detailed information about the electronic states close to the Fermi level is required as these are the orbitals that interact appreciably with adsorbates. Example calculated electronic structures of selected Pt–group metals are presented. The s– and p–states are combined and plotted in red and the d–states plotted in blue. The Fermi level has been set to zero.

crease in atomic interaction coupled with specific coordination geometry (octahedral or tetrahedral coordination) leads to a more molecular type electronic structure.

Oxides can be thought of as being constructed from building blocks consisting of a metal center surrounded by a specific geometry of oxygens. For example, many abundant oxides such as TiO_2, Al_2O_3, Fe_2O_3, SnO_2, IrO_2, and SiO_2 have octahedral or tetrahedral MO_x building blocks. Utilizing the symmetry of this building block allows us to understand the electronic structure of the extended oxide. In Figure 2.5, the molecular orbital diagram for an octahedrally coordinated metal atom is presented along side the DFT calculated density of states for Rutile TiO_2, which is build of octahedral crystal units. The d–states of the metal center are split by the field of six surrounding atoms. These states have varying degrees of bonding and anti–bonding character; thus, they are distributed at different energies (referenced to the Fermi level) accordingly. In the case of many oxides, the Fermi level (set to zero in DOS plots) falls in an energy gap, thus the material is insulating. In the case of metals, there are electronic states at the Fermi level, see Figure 2.4, thus the material may conduct electrons. The DOS of TiO_2 only shows the states very close to the Fermi level. The unpopulated states above (below) the Fermi level are comprised mostly of titanium (oxygen) electronic states. The calculated TiO_2 electronic structure is for stoichiometric TiO_2. When departing from stoichiometry, either reduction or over oxidation, the electronic structure of the oxide changes. These changes are oxide type (i.e., insulator, semi–conductor, metallic) specific and can dictate the oxide's surface chemistry.

2.5 Model System Specifics

Quantum chemical model systems consisted of Au atoms, clusters, nano–rods, and continuous layers supported by a rutile crystal of oxide. Employing many different metal geometries allowed critical variables to be determined which significantly

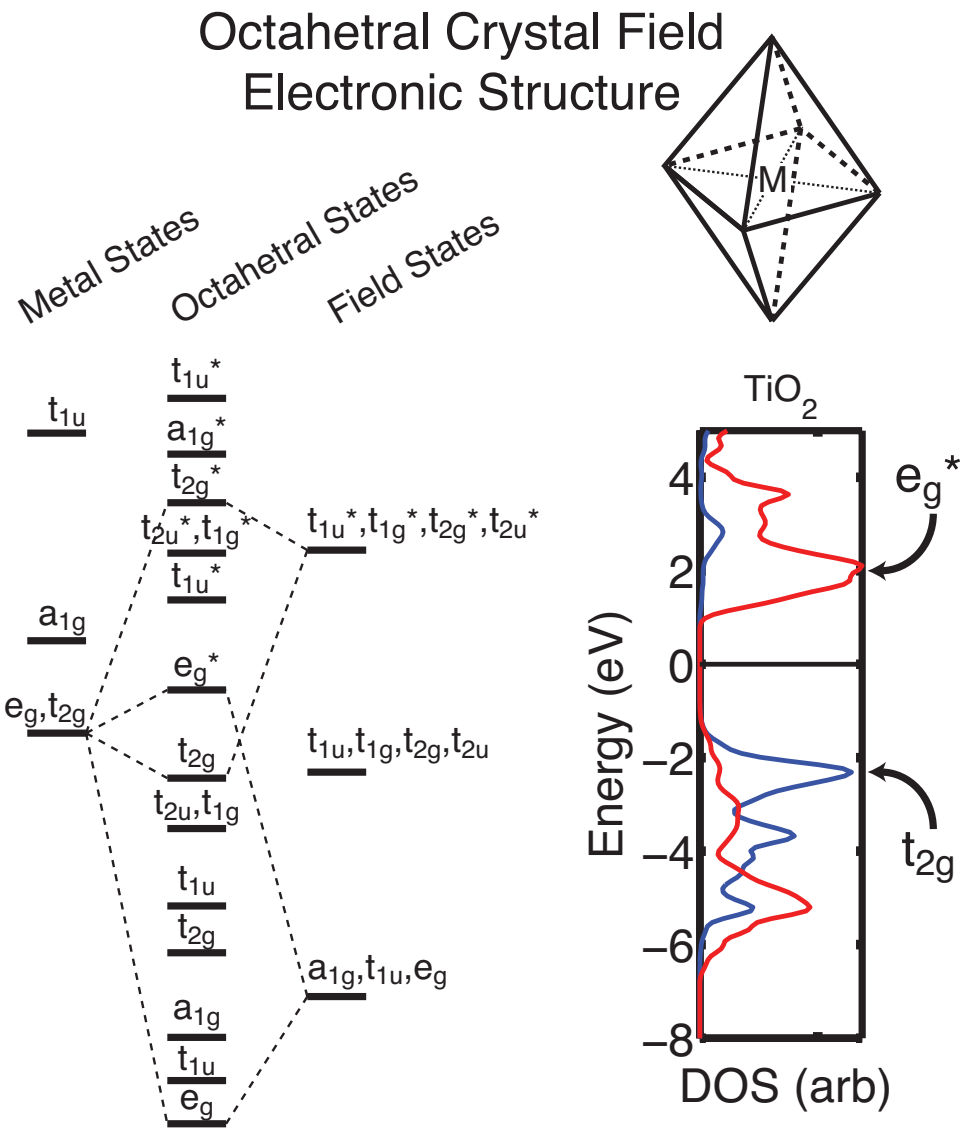

Figure 2.5: The oxide supports considered in this dissertation are calculated in the rutile crystal structure. The stoichiometry and octahedral oxygen coordination around the metal centers leads to specific electronic structure. The molecular orbital diagram of a d–block metal in an octahedral field is displayed. The calculated electronic structure of rutile TiO_2 about the Fermi level is displayed as an example.

affected the chemical dynamics of the model surface.

The oxides utilized as supports include TiO_2, SiO_2, IrO_2, and SnO_2. The rutile oxide crystal structure is the most thermodynamically favorable structure at room temperature and pressure for TiO_2, SnO_2, and IrO_2, and is a high energy low density form of SiO_2. The (110) surface of the rutile crystal is the most thermodynamically favorable crystal facet termination. The chemical termination of the surface is found to be stoichiometric under a wide range of external atmospheres. The rutile crystal structure and (110) termination are presented in Figure 2.6. The arrows mark the key characteristics of the oxide surface. The titanium cationic (titanium trough) and oxygen anion (oxygen bridge) rows are indicated by arrows. Partial reduction of the oxide surface is the removal of one or more of the oxygen bridge atoms. When extra oxygen is present on the oxide surface, adsorption is atop a titanium cation in the titanium trough.

Many Au structures were calculated ranging from single atoms to 1D, 2D, and 3D extended structures. The structures entertained are displayed in Figure 2.7. The Au model systems were chosen specifically to model Au geometries found experimentally in powdered catalysts and in model catalyst studies. Au structures were adsorbed both on stoichiometric and defective oxide surfaces to investigate how local chemical environment of the Au/oxide could affect the Au chemistry. The purpose of testing several model systems is two fold. First, ensures that conclusions drawn are not model system dependent and are indeed general, and, also helps to limit the effect of circumstantial experimental findings, i.e., Au structures measured under specific experimental conditions may not be present under actual reaction conditions.

2.6 Conclusion

In summary, we presented the theoretical framework for the quantum chemical and *ab initio* thermodynamic calculations along with a brief background on molecular

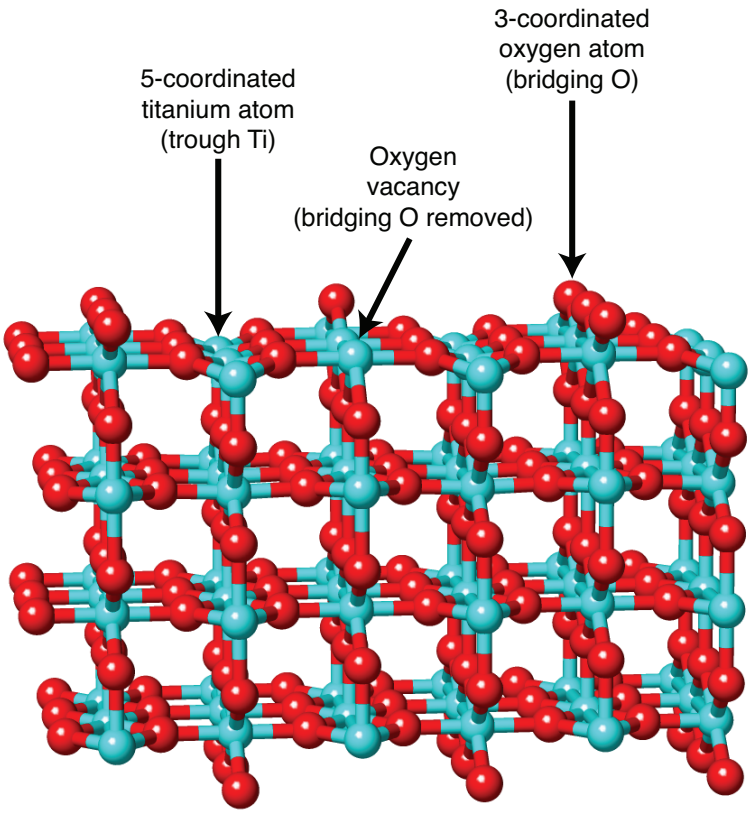

Figure 2.6: Model rutile crystal utilized in the quantum chemical calculations. Arrows indicate the three major features of the oxide surface. The titanium trough, oxygen bridge, and oxygen vacancy. The exposed surface in the z–direction is the (110) surface, the most thermodynamically favorable facet of the rutile crystal structure. Red and light blue spheres correspond to oxygen and metal respectively.

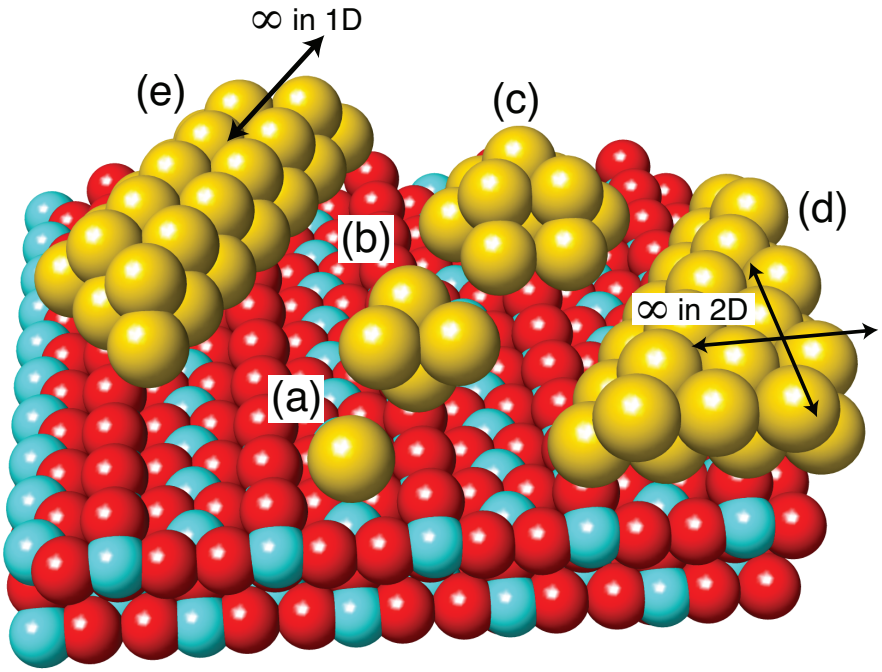

Figure 2.7: A selection of the Au geometries entertained for the quantum chemical calculations. (a) Atomically dispersed, small clusters truncated in the xy–plane (b) Au_4 and (c) Au_{10}, and extended structures (d) 2ML Au continuous in two directions and (e) Au nano–rod continuous in one direction. These different models systems present various types of adsorption sites for probe molecules and were used to ensure conclusions reached were not model system dependent. Gold, red, and light blue spheres correspond to gold, oxygen, and oxide metal respectively.

and extended electronic structure. All of these aspects of the theoretical calculation are important to understand as much of the dissertation relies upon connecting surface chemistry to the electronic structure. It will be seen in the forthcoming chapters that the electronic structure both of the oxide and Au play a critical role in understanding the dynamics of adsorption and activation of O_2, surface reactivity of Au, and the stoichiometric state of the oxide surface. Theoretical insights that help to understand the dynamics of the Au/oxide surface under catalytic reaction conditions.

CHAPTER III

Experimental Methods

3.1 Overview

In this section we discuss the experimental methods used to compliment and motivate our first principles calculations. In our experimentation we focused on the Au/TiO_2 catalyst. Herein, we present the procedures used to produce and characterize catalysts, discuss pertinent physical mechanisms that affect the procedures, and give reasons why the specific procedure was used.

3.2 Introduction

In this dissertation we used a combined theoretical/experimental approach to gain insight into the fundamental physical mechanisms that govern Au/oxide catalyzed low–temperature oxidation. In this section, we describe the experimental aspects of our combined approach. As in our first principles calculations, we focus on Au/TiO_2. We start by discussing the materials used in our catalyst preparation procedures and the procedures themselves. Then, we present the reactor design and reactor studies used to characterize the activity, chemical kinetics, and temporal stability of our samples. Finally, we describe the spectroscopic and microscopic techniques used to characterize the catalyst preparation procedure and catalytic material. In discussing our procedures we will also present a short background on the dominant physical mechanisms that dictate the dynamics of the procedure.

3.3 Materials and Material Preparation

Au/TiO_2 catalysts of various metal loadings (0.5–2.0 wt% Au) were prepared from Degussa P25 TiO_2 and Au chloride salt ($HAuCl_4 \cdot 3H_2O$). The oxide support Degussa P25 TiO_2 consisted of ∼25–30 nm TiO_2 non–porous single crystal particles. It has a measured BET surface area of approximately 50 m^2/g and is comprised of ∼75% anatase and ∼25% rutile crystal phases as–received. The purity of TiO_2 was reported as 99.99% on the metal basis. Prior to use, the oxide support was calcined under flowing ultra-high purity air over night at 500 °C to clean the as–received oxide. The cleaning procedure did not result in particle sintering, i.e., the surface area was unchanged. The as–received and calcined support were characterized by Raman spectroscopy, and it was found that both anatase and rutile crystal structures were present after calcination.

The Au salt, $HAuCl_4 \cdot 3H_2O$, was purchased from Alpha Aesar and had a reported

purity of 99.99% on the metal basis. The Au metal content of the salt was 49.94 wt%. The as–received salt was in solid form. The salt reacts readily with many materials, is hygroscopic, and light sensitive. The salt was stored under dry N_2 in a opaque bottle at ∼5 °C. Catalysts were prepared from the as–received solid Au chloride salt or from a 30 wt% Au in 5 wt% HCL in H_2O solution. The HCl was purchased from Fischer Scientific as a concentrated solution (37.5 wt%) and diluted with deionized H_2O to 5 wt% HCl. Au deposition via the HCl solution was found to yield more reproducible results. We determined that the rate at which the Au salt transformed into Au chloro–hydroxide or Au hydroxide, upon change in pH, depended greatly on the Au starting material, i.e., solid or solution.

The catalyst preparation was carried out in a 250 mL Erlenmeyer flask placed a top a heated stir plate. A Teflon coated magnetic stir bar of 4 cm length was used to vigorously stir the solution. The temperature of the solution was checked periodically by k–type thermocouple. The catalyst solid was removed from solution with ashless filter paper using vacuum filtration. The filter cake was further dried in a tube furnace under ultra–high purity air (∼250 SCCM) at 120 °C.

3.4 Catalysts Preparation Procedure: Theory and Procedure

Three catalyst preparation procedures were used to produce samples: dry–impregnation, modified incipient–wetness, and deposition–precipitation. The preparation procedures were chosen such that comparisons could be made between our results and literature results.

3.4.1 Dry–Impregnation (Imp) and Modified Incipient–Wetness (Mod–IW)

The Dry–impregnation and incipient–wetness catalyst preparation methods involve similar physical mechanisms and may be used to deposit a wide range of precursors on many supports [87, 88]. In these methods the oxide support is forced into contact with the metal precursor by mechanical mixing or by concentrated precursor solution. Because the deposition mechanisms is predominately physical in nature attractive precursor–support interactions are not required. This allows virtually any precursor to be deposited on any oxide via these methods. The overall dispersion, however, is directly affected by the precursor–support interactions and may vary greatly as various precursor/support combinations are entertained. In both dry–impregnation and incipient–wetness, the chemical form of the precursor is not changed upon deposition. Therefore, in most cases, catalyst pretreatment procedures are required to produce the catalytically active species. High temperature oxidation or reduction is used to liberate the active metal centers from the precursor complex. Here, the interaction between the metal contained within the precursor and the support surface further affects the overall dispersion.

3.4.2 Deposition–Precipitation

The deposition–precipitation (DP) method relies upon chemical reaction and attractive interactions between the precursor and support to drive precursor deposition. In this preparation method, the support and precursor are both present in low concentrations in solution. The precursor is then reacted with an additional substance to cause precipitation of another complex or fully reduced metal. The precipitate is drawn to the support by attractive electrostatic interactions [87]. In the case of directly depositing metal particles, the particles simply precipitate onto the support. Because this method relies upon 1) a reaction and 2) attractive precursor–support

interactions, a relatively small number of catalysts have been successfully prepared by this technique. Because the rate of deposition may be carefully controlled high dispersions may be achieved. Furthermore, if the precipitated precursor attracts to the support surface very highly loadings can also be produced. In this method, as in dry–impregnation and incipient–wetness, the as–deposited precursor may or may not be catalytically active and may require oxidative or reductive pretreatments.

3.4.3 Step–by–step Procedure

Next we present a step–by–step procedure for the three preparation methods. In the three procedures the same drying step was used and no pretreatments were employed.

3.4.3.1 Specific Procedure for Dry–Impregnation (IMP)

To produce ∼250 mg of Au/TiO_2 catalyst via the dry–impregnation method oxide support was mechanically mixed with solid metal precursor. The metal precursor is highly sensitive to H_2O and light and will readily react with metal spatulas, thus care should be taken when handling the precursor. The solid mixture was mechanically mixed using a mortar and pestle for approximately five minutes and then transfered to a quartz boat for drying. The quartz boat was placed in a 6 cm ID glass tube furnace and heated to 120 °C at a rate of 1.5 °C/minute. Ultra–high purity air was flown over the boat with a rate of ∼250 SCCM. The powder was allowed to dry over night for 12 hours in the furnace. After drying, the powder was again mixed, pulverized, stored in a desiccator under roughing vacuum (∼5E-2 torr) in a refrigerator away from light.

3.4.3.2 Specific Procedure for Modified Incipient–Wetness (Mod–IW)

To produce ∼100 mg of Au/TiO_2 catalyst via the modified incipient–wetness procedure, we first determined the volume of H_2O required to reach incipient–wetness

for 250 mg TIO_2. Then a solution was produced of $HAuCl_4 \cdot 3H_2O$ in 5 wt% HCl ($\sim$16.7 μL per 250 mg TiO_2) such that the final loading of the active metal would be 1.0 wt%. The proper volume of this liquid was deposited directly onto dry TiO_2 powder and mixed for several minutes to distribute the Au salt over the oxide. After the deposition step the mixture was suspended in 100 mL of H_2O at 25 °C and the pH was adjusted to 7. After the adjustment the mixture was centrifuged and washed with $\sim$2 L of H_2O per 250 mg catalyst. The washed mixture was then vacuum filtered with ashless filter paper until dry enough to transfer to the drying furnace. The catalyst was then dried and stored as in the dry–impregnation procedure.

3.4.3.3 Specific Procedure for Deposition–Precipitation (DP)

To produce $\sim$100 mg of Au/TiO_2 catalyst via the deposition–precipitation method, first 250 mL of purified H_2O was heated in a Erlenmeyer flask to 70 °C. The solution was mixed continuously buy a 4 cm teflon coated magnetic stir bar. 250 mg of TiO_2 was added to the flask and allowed to mix thoroughly. A timer was started upon the addition of the Au salt solution (30 wt% $HAuCl_4 \cdot 3H_2O$ in 5 wt% HCl/H_2O). The pH of the solution was measured continuously by a dual probe Fisher Scientific Accumet AB15+ pH meter. The pH of the solution was slowly and continuously adjusted to the desired value, between 2 and 10, by 0.1 N NaOH (NaOH purity was 99.995 % on a metal basis) over $\sim$10 minutes. The solution was allowed to age for one hour with continuous adjustment of the pH throughout the entire hour. This ensures equilibrium concentrations of Au chloride, Au chloro–hydroxide, and Au hydroxide species in solution. After aging, the catalyst was centrifuged and washed with $\sim$2 L of H_2O and then vacuum filtered. The filter cake was transfered to the drying furnace and underwent the same drying procedure as previously described.

3.5 Characterization Methods

The catalysts were characterized using an array of experimental spectroscopy and microscopy techniques. A custom built bench–top reactor was used to test catalyst activity and temporal stability. Transmission electron microscopy operated in the High Angle Annular Dark Field (HAADF) Scanning mode (STEM) was used to investigate the presence of particles and quantify their size if present. The chemical composition of the catalyst and the local chemical environment about the Au metal was quantified by X-ray photoelectron and Raman spectroscopy. X-ray photoelectron spectroscopy was used to directly measure the oxidation state of Au and the presence of chlorine on the catalyst surface. Raman spectroscopy was used to investigate the Au species under ambient conditions. Ultra–violet/visible absorption spectroscopy was used to characterize the Au species present in the deposition–precipitation catalyst preparation solutions.

3.5.1 Reactor Studies

Reactor studies were performed using a temperature controlled custom built bench–top reactor. The reactor consisted of a 35 cm total length quartz u–tube reactor one leg encased in a heater. The reactor was fed ultra-high purity reactant gases metered by mass flow controllers. The composition of the effluent was measured by a Varian CP-3800 gas chromatograph equipped with a 60 meter CP-Sil 5CB column. A diagram is presented in Figure 3.1 of the reactor design. The catalyst sample, usually 1–5 mg, was mixed with ∼150–200 mg low surface area SiO_2 to minimize heat and diffusion effects and placed between two quartz wool plugs within one leg of the u–tube reactor. The catalyst plug was placed approximated 12 cm down the temperature controlled leg. A k–type thermocouple was fed to the top of the catalyst bed to within half a centimeter to control the temperature of the reactor. The effectiveness of this setup was checked by submerging an unsheathed thermocouple in the

catalyst bed and comparing the temperature measured there with the thermocouple directly above the bed. The temperatures were comparable within three degrees. The reaction gases used were ultra–high purity O_2, CO, and N_2 and fed fed to the reactor via Swagelok tubing. The mass flow controllers were purchased from Hastings and were of model type HCF–302 and HCF–202. Standard operating flows were 30 standard cubic centimeters per minute (SCCM) CO, 200 SCCM O_2, and balance N_2 for a total flow of 280 SCCM to 1000 SCCM. The effect of diffusion on the measured reaction rate was determined by varying catalyst mass and volumetric flow rate of the reactants. It was determined that diffusion did not play a major role in the measured rates or the kinetics determined.

Three reactor study approaches were employed to test catalytic activity and stability: temperature programmed reaction, kinetic, and temporal stability studies. Temperature programmed reaction may be used to investigate the effect of temperature on the activity of the catalyst. These studies are strictly not catalytic measurements, but may be used to understand how the catalytic activity of a surface changes over a wide range of temperatures. Kinetic studies were performed to quantify the apparent activation barrier for reaction over selected catalysts. In these studies we investigated how the apparent activation barrier was affected by catalyst preparation procedures and temperature. Temporal stability studies were performed to quantify the deactivation of the catalyst samples.

3.5.1.1 Determining Kinetics of Reaction

To determine kinetic parameters for a given sample, the sample was allowed to reach steady–state near room temperature. This usually occurred within 30 minutes of contacting the sample with the reactant gases. The temperature of the sample was then ramped and the catalytic rate was measured. The data was analyzed by

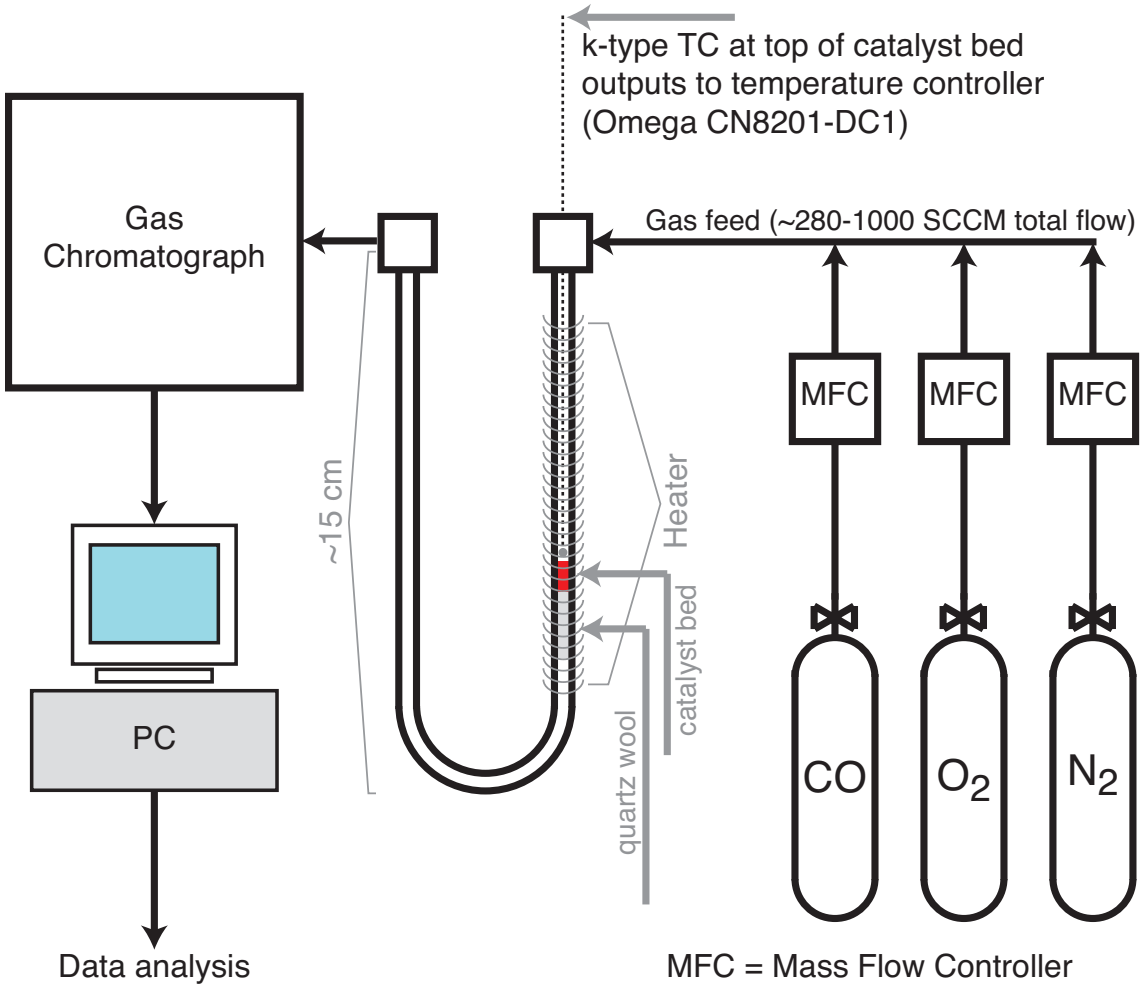

Figure 3.1: Schematic of custom–built reactor. Ultra–high purity gases were metered through mass flow controllers to a temperature controlled u–tube reactor. The effluent was analyzed by a gas chromatograph every 5.75 minutes. The geometry of the u–tube reactor is accentuated to show the catalyst plug, heater, and point of temperature measurement.

manipulation of an Arrhenious type equation:

$$rate = A \cdot e^{\left(\frac{-E_a}{RT}\right)} \tag{3.1}$$

Where 'A' is the pre–exponential factor or frequency factor, E_a is the apparent activation barrier for the reaction to take place, 'R' is the ideal gas constant (8.314 J/mole/K), and 'T' is temperature in Kelvin. Taking the natural log of the Eqn. 3.1 leads to:

$$ln(rate) = ln(A) - \frac{E_a}{RT} \tag{3.2}$$

Which may be plotted as ln(rate) vs. 1/RT and the Arrhenious parameters, A and E_a may be easily extracted as the slope and intercept of the line produced. In Figure 3.2 an example analysis for three catalysts is presented.

The kinetics were determined within the differential conversion regime such that the forward rate constant dominated the measured rate. The effect of diffusion was checked by varying catalyst loading and gas flow rates, and It was determined that film diffusion did not play a major role in the measured kinetics. For a more complete description of the dynamics of chemical kinetics see reference [89].

3.5.1.2 Determining Temporal Stability

The temporal stability of the catalysts was tested by subjecting ∼1-5 mg catalyst to reactant gases over an extended amount of time. In these studies, changes within the catalyst under isothermal operation could be measured. An example of a stability study is presented in Figure 3.3.

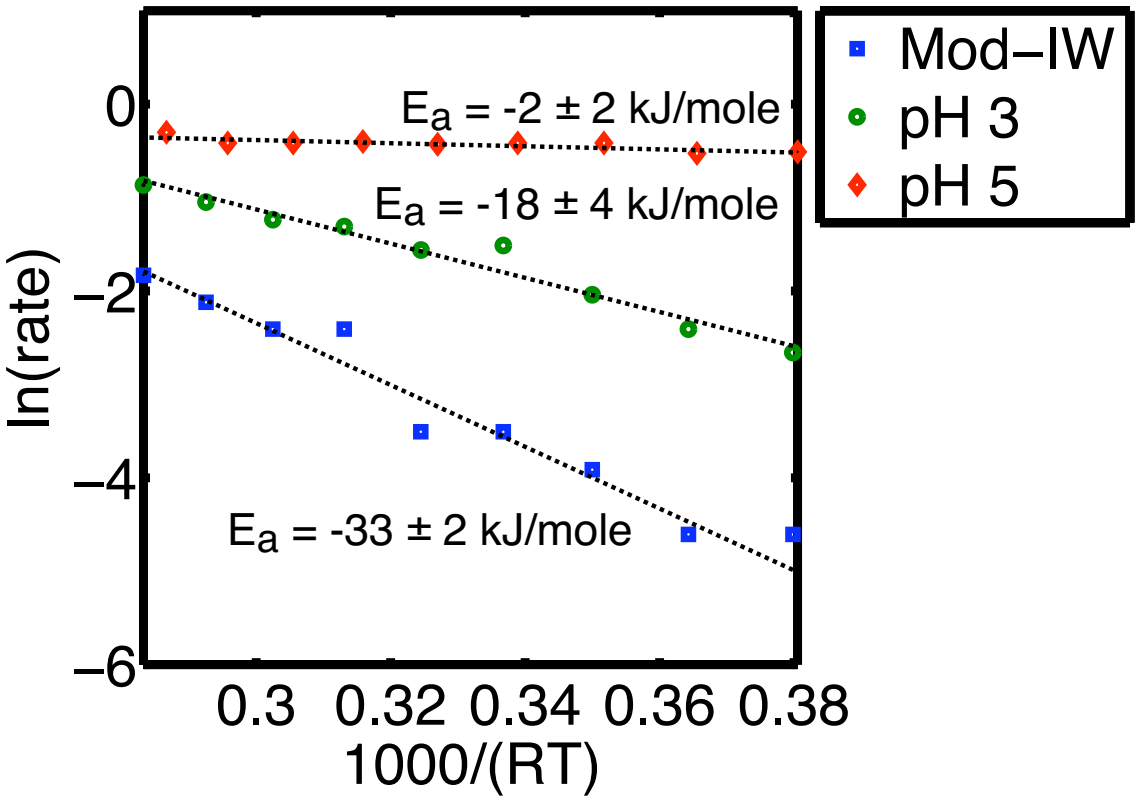

Figure 3.2: Example calculated kinetics for low–temperature CO oxidation over selected Au/TiO_2 catalysts. The catalysts were produced by modified incipient–wetness (Mod–IW), and deposition–precipitation at a pH of 3 and 5.

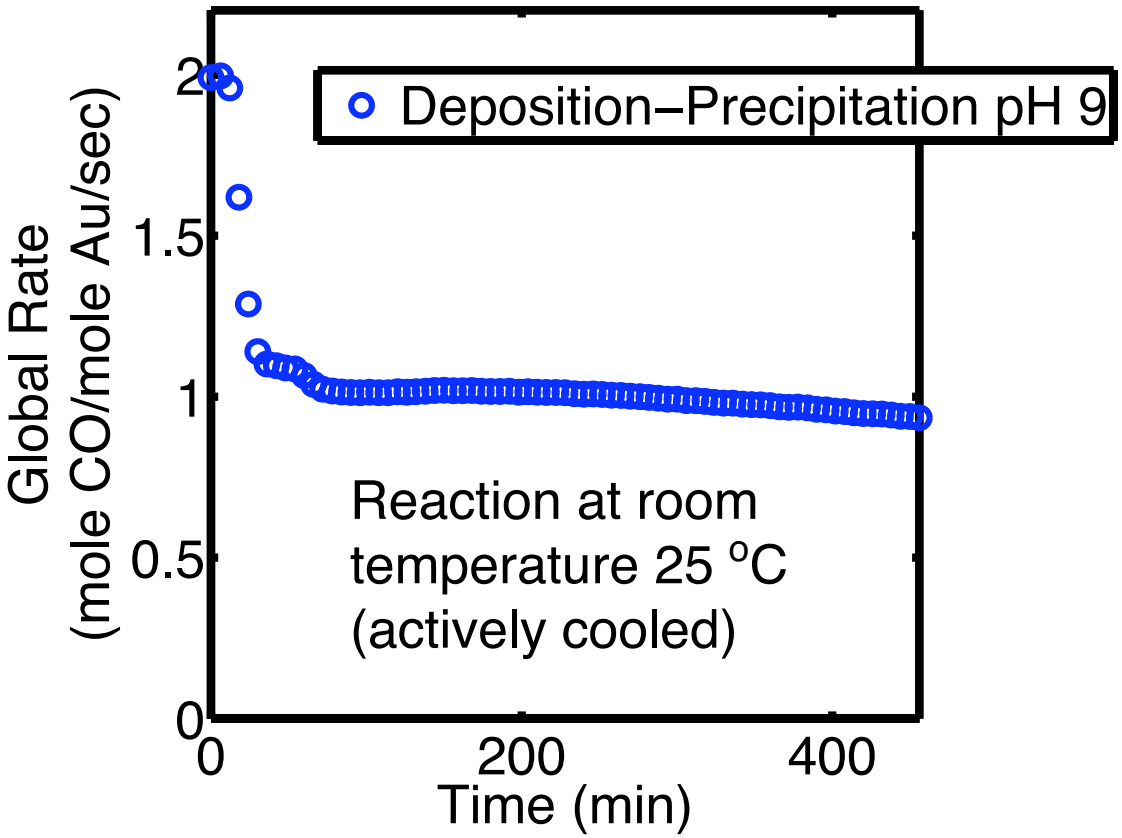

Figure 3.3: Example stability test for Au/TiO_2 catalyst prepared via the deposition–precipitation method at a pH of 9.

3.6 Microscopy

3.6.1 Transmission Electron Microscopy

The geometric structure of the oxide support and the deposited Au was determined by a 2010F JEOL Transmission Electron Microscope operated in bright field imaging or high angle annular dark field scanning mode (HAADF–STEM). Transmission electron microscopy utilizes high energy electrons (∼100 keV+) to image the atomic structure of a material. Many techniques are available when using TEM, however, we focused upon bright and dark field imaging to investigate the geometric structure of our catalysts. A bright field image is produced by measuring the amount of electron beam transmitted through the sample at high magnification and resolution. This technique may be used to produce images with atomic resolution (∼0.17 nm). However, this technique does not directly indicate chemical composition and may result in significant sample damage and reconstruction as the electron beam is continuously bombarding the sample as the image is acquired. It was found that bright field imaging significantly damaged the sample and led to drastic changes in Au species that may be visualized while imaging.

To circumvent the harsh environment of the electron beam, a scanning beam technique was employed (STEM). Operating in scanning mode the electron beam was focused to a spot size of 0.15–0.5 nm and rastered across the sample. In this mode the sample surface was contacted by the electron beam at discrete points for short times thus led to a much more stable sample while imaging. The STEM was operated in high angle annular dark field imaging mode, which collects the diffracted electrons in a high angle annular region and reconstructs an image into real space. This technique, because it utilizes diffracted electrons, contains information pertaining to the elements that diffracted the electrons i.e., the heavier elements diffract electrons at a larger angles than lighter elements. Therefore, this imaging technique allowed us

to not only visualize the geometric structure of the catalyst, but also determine the spacial distribution of Au on the support simultaneously. It should be noted that the diffraction in STEM also depends upon the density and oxidation state of the sample material. Therefore, oxidized species such as $AuCl_x$ and AuO_x may be undetectable because of their decreased density and increased oxidation state as compared to metal Au nano–particles. This was confirmed by STEM imaging of as–prepared catalysts where Au particles could not be detected, yet under x-ray photoelectron spectroscopy it was clear Au was present.

The microscope electron source operated at 200 keV energy with a beam spot size of either 0.5 or 0.17 nm. The sample chamber was held at $\sim$1.5E–7 torr vacuum. Sample preparation involved dispersing dry powder on copper grid supported carbon film or holey carbon film.

3.7 Spectroscopy

3.7.1 X–ray Photoelectron Spectroscopy

X–ray photoelectron spectroscopy was used to investigate the chemical composition of the catalyst surface and quantify the oxidation state of Au. X–ray photoelectron spectroscopy is based on the photoelectric effect, where a photon of energy is absorbed by a solid ejecting an atomic particle with the same energy, see Figure 3.5. In the case of XPS core state electrons are ejected and the energy at which they were bound in the atom is calculated by Eqn. 3.3

$$E_{binding} = E_{photon} - E_{kinetic} - \Phi_{WF} \tag{3.3}$$

Where $E_{binding}$ is the binding energy of the ejected electron, E_{photon} is the energy of the incident photons, $E_{kinetic}$ is the kinetic energy of the ejected electron, Φ_{WF} is the work function of the spectrometer. Shifts in the binding energy of the electrons may

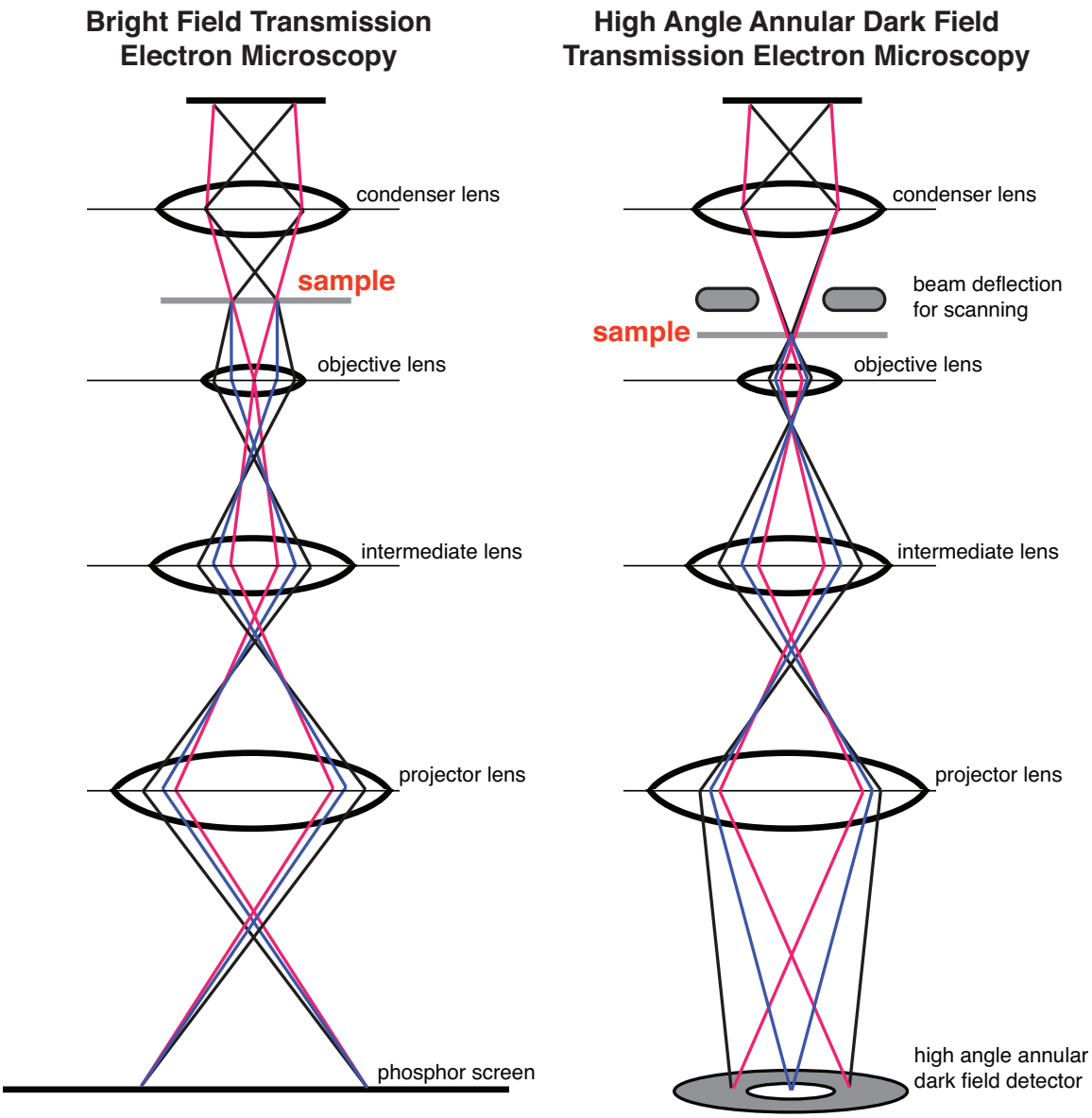

Figure 3.4: Schematic of the transmission electron microscope operated in bright and dark field imaging modes. In bright field imaging the real space image obtained is produced directly from the electrons transmitting through the sample. In dark field operation the image is reconstructed from the electrons diffracted by the sample. Therefore, the dark field image contains information about the atomic species which the diffracted electron encountered. This technique is commonly referred to as Z-contrast imaging.

be used to quantify the oxidation state of the parent atom. For example, electrons ejected from the $4f_{\frac{5}{2}}$ and $4f_{\frac{7}{2}}$ states of metallic Au have binding energies of 87.8±0.1 eV and 84.0±0.3 eV respectively [86]. Whereas, when Au is oxidized in an compound such as $CsAuCl_4$ the binding energies are 87.5 and 91.2 eV respectively [86]. XPS may also be used to quantify the relative amount of an atomic species present on the catalyst surface. By employing sensitivity factors, a measure of how sensitive the element is to electron ejection based on a standard, the relative atomic concentration may be calculated by Eqn. 3.4.

$$Atomic\ \% = \frac{A_i/S_i}{\sum_i A_i/S_i} \tag{3.4}$$

Where atomic % is the atomic percent of species 'i', A_i is the measured XPS peak area, S_i is the sensitivity factor for the element electronic state measured.

The instrument used was a Kratos Axis Ultra XPS with a monochromatic aluminum source (1486.7 eV). The sample transfer and analysis chamber pressures were ∼5E–7 and ∼5E–9 torr respectively. The time from sample introduction to spectra collection was commonly 12 hours, the time required to degas the sample and reach a vacuum favorable for spectra collection. Steps of 0.1–0.5 eV in energy were used to collect spectra with dwell times per point of ∼200 milliseconds. Due to the rapid reduction of Au under UHV conditions the time elapsed between sample introduction and spectra collection was minimized.

3.7.2 Ultra–violet Visible Absorption Spectroscopy

To quantify the chemical complexes present in the catalyst preparation solution we utilized Ultra–violet/visible light absorption spectroscopy. In this spectroscopy electromagnetic radiation of the ultra–violet and visible spectral range is used to excite valence electrons to unpopulated low lying states. These electronic transitions

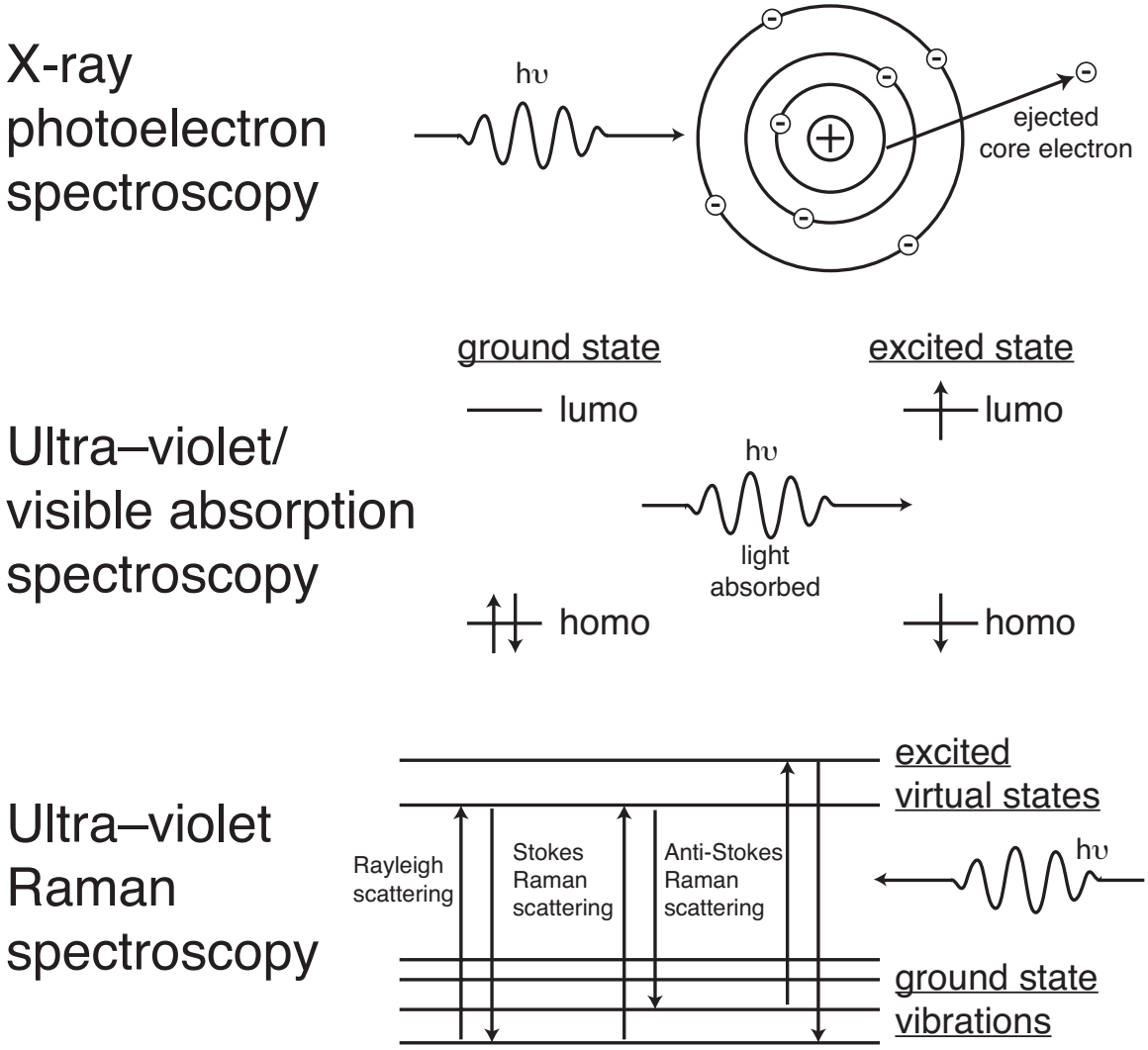

Figure 3.5: Schematic of the physical mechanisms underlying x-ray photoelectron, ultra–violet absorption, and Raman spectroscopy.

are accompanied by absorption of photons. Only specific electronic transitions are allowed and are indicative of the electronic structure of the sample. This spectroscopic technique can be used to track chemical transformations occurring under ambient conditions. A schematic of this process is shown in Figure 3.5. In our case, we utilized UV–vis to investigate the transformation of $HAuCl_4{\cdot}3H_2O$ to $Au(OH)_4$. The experiment was performed using deuterium/hydrogen and xenon lamps for the photon source. Solutions were produced identical to those used to produce our catalyst samples. The solutions was diluted $\sim$1000 fold to reduce the concentration of precursor and placed in a cuvette. The spectra was collected in transmission mode with the absorption of the source being plotted. Three samples were taken and averaged to reduce noise.

3.7.3 Raman Spectroscopy

Raman spectroscopy was used to further characterize the Au chemical species present on the oxide surface after catalyst preparation. Raman spectroscopy is based on gains or loses in energy of photons absorbed and reemitted by a molecule or solid. Three main phenomena dominate the Raman spectra: Rayleigh scattering, Stokes–Raman scattering, and anti–Stokes–Raman scattering. The first type of scattering is elastic where no energy is lost from the absorption to reemission. This scattering occurs when the material is not Raman active. When the material is active, i.e., the polarization of the electron cloud changes upon photon absorption, either Stokes–Raman or anti–Stokes–Raman occurs. In Stokes–Raman the excited virtual state relaxes to a state higher in energy than the vibrational ground state, on the other hand, anti–Stokes–Raman the virtual state relaxes to a lower energy vibrational state than the initial state. Raman spectroscopy can be used to detect molecules or modes that are invisible to infra–red vibrational spectroscopy. In our case we used Raman to verify the presence of $AuCl_x$ and AuO_x on the oxide surface and correlate their

Table 3.1: Raman shifts for various species of Au chloride, Au chloro–hydroxide, and Au hydroxide. Raman shifts presented in wavenumbers (cm^{-1})

Species	Au—Cl	Au—O
$AuCl_4^-$	347	na
$AuCl_3(OH)^-$	339	569
$AuCl_2(OH)_2^-$	356	576
$AuCl(OH)_3^-$	366	553
$Au(OH)_4^-$	na	580

presence with the catalytic activity measured. The experimental setup was as follows: approximately 25 mg of catalyst solid is pressed into a uniform pellet at a pressure of 3000 psi and placed in the beam path. The spectrometer was operated in reflectance mode. Spectra were collected with an integration time of 15–25 sec with 10-25 spectra averaged to obtain the final spectra. Key spectral signals for $AuCl_x$, $AuCl_x(OH)_y$, and $Au(OH)_y$ are given in Table 3.1, the values are from La Grange and co–workers [90]. Spectral signals from TiO_2 are 235, 445, and 612 cm^{-1} for the rutile crystal structure and 395, 515, and 638 cm^{-1} for anatase TiO_2. An example Raman spectra of an Au/TiO_2 catalyst prepared via dry–impregnation is presented in Figure 3.6.

3.8 Conclusion

In this section we have summarized our catalyst preparation procedures and the microscopic and spectroscopic techniques used to characterize them. The characterization techniques allowed information to be obtained about the physical geometry of the catalyst surface and its chemical composition. This information was coupled with first principles calculations to obtain a more resolved connection between the chemical composition of the catalyst surface and the measured catalytic activity.

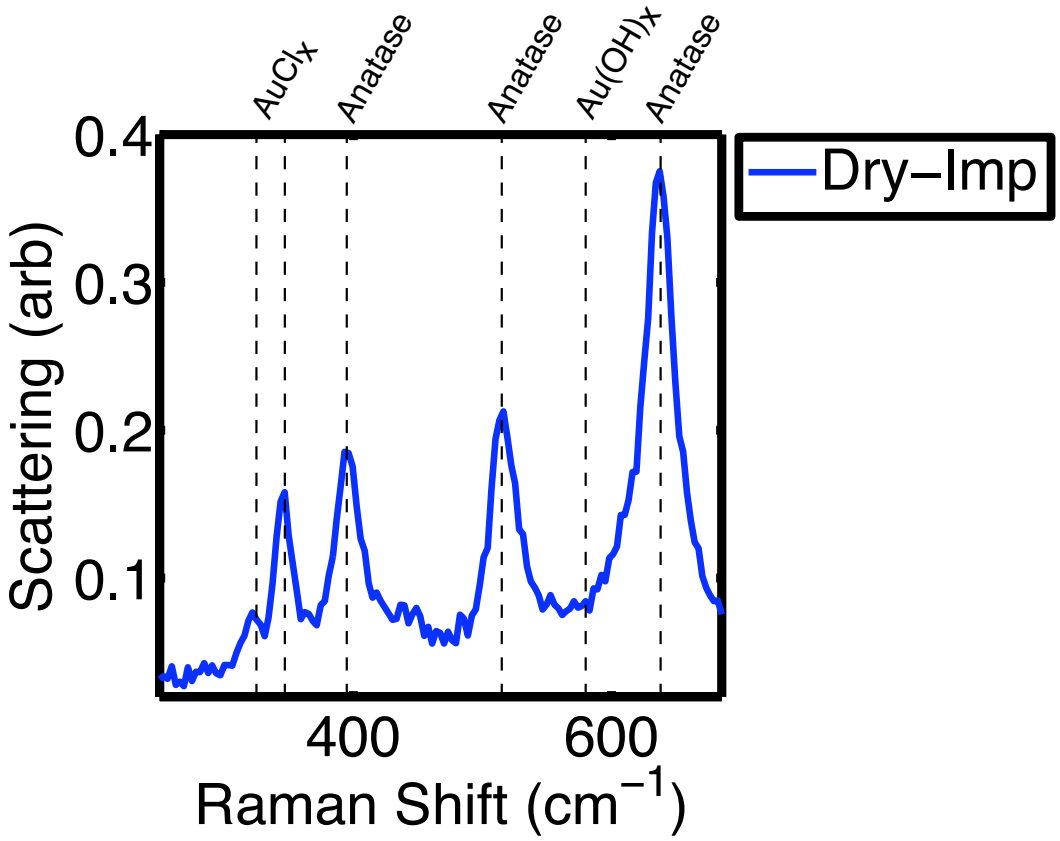

Figure 3.6: Example Raman spectra of Au/TiO_2 prepared via the dry–impregnation preparation procedure. The oxide was not pretreated in this sample thus the anatase phase of TiO_2 dominates the spectra.

CHAPTER IV

Oxide Specific Effects in Au Catalysis: promotion of oxygen adsorption

4.1 Overview

In this section, we focus on understanding how an oxide support can directly affect the chemistry of a supported Au nano–structure. We employ quantum chemical and *ab initio* thermodynamic calculations to investigate the activity of Au/TiO_2 and Au/SiO_2 surfaces toward binding atomic oxygen. We found that oxide surface defects, namely oxygen vacancies, at the Au/oxide interface can directly influence the chemistry of the supported Au a few Au—Au bond lengths away. The promotional effect of the oxygen vacancies was found to be oxide specific, with the more reducible oxide (TiO_2) promoting oxygen adsorption to a greater extent than the irreducible oxide (SiO_2). This oxide specific effect stemmed from how the oxides respond to surface reduction, and how the electronic structure accommodated the electron density left at the oxygen vacancy.

4.2 Introduction

Gold (Au) is chemically inert. However, Au nano–particles deposited on oxide supports are active in a number of catalytic reactions including low–temperature CO oxidation and propylene epoxidation [72, 91]. Even though oxidation reactions over Au/oxide catalysts have been studied extensively, there are many fundamental questions that remain unanswered. There is an intensive debate regarding the oxidation state of catalytically active Au [37, 42, 92–95]. While ultra–high vacuum (UHV) studies and theoretical calculations suggest that electronic charge is transferred from a support to Au yielding anionic Au [37, 42, 94], steady–state experiments suggest that cationic (oxidized) Au is responsible for the unusual activity [92, 93]. Another question that has been argued extensively is whether and how oxide supports impact the catalytic activity. It has been demonstrated that Au supported on reducible oxides (TiO_2, Fe_2O_3) is more active than Au supported on irreducible oxides (SiO_2, Al_2O_3) under similar conditions and for Au particles of identical size [32, 70]. Irreducible oxides are characterized by higher metal–oxygen bond strength and larger band gap than reducible oxides.

4.3 Summary

In this Letter, density functional theory (DFT) and *ab initio* thermodynamic calculations have been utilized to investigate *i*) the oxidation state of catalytically active Au and *ii*) the role of oxide supports. We focus on pressure–and temperature–dependent interactions of oxygen with Au deposited on a reducible (TiO_2) and an irreducible (SiO_2) oxide. We demonstrate that the oxidation state of Au is governed by external conditions (oxygen pressure and temperature) and by the chemical interactions between oxides and Au. We find that while under low oxygen chemical potentials, electron density is transferred from an oxide support to Au forming Au;

under catalytically relevant conditions there exists a thermodynamic driving force to oxidize Au and form cationic Au. Our calculations show that highly anionic Au, formed when Au is deposited on reducible TiO_2, interacts strongly with oxygen and is easily oxidized even at moderate oxygen chemical potentials. On the other hand, mildly anionic Au, formed when Au is adsorbed on irreducible SiO_2, interacts weakly with oxygen and high oxygen chemical potentials are required to oxidize the substrate. We propose a simple model, grounded in the first principles calculations, which can explain the oxide–specific catalytic activity of Au nano–structures adsorbed on oxide supports.

4.4 Model System

We utilize a model system with an Au(111) bilayer adsorbed epitaxially on an oxygen vacancy rich (4x1) unit cell of rutile TiO_2(110) and SiO_2(110), see Figure 4.1. Rutile is thermodynamically the most stable phase of TiO_2, while rutile SiO_2 is metastable under relevant conditions. We explore the oxide supports with oxygen vacancies, labeled R–TiO_2 and R–SiO_2, since it has been observed that the vacancy sites serve as anchoring points for Au nano–clusters [36]. These model systems, which are structurally almost identical for both oxides, allow us to focus on the support–specific aspects of Au/oxide chemistry. A similar model system containing an Au bilayer adsorbed on TiO_2 has been found to exhibit superior CO–oxidation activity in well–controlled high vacuum experiments [96]. The oxide surface is modeled with 50% of the bridge oxygen atoms missing. The Au bilayer is oriented so that the Au lattice stretch, caused by the lattice mismatch between Au and the oxides, is minimized for the explored (4x1) oxide unit cell. This orientation yields the TiO_2–induced Au lattice stretch of 12% in the Au(112) direction, consistent with the experimentally reported values [24], and no stretch or compression for Au on SiO_2. The lattice constants of the Au/oxide systems have also been optimized in the DFT calculations which showed

that the lowest energy state is the one where the bilayer accommodates the lattice constant of the underlying oxide support.

4.5 Calculation Parameters

We utilize periodic pseudo–potential plane–wave DFT calculations with Perdew–Wang Generalized–Gradient–Approximation functional (http://www.camp.dtu.dk). The calculations were converged with respect to k-point sampling, number of oxide layers, plane wave cutoff, and the force convergence threshold of 0.05 eV/$\mathring{A}$. The top 2 Au layers are relaxed in the z-direction while oxygen adsorbates were relaxed in all three directions. We have performed a number of studies, for different oxygen vacancy concentrations, where all Au and O atoms were allowed to fully relax in all directions. While, depending on the oxygen-vacancy concentration, there might be surface restructuring and shifts in oxygen adsorption energy, the results of the fully relaxed calculations are in qualitative agreement with the results reported in Figure 4.2.

Oxygen adsorption is modeled by oxygen atoms occupying threefold hollow sites on the Au surface and interstitial Au subsurface sites [93]. Figure 4.2 shows the surface free energy of adsorption calculated for oxygen adsorbed on Au(111), Au supported on R–TiO_2, and Au supported on R–SiO_2 as a function of oxygen chemical potential [97, 98]:

$$\begin{aligned} \Delta G_f(T, P_i) &= \frac{N}{A}\left(E_{ads} - \Delta\mu_O(T, P_O)\right) \\ &= \frac{N}{A}\left(E_{ads} - \Delta\mu_O(T, P^o) - \frac{1}{2}kTln(\frac{P_O}{P_O^o})\right) \end{aligned} \tag{4.1}$$

Where N is the number of oxygen atoms per unit cell while A is the surface area of

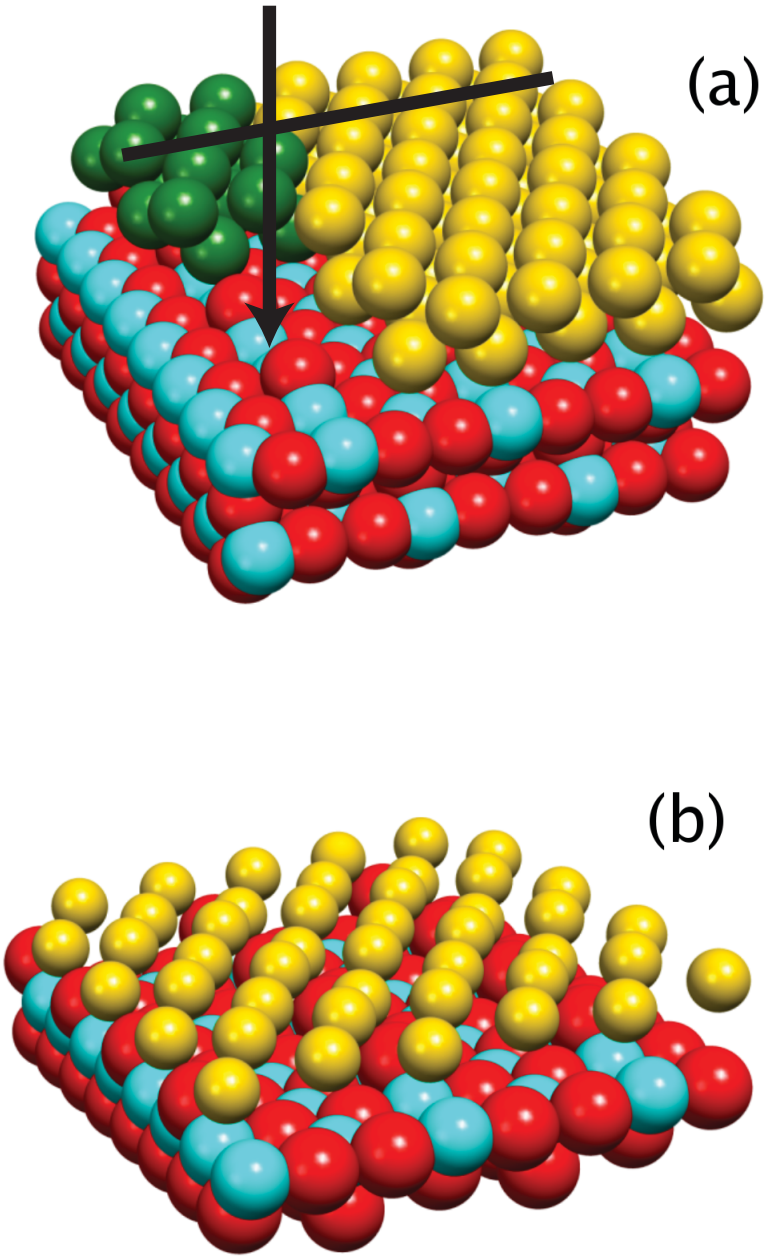

Figure 4.1: (a) The model system contains an Au(111) bilayer adsorbed on rutile TiO_2(110)–(4x1) and SiO_2(110)–(4x1). The unit cell is colored in green. The arrow points towards an oxygen vacancy. The dark line depicts the direction of the Au stretch required to accommodate the TiO_2 lattice. There is no stretch for Au supported on SiO_2. O atoms are red, Ti or Si are blue, while Au is yellow. (b) The layer of Au, bonded to the support, is depicted. Notice the relaxation of Au atoms towards oxide vacancies.

the unit cell. The adsorption energy (E_{ads}) per O_2 is obtained as:

$$E_{ads} = \left(\frac{1}{N} E_{O/substrate} - E_{substrate} - \frac{N}{2} E_{O_2} \right) \tag{4.2}$$

Where the relevant energies are calculated in the DFT calculations. Temperature and pressure effects on the free energy of O_2 are included through O, which can be computed from first principles using appropriate partition functions or obtained from thermochemical tables [86]. We note that metal–oxygen vibrations, which are approximated to contribute a maximum of 2–3 meV at 300 K, and slab phonon contributions, which to a large extent cancel each other in the formulation of the free energy, are neglected.

4.6 Results

4.6.1 *Ab Initio* Thermodynamics of Oxygen Adsorption

The configuration with the lowest free energy at a given oxygen chemical potential is thermodynamically the most stable at the external conditions (pressure and temperature) that correspond to the chemical potential. The term "the most stable structure" refers to the energetically favorable structure among the tested trial structures. While one cannot exclude the possible existence of other more stable configurations, this uncertainty has little effect on our conclusions. Figure 4.2 shows that oxygen adsorption on Au(111) (dashed lines) is thermodynamically unfavorable for all realistic oxygen chemical potentials. This observation corroborates the chemical inertness of Au. Figure 4.2 also shows that oxygen does not adsorb on Au/R–SiO_2 (dash–dotted lines) at the chemical potentials lower than –0.27 eV, which corresponds to atmospheric pressure and room temperature (RT). However, at the chemical potentials higher than –0.27 eV, the most stable configuration has $\frac{1}{2}$ML of oxygen adsorbed. In this configuration, which is effectively a 2D surface oxide, $\frac{1}{2}$ML oxygen is adsorbed

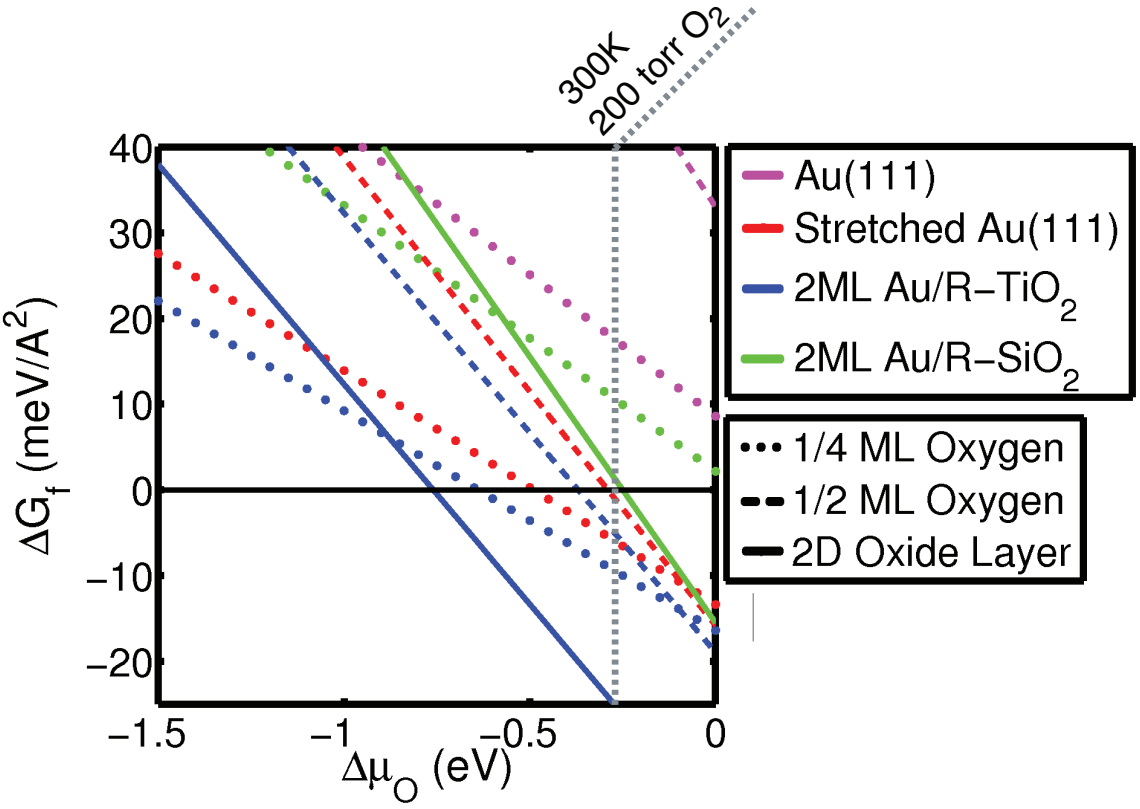

Figure 4.2: Surface Gibb's free energy of adsorption for oxygen adsorbed on Au(111), stretched Au(111), Au/R–TiO_2 and Au/R–SiO_2. The line $\Delta G_f = 0$ corresponds to the reference state of an adsorbate free Au/Oxide surface and gas phase O_2. The vertical dashed gray line corresponds to $\Delta\mu_O$(T,P) at a temperature and pressure of 300 K and 200 torr O_2. $\Delta\mu_O$ equal to zero is referenced to the electronic energy of O_2, therefore, corresponds approximately to a $\Delta\mu_O$ value where O_2 would condense on the surface irregardless of favorable electronic bonding.

on the Au surface and $\frac{1}{4}$ML is in the Au subsurface sites close to the oxygen vacancy. In the case of Au/R–TiO_2 (full lines), the $\frac{1}{2}$ML oxidic structure is thermodynamically the most stable even at very low oxygen chemical potentials (μ_O>–0.7 eV).

Since Au adsorbed on R–TiO_2 is slightly stretched, it is important to decouple the stretching effect from the electronic effect due to the chemical interactions between Au and R–TiO_2. To decouple these effects we have studied oxygen adsorption on stretched but unsupported Au(111) (dotted lines). The Au(111) lattice is stretched so that the lattice constant corresponding to Au/R–TiO_2 is reproduced. Figure 4.2

shows that while on Au/R–TiO_2 the $\frac{1}{2}$ML oxidic structure is the most stable for a wide range of external conditions, on stretched Au(111) the most stable configuration has oxygen adsorbed on–surface at $\frac{1}{4}$ML coverage.

Figure 4.2 shows that Au/R–TiO_2 binds oxygen more strongly than Au/R–SiO_2 and stretched Au(111) for all examined oxygen coverages and configurations. The observed behavior is not a consequence of the TiO_2–induced Au lattice stretch but rather it is the result of oxide–specific electronic interactions between the support and Au.

4.6.2 Electronic Structure Analysis

To understand the observed oxide–specific behavior of the Au/oxides we have investigated their electronic structure. When an oxygen vacancy is created on an oxide, two electrons remain in the vacancy. The redistribution of this electron density is oxide specific. Figure 4.3 shows the local density of states (LDOS) projected onto the bridge Ti and Si atoms of the stoichiometric and vacancy-rich versions of the respective oxides. The Ti LDOS suggests that the electron density, freed upon the formation of the vacancy, shifts to low laying Ti 3d–states of the neighboring bridge Ti atoms. These orbitals are unoccupied in the stoichiometric S–TiO_2. Bader charge analysis shows that the bridge Ti atoms gain 0.4 e^- each and move apart by additional one Angstrom, compared to the Ti—Ti distance in S–TiO_2. Figure 4.4 also shows the localized Wannier orbital corresponding to a 3d–state that gains the electron density from the vacancy.

On the other hand, the Si–projected LDOS shows that the electron density, freed upon the formation of the oxygen vacancy on SiO_2, is utilized to form a Si—Si bonding state at 0.85 eV below the Fermi level. This electron density is localized along the Si—Si bond, which is formed at the oxygen vacancy. This is corroborated by the Wannier orbital corresponding to this state, shown in Figure 4.4. The formation of

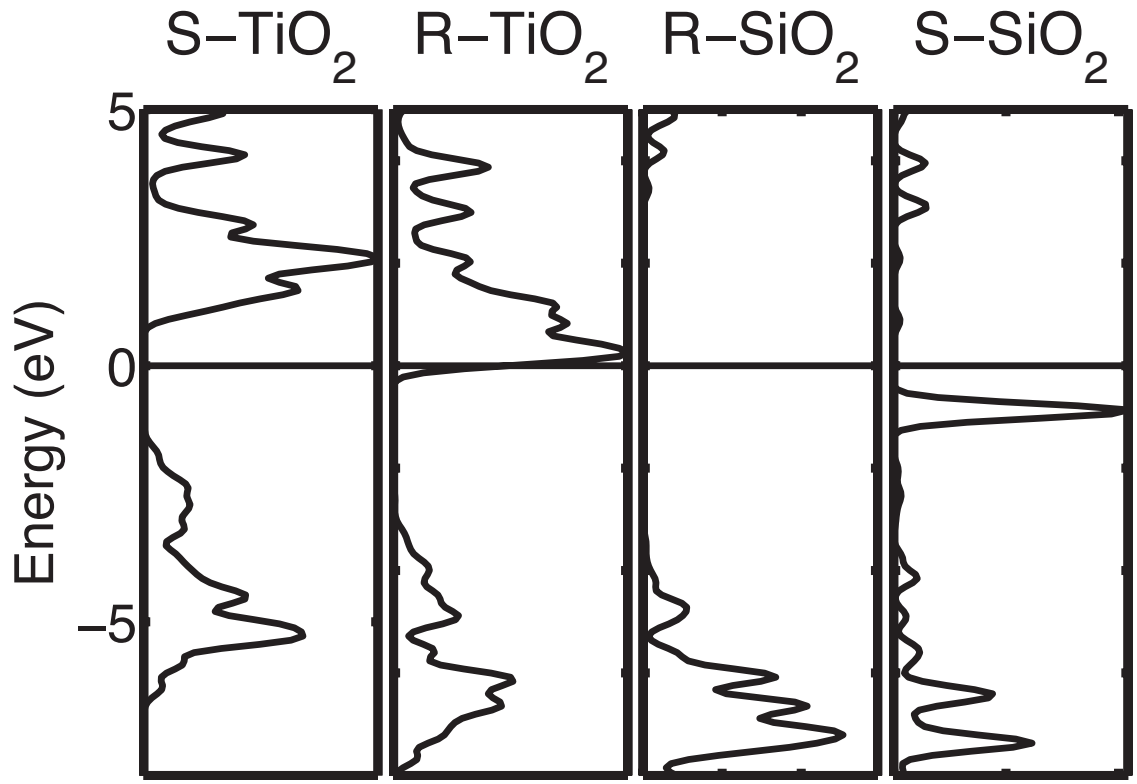

Figure 4.3: The density of states projected on the metal atoms present at the location of surface reduction are plotted. The local density of states (LDOS) show that in the case of R–TiO_2 the surface reduction produces electronic states at the Fermi level with 3d–state character. The electrons in these states are highly activated and may be transfered up into the supported Au nano–structure. On the other hand, in the case of R–SiO_2 the electrons are accommodated in an Si—Si bond formed after surface reduction. Transfer or sharing of these electrons is energetically unfavorable since that would involve breaking the Si—Si bond formed. This effectively reduces the electron transfer to Au in the Au/R–SiO_2 system. The Fermi level is set to an energy of zero.

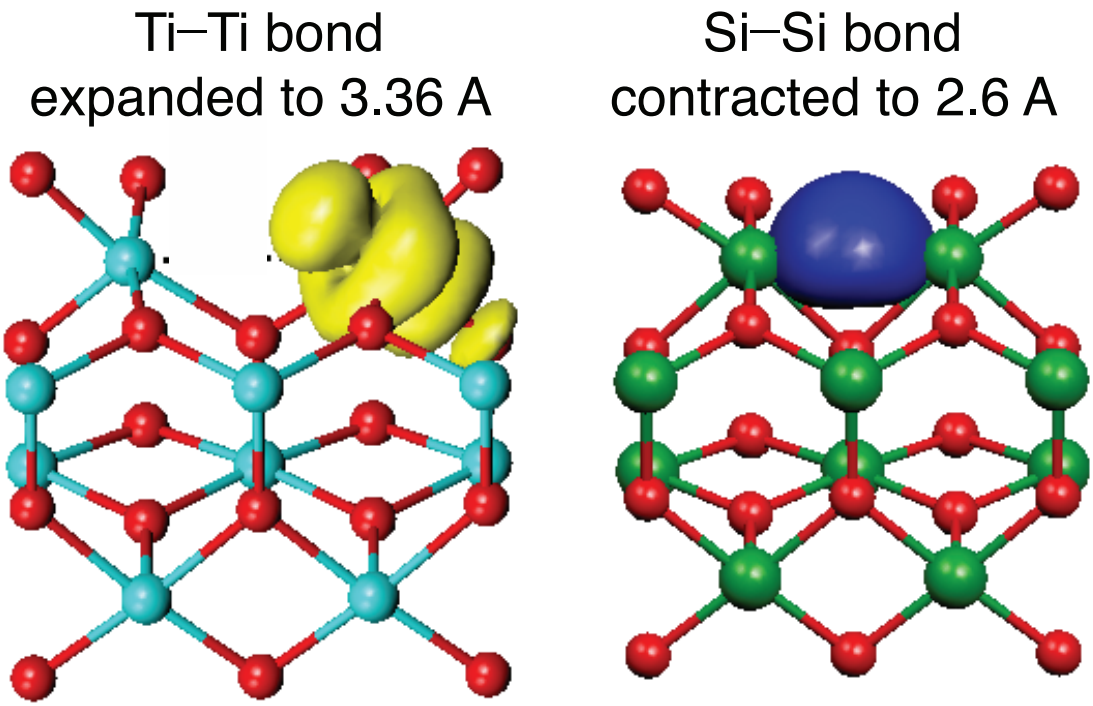

Figure 4.4: The electronic states resulting from oxygen vacancy generation may be visualized using a unitary transformation. The total wave–function is projected onto atomic orbital basis sets at the atomic centers and then the orbital–orbital overlap is iteratively reduced. This treatment was pioneered by Wannier. The orbitals at the oxygen vacancies for TiO_2 or SiO_2 are displayed. The electronic states correspond to either the Ti 3d–state or the Si—Si bond formed.

the Si—Si bond is also supported by the fact that the Si—Si distance is shortened from 2.8 $\mathring{A}$ for S–SiO_2 to 2.6 $\mathring{A}$. The oxide–specific electron density redistribution has significant impact on the chemical behavior of Au deposited on the oxide surfaces.

When Au is deposited on R–TiO_2, there is a considerable chemical interaction between the Au and the oxide which results in high Au bilayer binding energy, calculated to be 1.97 eV/vacancy. The electron density, accumulated in the Ti 3d–states upon the vacancy formation, is redistributed as Au—Ti bonds are formed. This density is not only localized along the Au—Ti bonds but it is distributed among neighboring Au atoms. We calculate that the Bader charge on the Au atom at the oxygen vacancy is 0.46 e^-, while the Au atoms in the top Au layer gain 0.1 e^- per atom.

Bader charge analysis suggests the formation of anionic Au, which is in agreement with other theoretical calculations [56, 94, 95] and with UHV experiments [37]. The driving force for the observed electron density shift is that the Au/R–TiO_2 system can reduce its energy by electron transfer from Ti 3d–states to energetically lower Au states.

Compared to Au/R–TiO_2, the interaction between Au and R–SiO_2 is weaker as corroborated by the lower Au bilayer binding energy, calculated to be –1.07 eV per vacancy. Bader charge analysis indicates that only 0.22 e^- are transferred from R–SiO_2 to the Au atom at the vacancy. The calculated Bader charge transfer is a consequence of the covalent charge localization along the bridge Si—Au bonds. Unlike in the case of Au/R–TiO_2, the Au atoms in the top layer do not gain electron density.

The proposed oxide-specific interactions between Au and the vacancy–rich oxides are further supported by the LDOS projected on an Au atom in the top Au layer, shown in Figure 4.5. The Au LDOS associated with Au/R–TiO_2 has shifted upward in energy more than the Au LDOS associated with Au/R–SiO_2 and stretched Au(111). The accentuated shift upward in the Au LDOS for Au/R–TiO_2 is another consequence of the larger electron density transfer from R–TiO_2 than from R–SiO_2.

The extent of the electron density transfer from R–TiO_2 and R–SiO_2 to Au impacts the chemical behavior of Au nano–structures deposited on these oxides. One manifestation of this is that an Au atom cohesive energy for Au/R–TiO_2 is lower than the respective cohesive energies for Au/R–SiO_2 and stretched Au(111). This has a direct impact on the chemical activity since the low Au cohesive energy allows for a less rigid Au nano–structure, which can easily adjust its geometry to adsorbates and relevant transition states and yield reaction pathways with low activation barriers. Also, due to their anionic character, the Au atoms adsorbed on R–TiO_2 interact strongly with electronegative adsorbates such as oxygen. We calculate that the adsorption energy of molecular O_2 adsorbed on Au/R–TiO_2 is by 0.5 and 0.3 eV more exothermic than

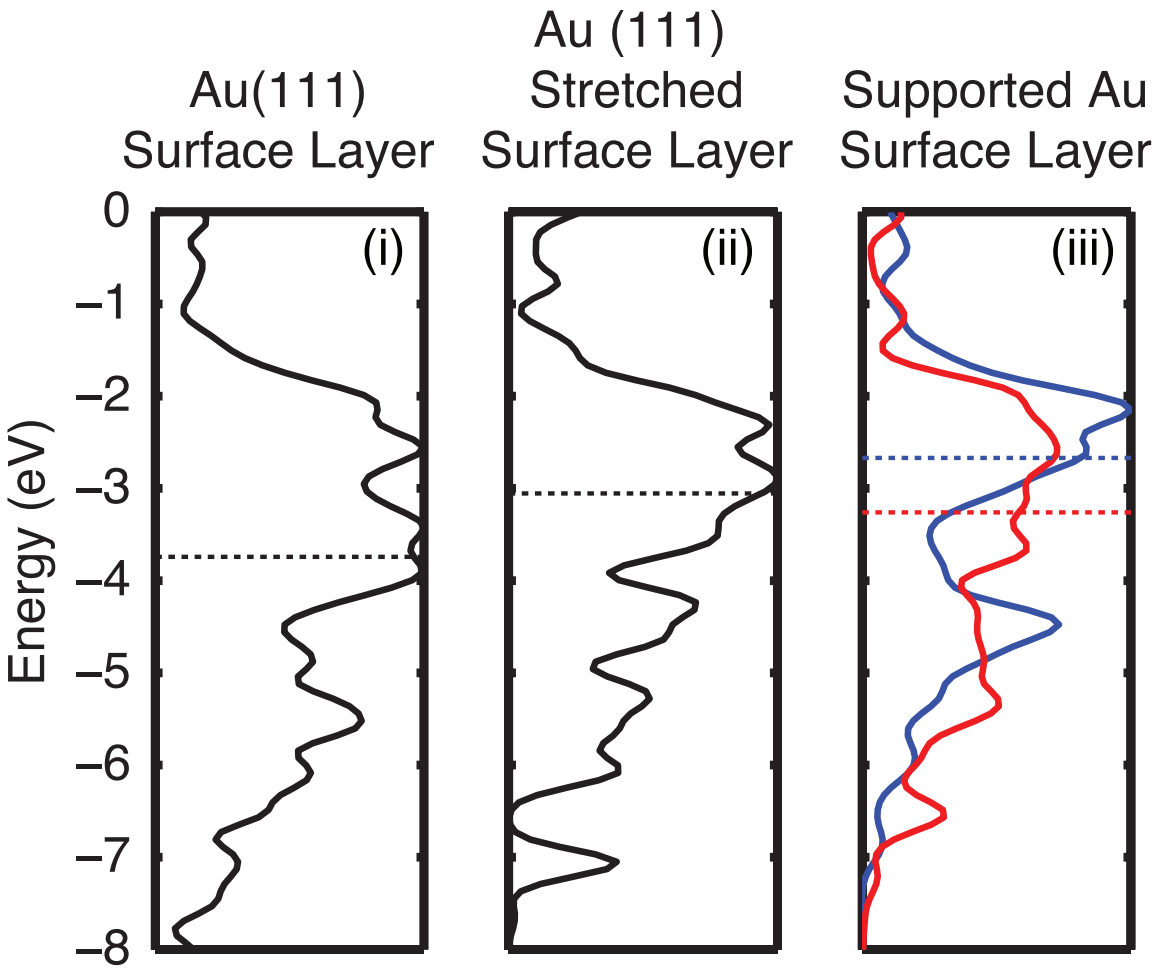

Figure 4.5: LDOS projected on an Au atom in the top Au layer for: (i) Au(111), (ii) stretched Au(111), (iii) Au/R–TiO_2 (blue line), and Au/R–SiO_2 (red line). Horizontal blue and red lines show the position of the center of the Au LDOS for Au/R–TiO_2 and Au/R–SiO_2, respectively. The Fermi level is set to zero.

for O_2 on Au/R–SiO_2 and stretched Au(111), respectively. The main interaction is through electron charge transfer from anionic Au to O_2 anti–bonding π^* orbital. This charge transfer weakens significantly the O_2 bond. Similarly, atomic oxygen binds more strongly to Au/R–TiO_2 than to stretched Au(111) or to Au/R–SiO_2 as illustrated in Figure 4.2. These results suggest that O_2 activation is energetically more favorable over Au nano–structures on R–TiO_2 than over Au/R–SiO_2 and stretched Au. The dissociation of O_2 was calculated using the Nudged–elastic–band approach (see Figure 4.6) and it was found that the presence of the reducible oxide did in deed reduce the barrier for O_2 dissociation markedly compared to unsupported or SiO_2 supported Au.

We calculate that highly anionic Au, formed when Au is deposited on R–TiO_2, binds oxygen stronger than Au/R–SiO_2. This observation might explain the apparent paradox discussed above, where UHV experiments and DFT calculations showed that Au adsorbed on oxides is negatively charged (anionic), while steady–state studies suggested that the activity of Au/oxide catalysts is directly proportional to the concentration of cationic Au atoms. Simply stated, anionic Au is needed to adsorb and activate O_2. However, as Au—O bonds are formed, the electronic fingerprint of Au is reversed from anionic to cationic due to the high electronegativity of oxygen. This behavior is illustrated in Figure 4.5, which shows the Au electronic fingerprint as a function of the support and external conditions. Under low oxygen chemical potential, corresponding to low pressure (UHV conditions) and high temperature, Au is anionic when adsorbed on both oxides. As oxygen chemical potential is increased the interactions between oxygen and Au/oxide are turned on, eventually yielding oxidized (cationic) Au . The transition from anionic to cationic Au takes place at a lower oxygen chemical potential for Au/R–TiO_2 than for Au/R–SiO_2. Our *ab initio* thermodynamic calculations suggest that under catalytically relevant conditions there exists a thermodynamic driving force to oxidize the regions of Au nano–structure that

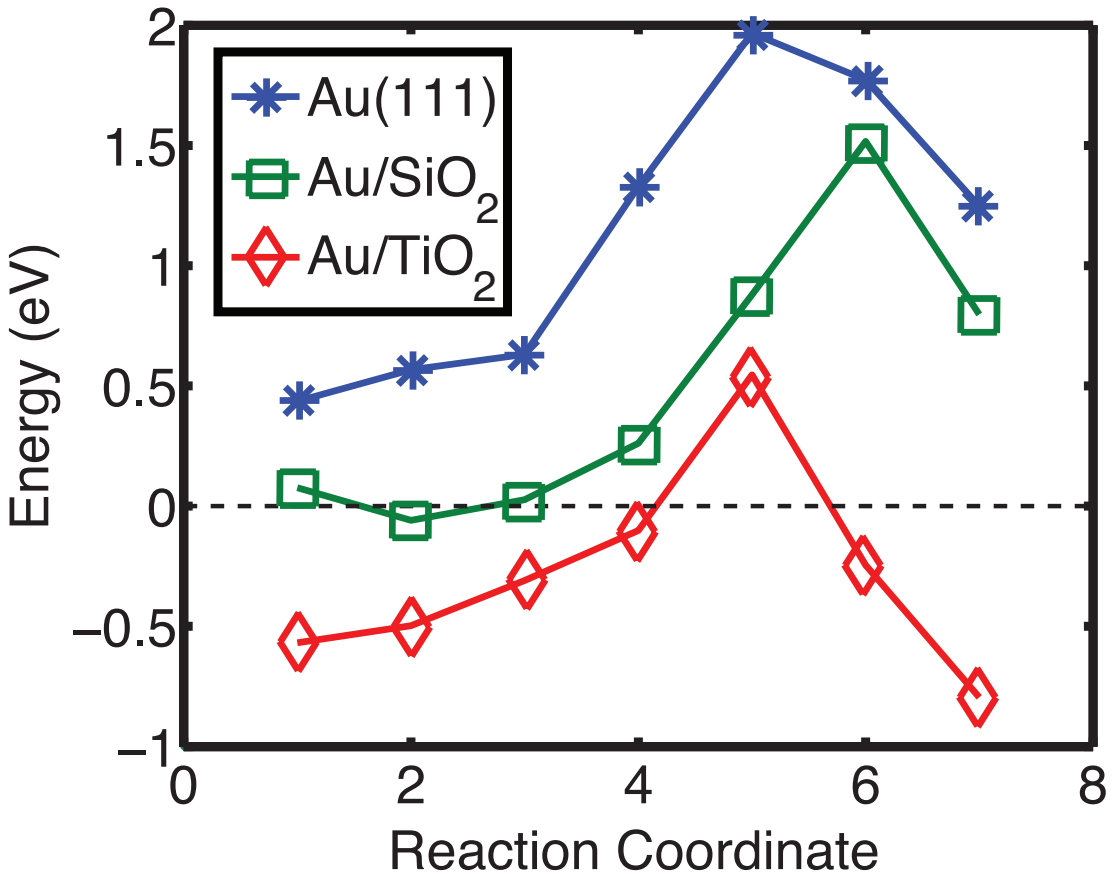

Figure 4.6: O_2 dissociation path way over Au/R–TiO_2, Au/R–SiO_2, and Au(111). Dissociation over Au/R–SiO_2 and Au(111) both result in large activation barriers and endothermic adsorption of the product atomic oxygens. On the other hand, Au/R–TiO_2 results in exothermic dissociation and a much reduced dissociation barrier. The reference energy of zero here is an adsorbate free model surface and gas phase molecular oxygen O_2, therefore, positive and negative energies correspond to an endothermic or exothermic state respectively when compared to the reference.

are close to the R–TiO_2 vacancies, while for Au/R–SiO_2 these regions will not oxidize at these conditions. We note that cationic Au, formed in the process of the Au—O bond formation, interacts with CO and propylene favorably, therefore providing an ideal environment for the low-temperature oxidation reactions [99].

The above described studies suggest a simple mechanism that might be able to account for the observed oxide–specific catalytic activity of supported Au nano–structures. Reducible oxides such as TiO_2, which are characterized by a small band gap, accommodate the electron density, released upon oxygen–vacancy formation, by the charge transfer to low laying d–states. The electronic charge accommodated in the Ti 3d–states, which cut through the R–TiO_2 Fermi level, is readily transferred to Au. On the other hand, irreducible oxides such as SiO_2, which are characterized by a larger band gap, undergo geometric restructuring, and Si—Si binding states are formed at the vacancy. The charge transfer from R–SiO_2 to Au is limited due to the fact that the Si—Si binding states are stabilized below the Fermi level. Since more charge is transferred from reducible oxides to Au, the Au adsorbed on these oxides interacts more strongly with oxygen providing an ideal environment for O_2 activation and for the oxidation reactions. The capacity of Au atoms adsorbed on reducible oxides, such as TiO_2, to be readily oxidized and reduced at mild conditions might explain the unique low–temperature oxidation activity of Au nano–structures adsorbed on reducible oxides.

CHAPTER V

Insight into the General Effect of Oxide Surface Off-stiochiometric Defects

5.1 Overview

In this section, we attempt to connect seemingly dissimilar experimental results pertaining to the catalytically active species in low–temperature CO oxidation over Au/TiO_2. From previously published literature, every oxidation state of Au had been implicated as the active species in low–temperature CO oxidation. By utilizing quantum chemical model systems that closely mimicked various catalyst preparation procedures we determined the fundamental physical mechanisms that may play direct roles in producing catalytically active Au. In short, we found that the activity of Au was more closely connected to chemical changes at the Au/oxide interface that destabilized Au increasing its chemical activity. Furthermore, that the Au surface activity was not directly connected to Au charge, however, the oxidation state of Au did appear to play a secondary role in binding and dissociating adsorbates.

5.2 Introduction

Gold is chemically inert [17, 18, 100]. However, Au nano–clusters anchored on oxide supports are active in many heterogeneous reactions [72]. Multiple factors including particle size and shape [101], charge transfer between Au and the oxide support [37, 42], metal–to–insulator transition [91], the presence of under–coordinated Au atoms [20], quantum size effects [96], lattice strain [22], and the Au/oxide interface perimeter [102] have been correlated with the catalytic activity. While these contributions have shed light on many aspects of the chemistry of Au, there is a lack of agreement regarding the nature of chemically active Au sites. For example, multiple reports indicate that anionic Au is required to facilitate catalytic reactions, while others have argued that cationic Au is present and active under relevant reaction conditions [37, 57, 92].

5.3 Summary

In this contribution we show that the chemical activity of an Au nano–structure on oxide supports is also enhanced significantly due to the strong chemical interactions between the An nano–structure and the oxide support. Our conclusions are obtained by comparing the chemical activity of Au nano–structures, anchored on an oxide surface which is rich in off–stoichiometric defects, to the activity of the identical Au nano–structures on the defect–free, stoichiometric surface of the same oxide. The investigated off–stoichiometric defects were either extra oxygen atoms or oxygen vacancies at the oxide surface. It has been shown previously that these defects might be present at Au/Oxide interfaces under external conditions associated with oxidation reactions [55]. We show that the defects interact strongly with the Au nano–structure, reducing the Au—Au bonding within the nano–structure, and forming chemically active Au sites. When the oxide surface is defect–free (stoichiometric),

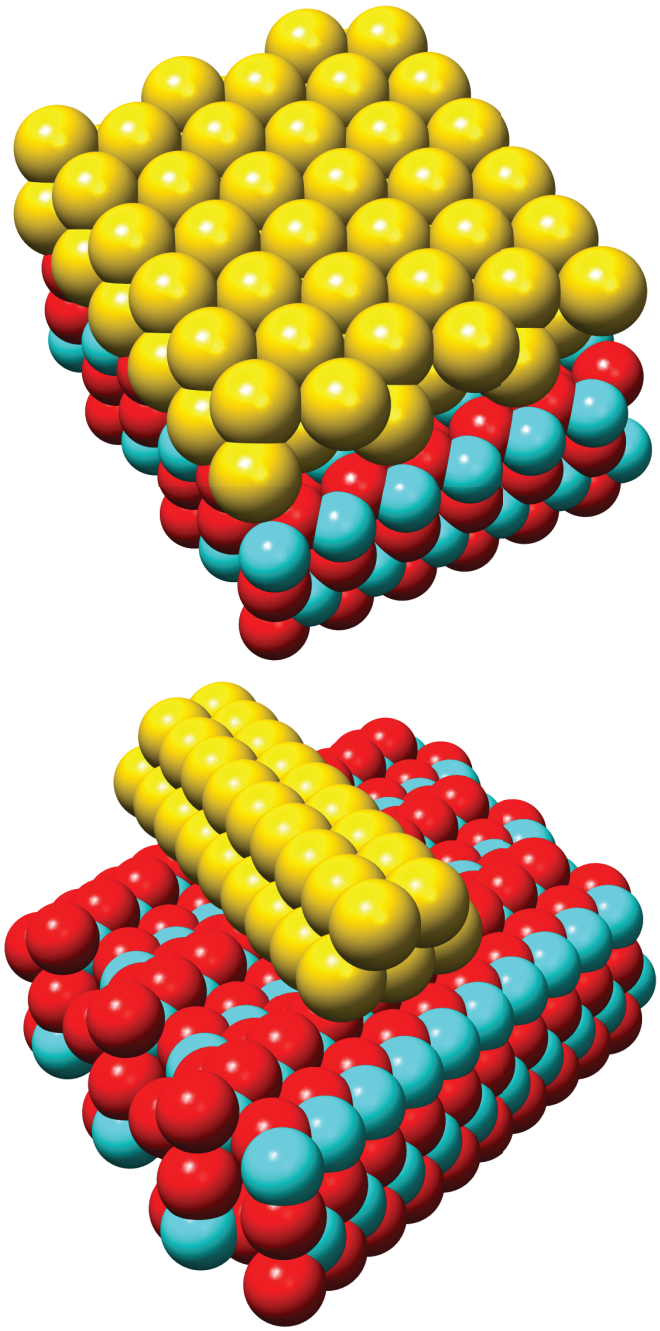

Figure 5.1: Au/TiO_2 model systems used for quantum chemical calculation consisted of a 2ML Au continuous layer of Au and a nano–rod continuous in one dimension. The 2ML Au model is used to model large Au facets, whereas, the Au nano–rod the Au/oxide interface perimeter and the effect of Au under coordination.

the interaction between Au and the oxide is minimal and Au behaves much like bulk Au. Our analysis also shows that there is no clear correlation between the nominal charge on Au and its chemical activity, and that the enhanced activity of supported Au can be related to the existence of strong polarized covalent bonds between the off–stoichiometric defect on the oxide and the Au nano–structure.

5.4 Approach and Model System

To study the chemical activity of supported Au nano–structures we employed Density–Functional Theory (DFT) and ab initio thermodynamics calculations. We investigated the adsorption and dissociation of oxygen and the adsorption of CO on Au supported on off–stoichiometric and stoichiometric TiO_2 as probe reactions. These reactions are important in low temperature oxidation, partial oxidation, and the water gas shift catalytic processes. We present concrete results for two different Au model systems, one consisting of two continuous Au layers on stoichiometric and off–stoichiometric TiO_2 surfaces and the other containing two atomic layers thick Au nano–rods on identical TiO_2 surfaces. The model systems and Au/TiO_2 interfaces are shown in Figure 5.1 and 5.2. Similar model systems have been utilized previously [40, 44]. We note that scanning tunneling microscopy (STM) and scanning transmission electron microscopy (STEM) measurements showed that the continuous bi–layers and bi–layer clusters of Au supported on oxides (TiO_2 in ref.[91] and Fe_xO_y in ref.[103]) exhibit the highest turnover frequencies in the oxidation of CO at low temperatures [91, 103]. Since the objective was to investigate the impact of the support on the chemical activity of the Au atoms in the neighborhood of the support we focus exclusively on the chemistry of Au sites on the model systems, i.e., the sites on the TiO_2 support and at the Au/TiO_2 interface (where adsorbates are shared between Au and the support) were not probed in this study. It is important to note that we have also studied a number of other Au model systems obtaining

quantitatively identical conclusions.

The (110) surface termination of rutile TiO_2 was utilized to model the TiO_2 support as this is the most stable surface for rutile TiO_2. The oxide support was modeled by two tri–layers of TiO_2. To investigate the affect of the number of oxide layers, we performed calculations using four tri–layers of oxide support. We found that the adsorption energies changed by less than 2%. Super cells of 2x1 and 5x1 with respect to the TiO_2(110) surface were used for the continuous monolayer and Au nano–rod systems respectively. The (4x4x1) and (2x2x1) Monkhorst–Pack k–point sampling for the monolayer and nano–rod system respectively was required to achieve relative convergence in the energy calculations. The relevant transition states were identified using the climbing nudged elastic band approach [104]. The total energy code DACAPO was utilized to perform the DFT calculations (https://wiki.fysik.dtu.dk/dacapo). While we discuss in detail our results for the Au/TiO_2 systems, we found that the conclusions presented herein are qualitatively consistent for Au nano–structures anchored on other insulating and semiconducting oxides (i.e., SiO_2, Fe_2O_3).

We have considered three different Au/Oxide model interfaces: (i) Au on stoichiometric TiO_2 (Au/S–TiO_2), (ii) Au on partially reduced TiO_2 (Au/R–TiO_2), with one bridging oxygen atom in the oxide surface layer per unit cell missing, and (iii) Au on oxidized TiO_2 (Au/O–TiO_2), with one coordinatively unsaturated Ti atom in the top Ti layer per unit cell covered with an oxygen atom, i.e., with extra oxygen atoms on the oxide surface. The model interfaces are shown in Figure 5.2. The only difference among the three interfaces was in the concentration of the oxygen atoms at the metal/oxide interface. The three model interfaces have been experimentally observed and can be loosely related to a range of external environments as discussed below [36].

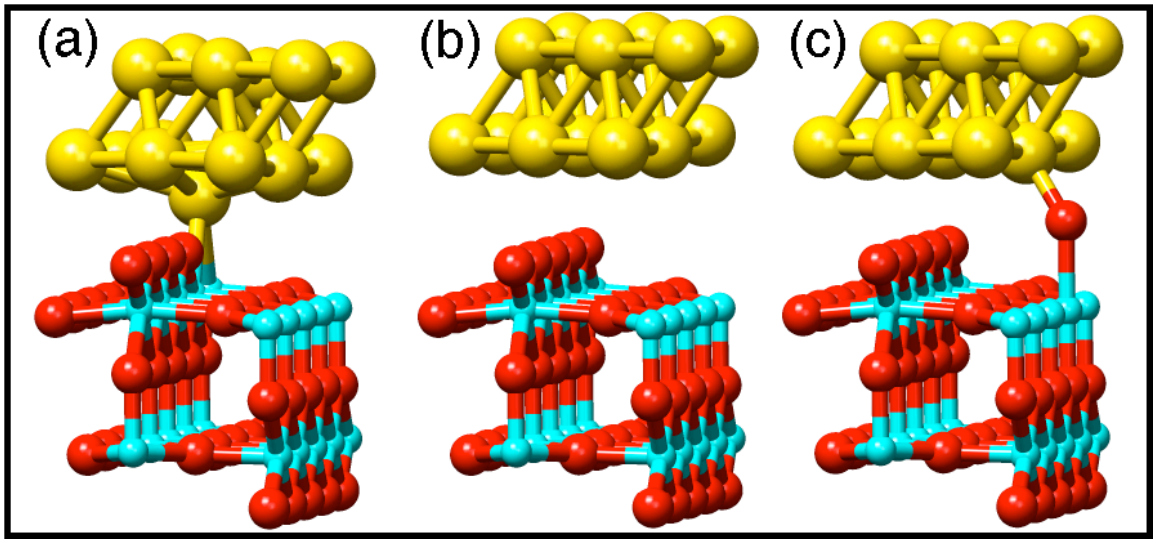

Figure 5.2: Ball and stick view of the three model interfaces showing the changes in stoichiometry at the Au/TiO_2 interface. From right to left, the Au/R–TiO_2 model interface has an oxide surface oxygen removed with Au interacting strongly with this defect, the Au/S–TiO_2 involves stoichiometric TiO_2 with no defects, and the Au/O–TiO_2 models an Au/oxide interface with extra oxygen present adsorbed between Au and the five–coordinated Ti^+ of the oxide surface.

5.5 Calculation Methodology

To evaluate the relative thermodynamic stability of the above–mentioned model interfaces in an oxygen atmosphere, we have employed an ab intio thermodynamic approach, which allows us to calculate the free energy of different systems as a function of temperature and partial pressure of gas–phase oxygen. The free energies of a system per unit cell with one oxygen defect (vacancy or extra oxygen) in the unit cell were calculated using the following expression:

$$\Delta G_f(T,P) = E_{final} - E_{Au/S-TiO_2} \pm (E_{O_2} + \Delta\mu_O(T,P)) \tag{5.1}$$

In Eqn. 5.1, E_{final} is the DFT calculated electronic energy of an Au nano–structure (nano–rod or bi–layer) adsorbed on a TiO_2 support (stoichiometric or off–stoichiometric), $E_{Au/S-TiO_2}$ is the DFT calculated electronic energy of the same Au

nano–structure on the stoichiometric TiO_2 support, E_{O_2} is the DFT calculated electronic energy of an O_2 molecule, and $\Delta\mu_O$(T,P) contains all temperature and pressure dependent free energy contributions due to the internal degrees of freedom of the O_2 molecule. We have verified that the entropic contributions to the free energy difference between Au/S–TiO_2 and Au/R–TiO_2 or Au/O–TiO_2 were insignificant at relevant conditions. In this formulation of free energy, an Au nano–structure (either nano–rod on bi–layer) adsorbed on stoichiometric TiO_2 (S–TiO_2) has the free energy of zero. Sufficient accuracy can be obtained by assuming that the gas phase oxygen is well described by the ideal gas law, which allows us to relate $\Delta\mu_O$(T,P) to temperature and the partial pressure of O_2 by the following expression:

$$\Delta\mu_O\left(T,P\right)=\frac{1}{2}\left(\Delta\mu_{O_2}\left(T,P^o_{O_2}\right)+k_bTln\left(\frac{P_{O_2}}{P^o_{O_2}}\right)\right) \tag{5.2}$$

$\Delta\mu_O$(T,P) can be either directly calculated from rotational, translational, and vibrational partition functions of the molecule, which are easily obtained from *ab initio* calculations, or obtained from tabulated values at standard pressure $\Delta\mu_{O_2}$(T,P_{O_2}) [86]. Both approaches yield almost identical results.

5.6 Results

5.6.1 Energetics of Oxide Surface Defect Formation

In Figure 5.3 we show calculated Gibb's free energies of formation for the three model interfaces as a function of oxygen pressure and temperature ($\Delta\mu_O$(T,P)). The free energy for Au nano–rod and Au bi–layer model interfaces are calculated with respect to the respective energies of the Au nano–rod and Au bilayer on stoichiometric TiO_2, i.e., the free energy of zero (black horizontal line in Figure 5.3) corresponds to the Au/S–TiO_2 structures where Au is either nano–rod or bilayer. Figure 5.3 shows that for the model systems considered in these calculations, the formation of the

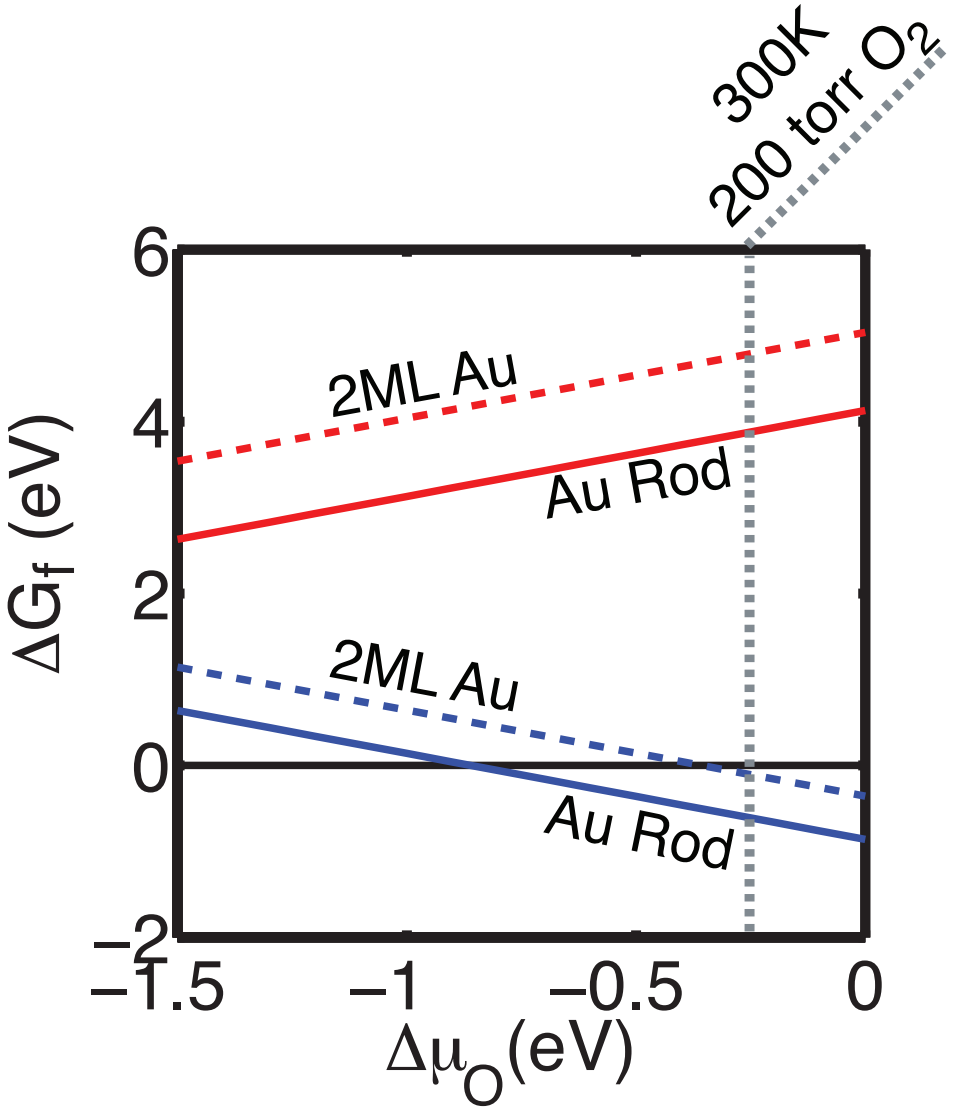

Figure 5.3: *Ab initio* thermodynamics of model system formation. The change in Gibb's free energy of formation is plotted for the three systems: Au/S–TiO_2 (black line at ΔG_f = zero), Au/R–TiO_2 (red lines positive slope), and Au/O–TiO_2 (blue lines negative slope). The thermodynamic stability of both 2ML and nano–rod model systems were tested, plotted as dashed and solid lines respectively. Note that positive changes in Gibb's free energy indicate the system would return to the reference state i.e., stoichiometrically supported Au and gas phase O_2, on the other hand, if $\Delta G_f < 0$ then the system would favorably form if not kinetically limited.

point oxygen vacancies (labeled with red lines in Figure 5.3) at the Au/TiO_2 interface is energetically very costly. This structure would be thermodynamically stable only under external conditions corresponding to very low oxygen chemical potentials. This suggests that for the point oxygen vacancies to exist at the Au/Oxide interface in significant concentrations in the configurations explored in these studies, the external reacting environment needs to be very reducing (high temperature, high pressure of reducing reactants, and low pressure of oxygen). Alternatively, the oxygen vacancies could be kinetically trapped. In fact, model systems containing Au nano–structures supported on the oxygen vacancy–rich TiO_2 surfaces have been synthesized under UHV conditions, and their structure was verified by STM [36]. In addition, it has been demonstrated that these structures are very active in the oxidation of CO [96]. For example, it was shown that bi–layers of Au supported on oxygen vacancy–rich TiO_2 exhibit turnover rates for CO oxidation that are among the highest reported [96].

Unlike Au adsorbed on the vacancy–rich TiO_2 ($Au/R–TiO_2$), Figure 5.3 shows that the systems containing Au on oxygen–rich TiO_2 ($Au/O–TiO_2$) are thermodynamically more favorable than Au on stoichiometric TiO_2 ($Au/S–TiO_2$) over a realistic range of the O_2 chemical potential. For example, for both model systems, Au nano–rod and bi–layer, the $Au/O–TiO_2$ structures are more thermodynamically stable than the respective $Au/S–TiO_2$ and $Au/R–TiO_2$ configurations for the O_2 chemical potential larger than those corresponding to atmospheric conditions. This suggests that under relevant reaction conditions the Au/TiO_2 interface might be enriched by atomic oxygen. The main reason for the high thermodynamic stability of $Au/O–TiO_2$ is the highly exothermic adsorption of atomic oxygen at the sites between coordinatively unsaturated Ti^{4+} cations and Au (Figure 5.2). The calculated high stability of the $Au/O–TiO_2$ structure is consistent with the experimental observations of Matthey et al., who demonstrated that oxygen–rich Au/TiO_2 interfaces can be realized even

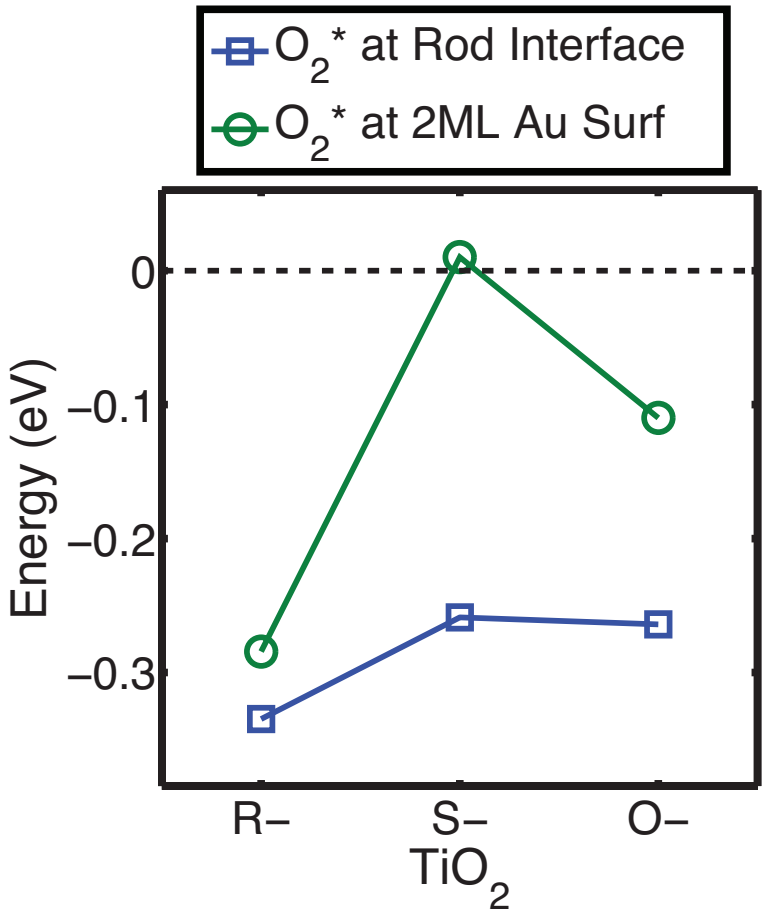

Figure 5.4: Molecular oxygen O_2 is adsorbed on Au–only sites in the proximity of the Au/oxide interface defects. On the 2ML Au model system this is at fully coordinated Au (111) surface site, on the Au nano–rod O_2 adsorption is at an edge site. In the latter case no favorable O_2 adsorption was found at Au–only locations other than the Au–rod edge away from the interface. However, strong binding sites exist at the rod perimeter, but that is the topic of a future communication. When interface defects are not present the adsorption of O_2 is weaker than the adsorption in the presence of the interface defects. The energy of zero is defined to be an adsorbate free surface and gas phase O_2.

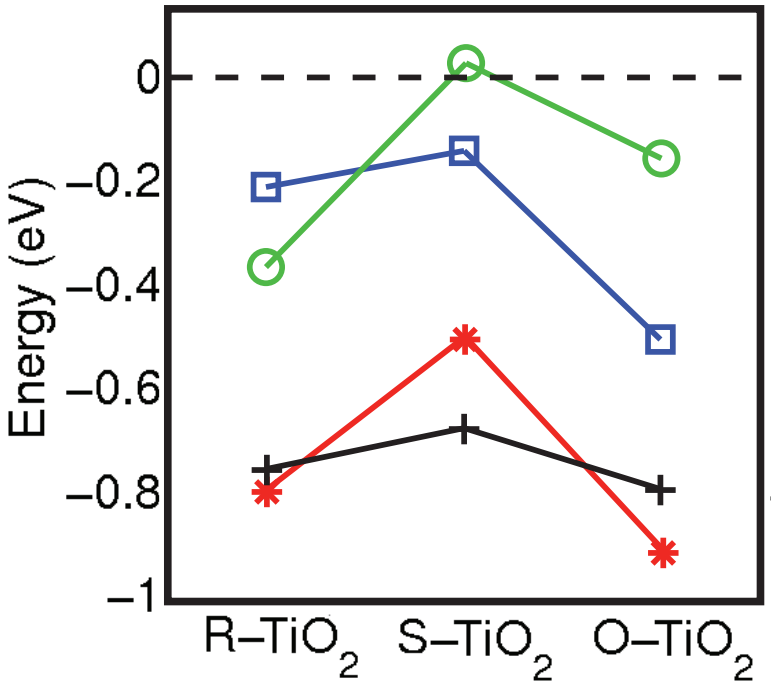

Figure 5.5: Adsorption of Atomic oxygen (on 2ML and rod, circle and square respectively) and CO (on 2ML and rod, asterisk and plus respectively) was tested as well. It was found that presence of defects at the Au/oxide interface promoted all adsorbates tested indicating a promotion mechanism which affects interaction between Au and the adsorbates in a general way. The energy of zero is defined to be an adsorbate free surface and gas phase O_2.

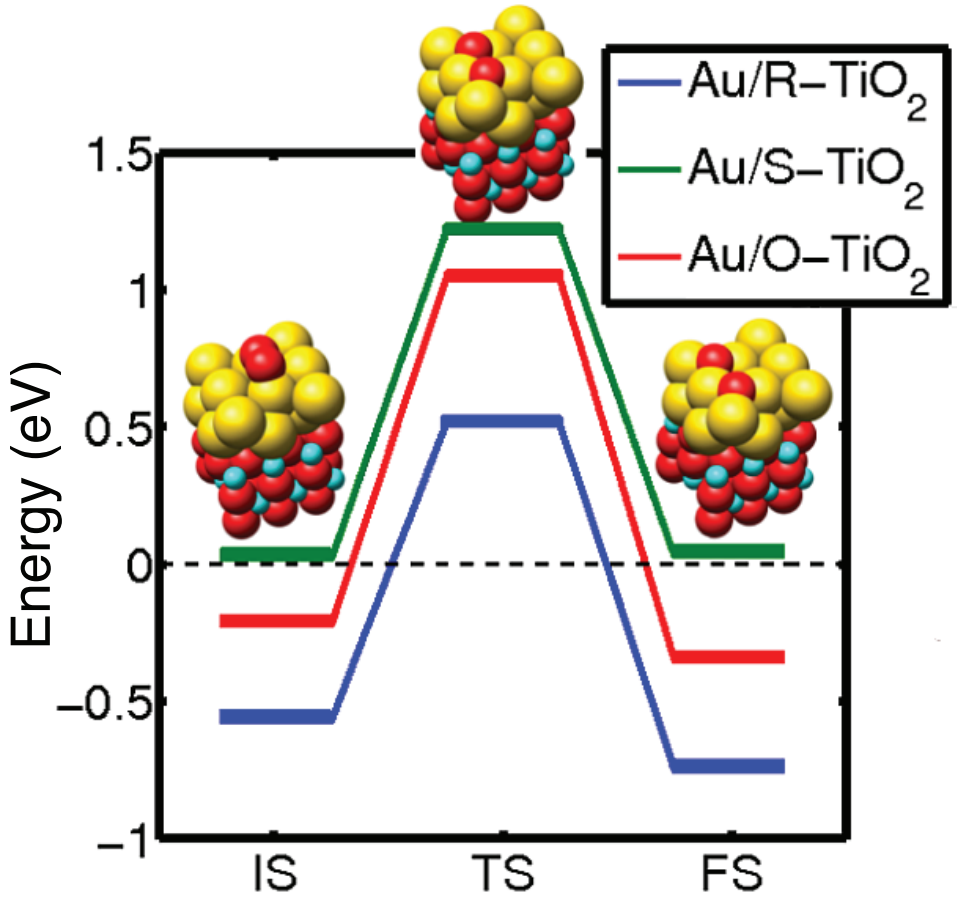

Figure 5.6: The effect of defects at the Au/oxide interface on O_2 dissociation was also investigated. The initial, transition, and final state of O_2 dissociation over the 2ML Au system for the three model interfaces are presented here. Similarly, to the effect found in our thermodynamics calculations, we find O_2 may dissociate more readily at Au sites near to a defective Au/oxide interface.

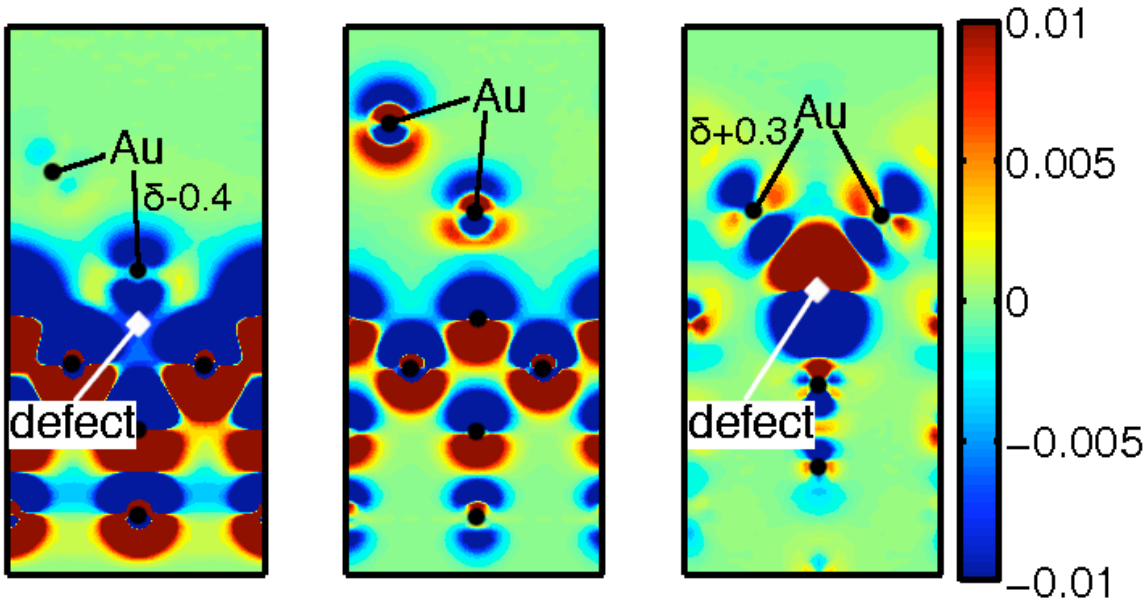

Figure 5.7: To better understand the types of bonds being formed at the Au/oxide interface we calculated the charge density difference upon Au adsorption for the 2ML Au/TiO_2 model interfaces. We found that the charge character of Au was affected by the oxide surface defects, with Au becoming partially negatively or positively charged when in contact with the oxygen vacancy or extra oxygen atom. Furthermore, the structure of the charge density difference indicates strongly polarized covalent bonds formed between the defects and Au.

under UHV conditions [55]. It was also found that extra interfacial oxygen atoms stabilize the Au nano–structures and prevent sintering [55, 56, 58]. Our calculations also show that the adsorption of oxygen on the Ti cations, without Au, is endothermic.

5.7 Adsorption and Dissociation of O_2 and Adsorption of CO

The three different model systems discussed above capture the three experimentally observed Au/TiO_2 interfaces and mimic the interface for a broad range of operating conditions (oxygen chemical potential) and catalyst preparation strategies. To investigate the chemical activity of Au for the three model systems, we have studied the dissociation of O_2 and the adsorption of atomic oxygen and CO, on various Au sites on the model systems. Figure 5.4 shows the adsorption energy of O_2 on the three

model systems with respect to gas phase O_2. Figure 5.5 shows adsorption energies for atomic oxygen and CO for the three model interfaces calculated with respect to gas phase O_2 and CO respectively for the Au adsorption sites that bind the adsorbates most exothermically. Figure 5.6 shows the calculated activation barriers for the dissociation of O_2 on the Au bi–layer supported on R–, S–, and O–TiO_2. We stress that we have focused exclusively on the chemistry of Au sites. We find that Au nano–structures supported on the off–stoichiometric surfaces of TiO_2 (Au/R–TiO_2 and Au/O–TiO_2) bind all adsorbates more exothermically and dissociate the O_2 molecule with lower activation barriers than the identical Au structures supported on stoichiometric TiO_2 (Au/S–TiO_2). This is somewhat surprising considering that in one case Au interacts with the oxygen deficient TiO_2 support, while in the other case Au is supported on the oxygen–rich support.

5.7.1 Electronic Structure Analysis

To shed light on this dilemma we have investigated the electronic structure of Au adsorbed on the oxygen vacancy–rich and oxygen–rich TiO_2 surfaces. We find that the main interaction between Au nano–structures and the off–stoichiometric oxide supports is the formation of polarized covalent bonds between Au atoms and the off–stoichiometric point defects (vacancies of extra oxygen atoms) on the support. The consequence of the formation of the polarized bond is that the critical chemical difference between Au adsorbed on the oxygen vacancy–rich TiO_2 and oxygen–rich TiO_2 stems from a different direction in the shift of electron density between an Au nano–structure and support. For example, the polarized covalent bond which is formed between Au and Ti, for Au on the oxygen vacancy–rich TiO_2, is characterized by a bonding state (orbital) that is Au–like, i.e., there is a transfer of electronic charge from the support to Au. On the other hand for Au on the oxygen–rich TiO_2, the bonding state is centered on the extra O atoms at the Au/O–TiO_2 interface,

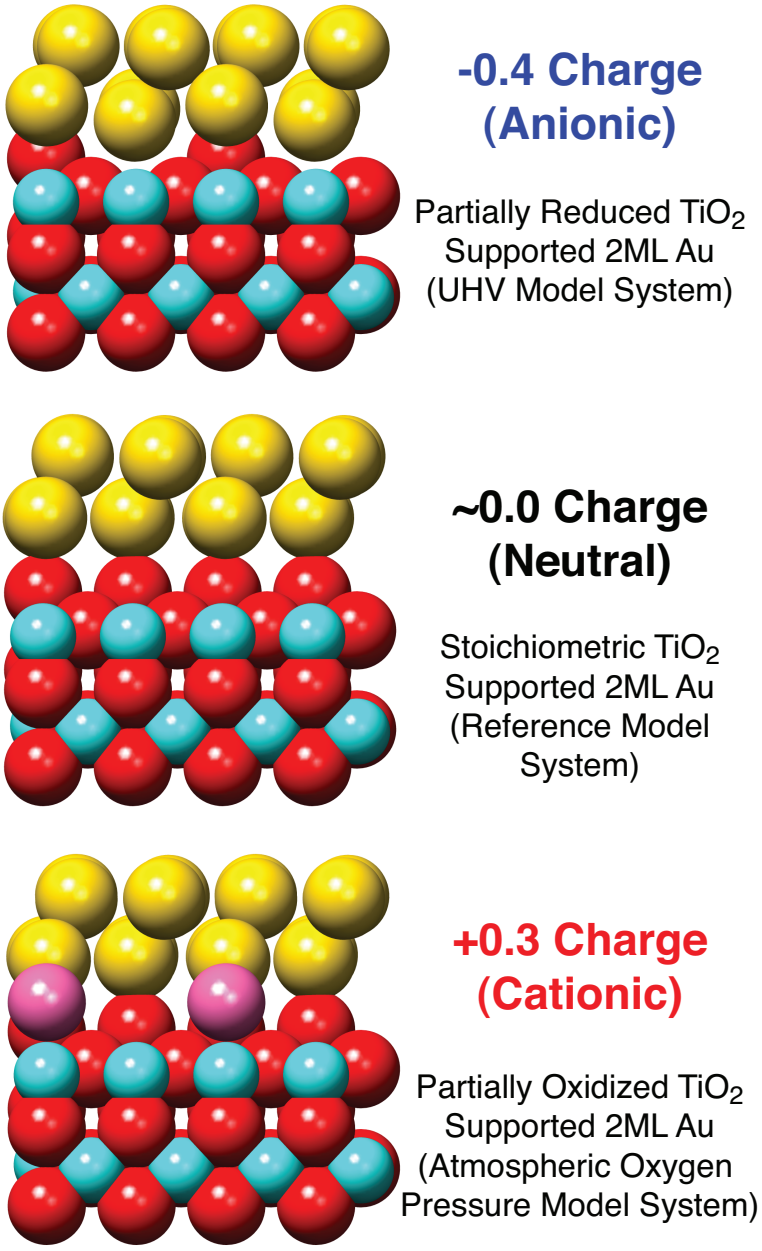

Figure 5.8: Calculated Bader charge of Au for reduced, stoichiometric, and oxidized Au/TiO_2 interfaces. Indicating that Au can act as an electron density source or sink depending on the local chemical environment.

suggesting charge transfer from Au. This picture is supported by calculated shifts in electronic density due to the interactions between Au and the oxide, shown in Figure 5.7. Furthermore, Bader charge (see Figure 5.8) analysis showed that the Au atoms adsorbed on the oxygen vacancy–rich TiO_2 are electron–rich (anionic), whereas for Au adsorbed on the oxygen–rich TiO_2 the electron density is shifted from Au to the interfacial oxygen atoms producing electron–deficient (cationic) Au. In contrast to these two situations we find that Au supported on the stoichiometric TiO_2 results in no significant charge transfer between the TiO_2 support and the Au atoms. This redistribution of electronic charge would suggest that depending on the external conditions the electronic fingerprint of those Au atoms that directly interact with the support might vary between anionic (on the oxide support that is rich in the oxygen vacancies) and cationic (on the support that is rich in extra oxygen atoms). Figure 5.5 and 5.4 suggests that regardless of whether electronic charge is transferred from the support to Au (Au/R–TiO_2) or from Au to the support (Au/O–TiO_2), the probe molecules bind with higher adsorption energies on Au nano–structures anchored on R–TiO_2 and O–TiO_2 than on Au/S–TiO_2.

5.7.2 Destabilization of the Au Internal Structure

Further investigation of the Au adsorption sites that bind the adsorbates most strongly shows that in both cases, Au/R–TiO_2 and Au/O–TiO_2, the most active Au sites are geometrically localized around the Au atoms that are bonded to the point defects (either oxygen vacancies or extra oxygen atoms) on the TiO_2 surface. Analysis of the local Au—Au geometry in the vicinity of the most active sites (Figure 5.9) shows that the bond distance between these chemically active Au atoms and the Au atom that is directly bonded to the off–stoichiometric defect on the support are significantly elongated for both, Au/R–TiO_2 and Au/O–TiO_2, model systems. On the other hand when Au is supported on the stoichiometric support the Au–

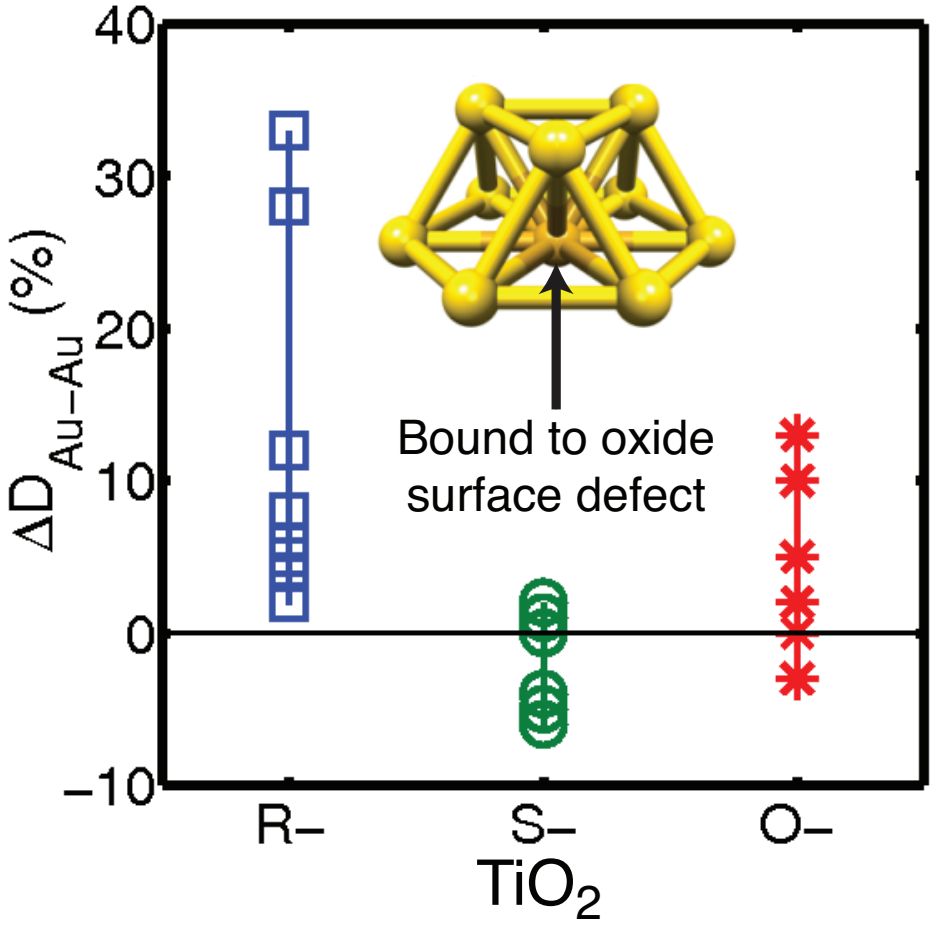

Figure 5.9: The geometric perturbation of the Au internal bonding was calculated. The percent change in Au—Au bond length for the Au atoms directly bound to the defect binding Au are presented referenced to the Au—Au bond distance in bulk Au. Drastic bond expansion is found in the model systems where defects are present indicating a reduction in Au—Au internal bonding caused by the strong bond formed between the oxide surface defect and the Au at the defect site. The ΔD_{Au-Au} is defined as the Au—Au bond distance in bulk Au, therefore, the calculated change indicates the amount of Au—Au interaction needed to achieve equilibrium bond energy.

Au bonds in the Au nano–structure are contracted with respect to bulk Au. These observations can be understood in terms of the bond order conservation arguments, where strong interactions between an off–stoichiometric center of the oxide and the Au atoms bonded to this center are accompanied by a weakening in the interaction between these Au atoms and the neighboring Au atoms in the Au nano–structure.

The bond order conservation argument is further supported by examining the electronic structure of the active Au atoms. The local densities of states (LDOS) projected on the most chemically active Au atoms (the atoms that surround the Au atom directly bonded to off–stoichiometric centers) for Au nano–rods supported on S–, R–, and O–TiO_2 are plotted in Figure 5.10 and compared to identical Au atoms in unsupported Au nano–rod . The Au LDOS shows sharp peaks around –7 eV, which can be attributed to the AuAu binding states. When the Au nano–rod is supported on S–TiO_2 the Au LDOS is almost identical to the Au LDOS associated with unsupported Au nano–rod. The absence of change in the electronic structure is consistent with the small adsorption energy of Au on the stoichiometric TiO_2 surface. However, when the Au nano–structure is supported on off–stoichiometric TiO_2 surfaces (R– or O–TiO_2) the AuAu bonding state at –7 eV is reduced and new states appear closer to the Fermi level. The net result of this restructuring of the LDOS is the expansion of the AuAu bond lengths and the reduction of the cohesive energy of Au within the Au nano–structure. Furthermore, the shift of electronic states towards the Fermi level increases the overall electronic energy of the Au nano–structure and results in a significant increase in the chemical activity of the Au atoms, as corroborated by the large oxygen and CO binding energies and low activation barriers for the dissociation of O_2. Identical analysis applies also for the Au bi–layer model systems.

The results presented above can begin to help us reconcile various seemingly contradictory reports regarding the electronic state of catalytically active Au. Many have

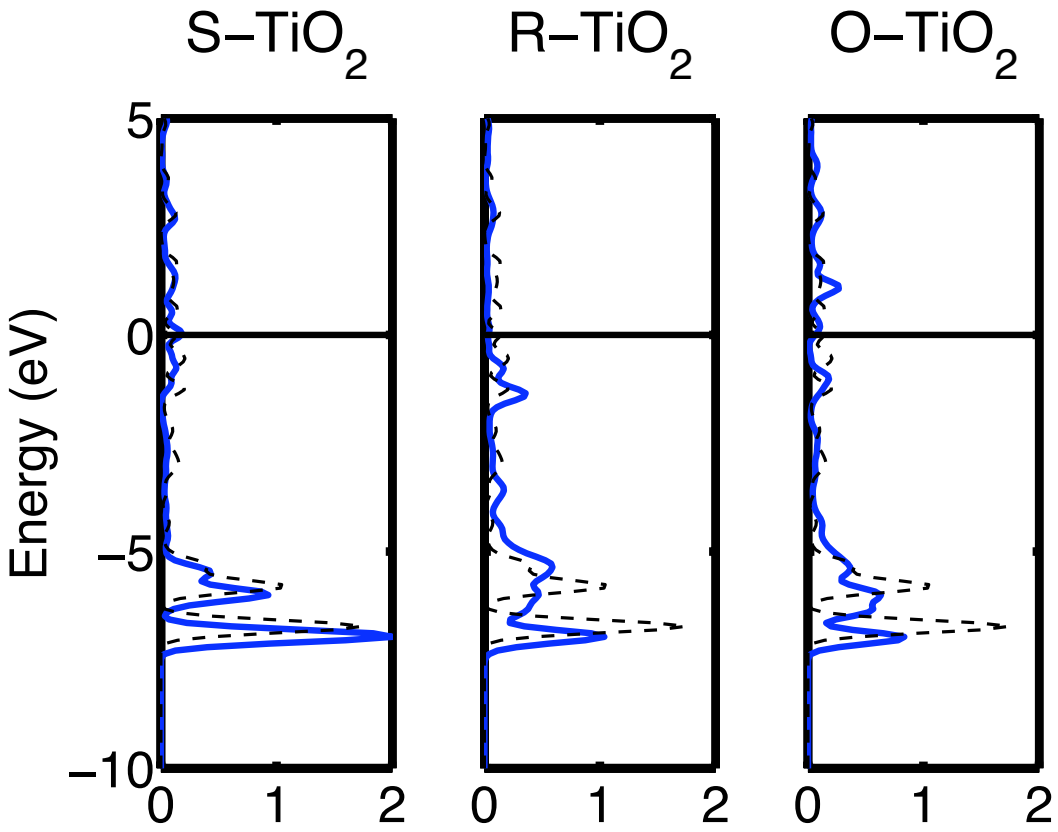

Figure 5.10: The combined s– and p–state were investigated to further verify the changes in Au—Au bonding. The dashed black line is the electronic structure of the unsupported Au nano–rod. From left to right: The electronic structure of the nano–rod supported by S–TiO_2 shows little restructuring upon adsorption indicating little Au–oxide interaction. The electronic structure of Au on R–TiO_2 and O–TiO_2 show electronic states redistributed to higher energy i.e., more positive energy values, indicating further that the Au—Au bonding is reduced by the presence of the oxide surface defect. The Fermi level is set to zero.

argued that anionic Au is required to activate O_2 and facilitate oxidization reactions, while others have suggested that the concentration of cationic Au scales well with the catalytic rates [92]. Our findings suggest that the Au atoms in an Au nano–structure interact strongly with off–stoichiometric centers on the oxide by forming polarized covalent bonds, with electronic charge centered either on the Au atoms (for Au on R–TiO_2) or on the extra O atoms at the Au/TiO_2 interface (for Au on O–TiO_2). The distribution of electronic charge in these covalent bonds yields Au atoms with either anionic (Au/R–TiO_2) or cationic (Au/O–TiO_2) electronic fingerprint. Irrespective of the electronic fingerprint of the Au atoms bonded to the off–stoichiometric centers on TiO_2, chemically highly active Au sites are identified in the vicinity of these Au atoms. The analysis suggest that the covalent bonds between Au atoms and the off–stoichiometric centers on the support play an important role in inducing the chemical activity on neighboring Au atoms. These observations suggest that the origin of the support–induced activity of Au nano–structure is conceptually different than the induced activity associated with the electron charging of gas–phase Au nano–clusters [30]. When an Au cluster is charged, the extra electron density is distributed in the surface states of Au nano–structure which are directly accessible to incoming adsorbates. On the other hand, if Au is deposited on an off–stoichiometric center on an oxide there is a significant rearrangement in the electronic structure of Au, which results in covalent bonding between the defect and Au. The electrons that are stored in these chemical bonds lead to the formation of active Au atoms in the vicinity of the Au/Oxide interface, characterized by electronic states close to or at the Fermi level.

5.7.3 Contrast with Previously Published Results

It is also important to discuss these results in the context of concrete experimental examples of oxidation catalysis on nano–Au/Oxide systems. It has been demonstrated

experimentally in the studies of well–defined model systems under controlled experimental conditions that the catalysts containing Au bi–layers supported on oxygen vacancy–rich TiO_2 (R–TiO_2) (Fig. 1 in [96]) are highly active in the oxidation of CO. The enhanced chemical activity has been related to a transfer of electronic charge from oxygen vacancies to Au and the formation of anionic Au. The results presented herein support this notion and further suggest that the high catalytic activity in these systems can be ascribed to the Au atoms that surround the Au atoms which form a chemical bond with the off–stoichiometric oxygen vacancy sites of the reduced TiO_2 support. This hypothesis is supported by recent DFT studies of Rodriguez and coworkers on a model system that resembled the one proposed by Chen et al. (Figure 1 in [105]). The results presented above also shed light on the experimental observations that under elevated pressures of O_2, the concentration of cationic (electron deficient) Au atoms is proportional to the rate of CO oxidation reactions. According to our *ab initio* thermodynamic calculations, under these conditions extra oxygen atoms may be present at the Au/Oxide interface. These structures are thermodynamically more stable than Au/S–TiO_2 and Au/R–TiO_2 over a wide range of external conditions. The presence of the interfacial oxygen atoms would on one hand yield Au atoms, at the interface, that have a cationic electronic fingerprint and on the other hand would result in the formation of highly active Au atoms surrounding the Au atoms bonded directly to the interfacial oxygen atoms. Recent aberration–corrected Scanning Transmission Electron Microscopy (STEM) measurements of Hutchings and coworkers showed that small bi–layer clusters of Au on iron oxide are much more active in low–temperature catalytic oxidation of CO than mono–layers or larger clusters. It was also shown in the XPS analysis of the sample that the Au^+ cations could be identified. These experimental observations are consistent with the analysis presented above which showed that the presence of cationic Au atoms at the interface would result in highly active Au atoms at the surface of the Au bi–layer. Furthermore,

anionic Au at the interface would be easily captured by XPS because of the small size of the bi–layer Au clusters.

5.8 Conclusion

In summary, DFT and *ab initio* thermodynamic calculations were employed to investigate the effect of off–stoichiometric oxide surface defects on the chemistry of oxide supported Au nano–structures. We find that off–stoichiometric defects (oxygen vacancies or extra oxygen atoms at the Au/Oxide interface) may be thermodynamically stable under appropriate conditions, such as UHV or steady–state atmospheric conditions. The defects interact strongly with the Au nano–structure, reducing the AuAu bonding within the structure and producing highly active Au sites. Depending on the nature of the off–stoichiometric surface defect, Au nano–structures anchored on the support might have anionic or cationic electronic character. Irrespective of the nominal charge character of the Au nano–structure, highly active Au atoms can be identified. The enhanced activity of supported Au is related to the existence of strong covalent bonds between the off–stoichiometric defect on the oxide support and the Au nano–structure. This study suggests that defects on oxide surfaces play a crucial role not only in anchoring metal particles, as had been proposed previously, but also in imparting chemical activity on the particles.

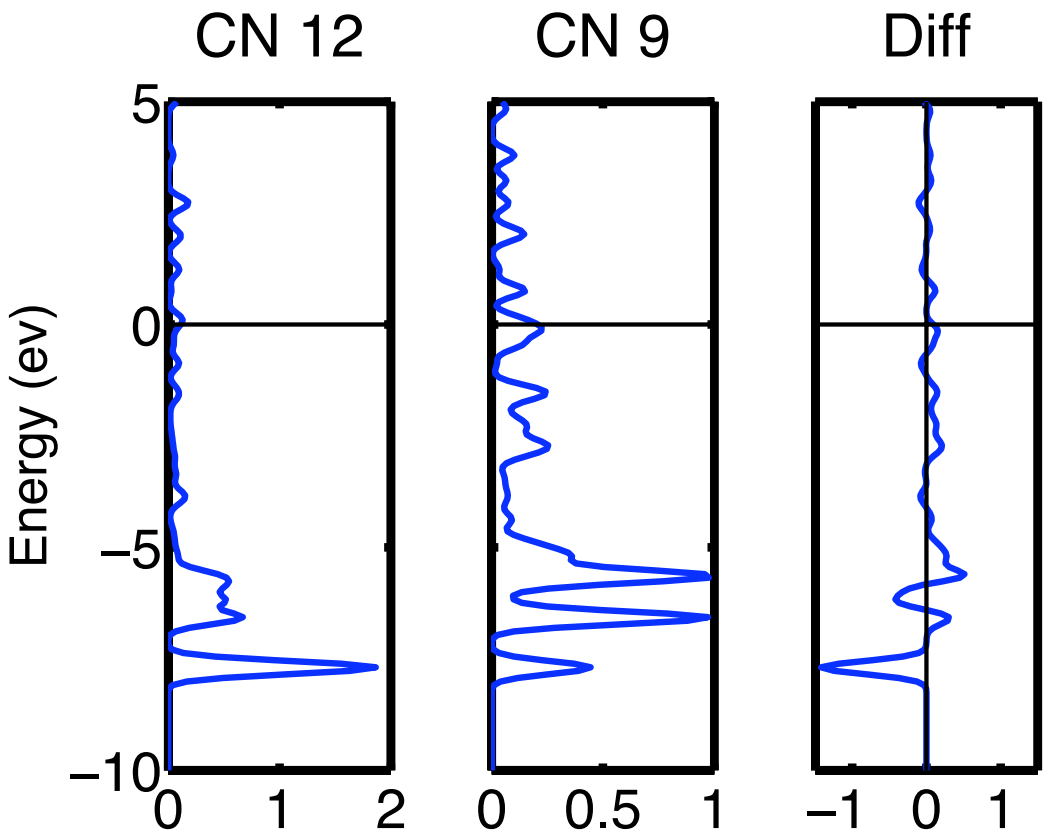

Figure 5.11: Change in DOS upon change in coordination environment.

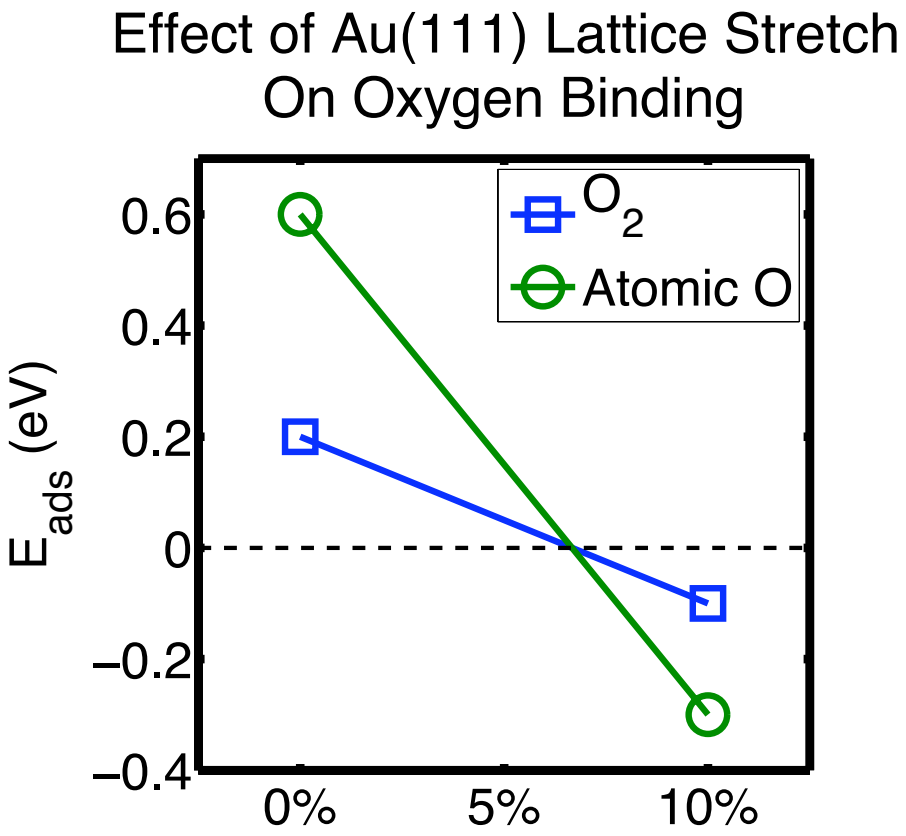

Figure 5.12: Effect of Au lattice stretch on molecular and atomic oxygen adsorption.

CHAPTER VI

The Chemistry and Electronic Structure of Oxide Supported Cationic Au Species

6.1 Overview

In this section, we attempt to further isolate the catalytically active Au species by focusing on catalyst preparation procedures and operating conditions. We investigated the activity of specific surface reaction sites on model Au/TiO_2 catalysts and found that a region at and close to the Au/oxide interface perimeter is highly active in binding and possibly dissociating oxygen. Moreover, this site is also calculated to be highly susceptible to chlorine poisoning, a result that is in line with experimentally observed effects of chlorine. By using multi–component *ab intio* thermodynamics insight into the mechanism of CO oxidation was achieved. We found that Au–only sites away from the Au/oxide interface are likely predominately populated by CO. Whereas, the sites at the perimeter of the Au nano–particle are populated by atomic and molecular species of oxygen. This mechanistic view is in line with inverse catalyst model results and operational powdered catalysts alike.

6.2 Introduction

Macroscopic gold (Au) structures are poor heterogeneous catalysts. However, when dispersed as nano–particles on oxide supports Au exhibits unusual catalytic activity in many important reactions [102, 106–111]. Many mechanisms explaining the catalytic activity of nano–Au have been proposed. These include the presence of cationic Au at the Au/oxide interface, charge transfer from oxide surface defects to Au forming anionic Au, metal–to–insulator electronic structure transition, and the presence of highly under–coordinated or geometrically strained Au sites [20, 42, 91, 108]. Although the previous studies have contributed significantly to the understanding of the chemistry of Au nano–structures, a consensus has not been reached with respect to the catalytically active Au site. Specifically, the charge character ($Au^{\delta-}$, Au^0, or $Au^{\delta+}$) and the location of catalytically active Au sites are under debate.

The lack of consensus regarding the active Au site stems from often contradicting literature reports implicating different oxidation states of chemically active Au ($Au^{\delta-}$, Au^0, or $Au^{\delta+}$). For example, several well defined surface science experiments preformed under ultra–high vacuum conditions showed that Au supported on partially reduced oxide surfaces, such as the TiO_2 surface rich in oxygen vacancy sites, is chemically active in CO oxidation reactions at low temperatures [38, 42]. This effect was rationalized through a transfer of electronic charge from oxygen vacancies to Au forming anionic Au. It has been proposed that anionic Au can easily activate O_2 forming adsorbed atomic O on the nano–structure which can perform oxidation reactions [39]. These experimental observations have been supported by quantum chemical calculations where the chemical activity of Au nano–structures supported on oxygen vacancy rich TiO_2 was studied [40, 44, 46, 112]. The question that naturally emerges from these studies is whether it is possible to sustain high concentrations of the oxygen vacancy sites on the oxide surface under relevant reaction conditions. Our recent *ab initio* thermodynamic analysis suggests that due to highly exothermic

dissociative adsorption of oxygen in the oxygen vacancy sites of TiO_2, the concentration of the vacancy sites under steady–state catalytic conditions may be too low to play an important role [46].

While the studies performed under ultra–high vacuum (UHV) conditions clearly indicated that electron–rich anionic Au is chemically active, studies performed under elevated pressures have lead to a number of contradicting conclusions. For example, in–situ x–ray absorption spectroscopy (XAS) measurements of Au catalysts (Au/TiO_2, Au/Al_2O_3, and Au/Fe_2O_3) prepared by the deposition–precipitation method using gold chloride precursors at a pH of above 8 indicated that the most active CO oxidation catalysts were dominated by electron–deficient cationic Au ($Au^{\delta+}$) [47]. It is important to note that the gold chloride precursor converts to $Au(OH)_x$ or AuO_x groups under high pH conditions [113]. Similar observations were made in studies utilizing catalysts prepared from an organic complex $Au(CH_3)_2(acac)$ where it was shown in XAS studies that active Au catalysts exhibited an Au whiteline intensity indicative of cationic Au [49].

It is interesting to note that very different conclusions were derived based on XAS studies of Au nano–structures supported on several oxides and prepared using a modified incipient wetness with the gold chloride precursor deposited at a pH lower than 5. Under low pH conditions, the gold may be deposited on a support in the form of $AuCl_x$ or $AuCl_x(OH)_y$. The studies showed, in complete contradiction to the observations discussed in the previous paragraph, that the as–prepared catalysts contained cationic Au, but were not catalytically active in CO oxidation. It was shown that these catalysts could be activated via a reduction pretreatment in H_2 at elevated temperatures. The reduction pretreatment was accompanied by a change in the Au electronic structure from cationic (characterized by a significant Au whiteline intensity in XAS measurement) to metallic. Based on these measurements it was argued that cationic Au is catalytically inactive and that metallic Au is required for

low temperature CO oxidation [65].

Clearly, the catalytic chemistry of Au is rich and complex. It appears that external operating conditions, precursors and conditions used in the preparation of catalysts, and the pretreatment of catalysts significantly affect the performance. In this contribution we have used DFT and *ab initio* thermodynamic calculations to address some of these complexities. We have identified the most likely arrangements for CO and O adsorbates on Au/TiO_2 model systems and proposed a likely mechanism for the oxidation of CO at low temperature conditions. Furthermore, we investigated the impact of external operating conditions, the choice of precursor in the synthesis of the catalyst, and the pretreatment of the catalyst on the electronic fingerprint of Au and on the catalytic activity of Au. We focus our attention of the potential role of Cl since gold chloride is often used as the precursor.

In the rest of the paper we discuss the model systems used in our studies and suggest the relationship between the model systems and "real" catalytic systems. This is followed by the description of the methodology and the discussion of the results. Throughout the paper we accentuate the relationships between the results of our analysis and previous experimental observations.

6.3 Model System

In our quantum chemical and *ab initio* thermodynamics calculations we employed two model systems which offer a compromise between computational efficiency and their potential to describe an operational catalytic system. To model the Au/TiO_2 catalyst we used 2–layer thick Au nano–rods supported on the $TiO_2(110)$ surface, see Figure 8.1. The nano–rods were oriented on the surface so that the strain within the Au nano–structure was minimized (below 1%). TiO_2 was chosen as the oxide support since it is the most used and well characterized oxide support [114] The rutile crystal structure of TiO_2 was utilized as this is the most studied and the most thermodynam-

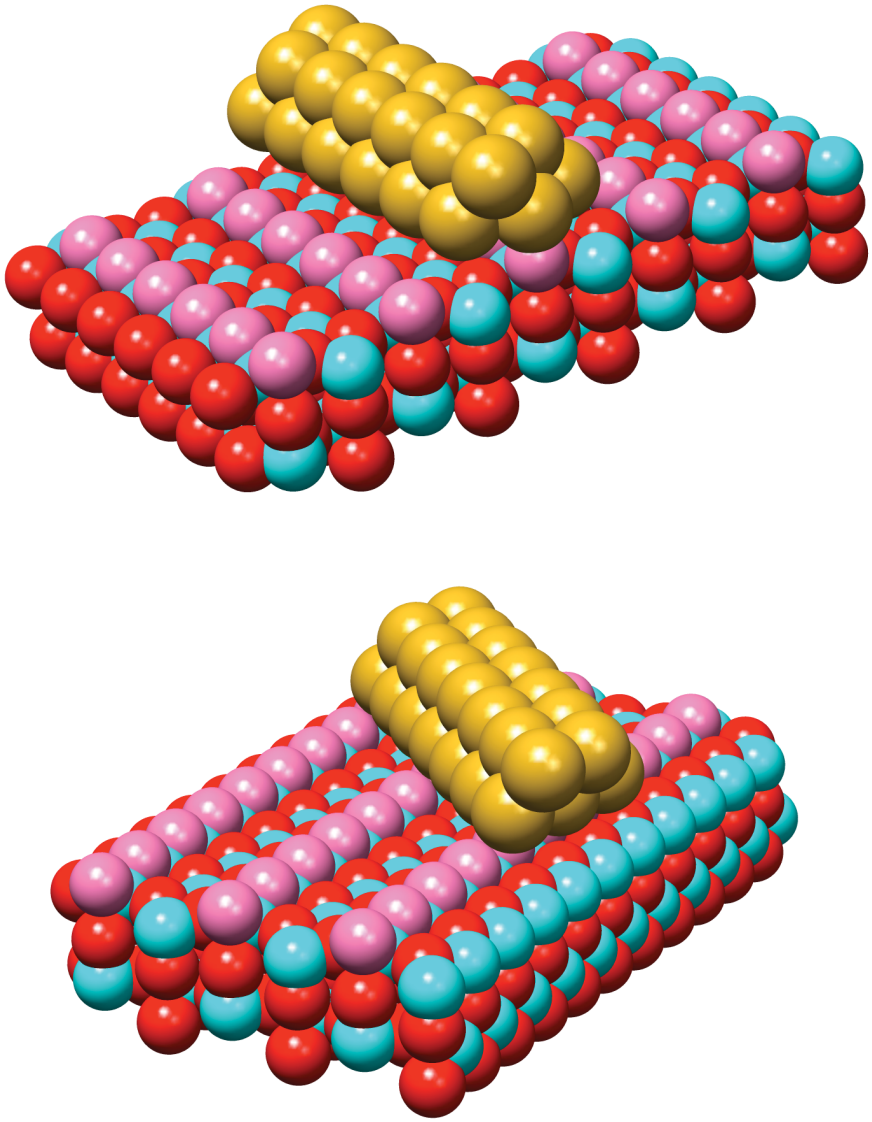

Figure 6.1: Au nano–rods supported by stoichiometric TiO_2 were utilized in our quantum chemical and *ab initio* thermodynamic study. These model systems allow both the Au surface and the Au/oxide interface to be probed. Geometries and supercell sizes were chosen so that the lattice stretch in the Au structure was less than 1%. Gold, red, and light blue spheres correspond to gold, oxygen, and titanium atoms. Light red spheres indicate bridging oxygen atoms in the stoichiometric TiO_2 surface.

ically stable structure of TiO_2. It should be noted that other polymorphs of TiO_2 are likely to produce similar conclusions since all polymorphs of TiO_2 appear to produce highly active Au catalysts in low temperature CO oxidation [115]. The (110) surface of the rutile crystal structure was chosen to model the TiO_2 oxide as this is the most thermodynamically stable facet. It is important to stress that since the electronic structure of the nano–rod model systems used in our calculations is consistent with the electronic structure of Au nano–particles, it is expected that these model systems will yield results consistent with supported 3–D Au nano–structures. We note that the model systems similar to those in Figure 8.1 have been used previously in DFT calculation [39, 40].

Several detailed experimental studies motivated the Au geometry used in our calculations. Goodman and coworkers postulated, based on UHV studies on well–defined model systems, that active Au nano–structures on TiO_2 were 2–3 atomic layers in height (raft–like) [91]. More recent studies utilizing aberration corrected Scanning Transmission Electron Microscopy (STEM) characterization of non–model supported catalysts also showed that Au nano–structures with the thickness of 2–3 atomic layers of Au on iron oxide were highly catalytically active in CO oxidation [103].

The model systems allow us to study a number of different catalytic sites. For example, the sites at the interface of the oxide support and the Au nano–structure are easily probed. Furthermore, the sites on the Au nano–structure, removed from the metal/oxide interface, can also be investigated. We note that the effect of metal/oxide interaction on the electronic structure of Au is rapidly dampened in the Au metal and the Au atoms which are more than two atomic lengths away from the interface would not be significantly affected by the interface.

6.4 Methodology

6.4.1 Quantum Chemical Calculations

Quantum chemical calculations were performed using Density Functional Theory (DFT) methodology with the DACAPO code [85]. The atomic cores were described by Vanderbilt ultra–soft pseudo–potentials [116]. The self–consistent wave function was calculated using the Perdew–Wang Generalized Gradient Approximation (GGA) functional to describe exchange and correlation effects [84]. The geometries were optimized to reduce inter atomic forces to below a value of 0.05 eV/angstrom. The electronic k–space was sampled by Monkhorst–Pack k–point sets of (2x2x1) and (1x2x1) for the 2x2 and 5x1 TiO_2 unit cells respectively. These k–point sampling grids led to converged adsorption energies. The distance between periodic Au structures in the x–y plane was greater than 5.5 angstroms to reduce interactions between periodic images. Vacuum space of 10 angstroms or larger was used between the slabs in z–dir. The dipole correction was used to minimize electrostatic coupling between slabs in z–dir. Adsorbates were allowed to fully relax on the nano–structure. Au atoms were relaxed in z–dir.

6.4.2 *Ab Initio* Thermodynamics Calculations

The electronic energies calculated in DFT calculations were corrected for the effect of temperature and pressure using the *ab initio* thermodynamics formalism discussed in detail by Scheffler and coworkers [98, 117]. The formalism allows for the identification of the structures with the lowest free energy for a given set of external conditions, i.e., external temperature and partial pressures of species in the gas phase. We discuss the approach by focusing on a general case where an Au/TiO_2 nano–structure is in contact with a gas phase reservoir which contains oxygen, chlorine, and CO. To identify the relative thermodynamic stability of Au/TiO_2 systems with various ad-

sorbates on the system we calculated the Gibb's free energy of adsorption for various structures.

$$\begin{aligned}\Delta G_f(T,P_i) = \frac{1}{A}\{&G_{(O,CO,Cl)^*Au/TiO_2} - G_{Au/TiO_2} \\ &- N_O\mu_O(T,P_O) - N_{CO}\mu_{CO}(T,P_{CO}) \\ &- N_{Cl}\mu_{Cl}(T,P_{Cl})\}\end{aligned} \tag{6.1}$$

$\Delta G_f(T,P_i)$ is the temperature and pressure dependent Gibb's free energy of adsorption. A is the area of the unit cell used in the adsorption energy calculation. $G_{(O,CO,Cl)^*Au/TiO_2}$ and G_{Au/TiO_2} are the Gibb's free energies of the Au/TiO_2 system with and without adsorbates respectively. N_X is the number of adsorbates X adsorbed on Au/TiO_2 and μ_X is the chemical potential of X. The gas phase chemical potential (μ_X) can be decomposed into an electronic contribution at T = 0 K and a contribution due to temperature and pressure effects, including zero–point vibrational energy (Eqn. 6.2).

$$\mu_X = \Delta\mu_X(T,P_X) + E_X^{elec} \tag{6.2}$$

The electronic energy is readily calculated using DFT, while the temperature and pressure effects on the free energy of gas phase molecules are included through $\Delta\mu_X(T,P_X)$ which can be computed from first principles using appropriate partition functions or obtained from thermo–chemical tables [86]. Both approaches yield almost identical results.

The Gibb's free energy of the solid Au/TiO_2 surfaces (with and without adsorbates) may also be decomposed using the following expression.

$$G_{surf} = E_{surf}^{elec} + E_{surf}^{vib} + PV - TS_{surf}^{conf} \tag{6.3}$$

Where E_{surf}^{elec} is the total internal energy, excluding the zero point energy, E_{surf}^{vib} is the vibrational free energy, including the zero point energy, while S_{surf}^{conf} is the configu-

rational entropy. We note that the pressure–volume term (PV) and configurational entropy contributions may be neglected as a first approximation. Order of magnitude estimation indicates these terms are insignificant when compared to electronic contributions. [117]. It is important to recognize that the formulation of Eqn. 6.1 assures that that the critical quantity, the free energy of adsorption, does not depend on absolute Gibb's free energies. It mainly depends on a difference in Gibb's free energies between adsorbate–laden and adsorbate–free Au/TiO_2 systems. This allows for favorable cancellations due to similar free energy contributions in the systems or due to similar errors in the computed energies. Coupling Eqn. 6.1, 6.2, and 6.3 one arrives at Eqn. 8.1.

$$\begin{aligned}\Delta G_f(T,P_i) \approx \frac{1}{A}\{&E^{ads}_{O,CO,Cl} - N_O\Delta\mu_O(T,P_O) - N_{CO}\Delta\mu_{CO}(T,P_{CO}) \\ &- N_{Cl}\Delta\mu_{Cl}(T,P_{Cl}) + \Delta E^{vib}_{ads}\}\end{aligned} \tag{6.4}$$

Where $E^{ads}_{O,CO,Cl}$ is the adsorption internal energy for N_X X molecules adsorbed. Evaluate of the vibrational contribution to the Gibb's free energy of adsorption (ΔE^{vib}_{ads}) would require a detailed analysis of vibrational fingerprints of various model systems used in the calculations. However, if one recognizes that the Au/TiO_2 surface does not undergo significant restructuring due to the adsorption of various adsorbates it can be assumed that the initial (adsorbate–free Au/TiO_2) and final model surfaces (the Au/TiO_2 surface with adsorbates) will have similar surface phonons thus ΔE^{vib}_{ads} associated with surface vibrations may be neglected. Therefore, the main vibrational contribution will be associated with the formation of chemical bonds between adsorbates and Au. If we approximate these vibrational modes to be between 100 and 300 cm^{-1}, it can be shown that at the temperature of interest in the process of CO oxidation on Au/TiO_2 (T = 300 K) the vibrational contributions to the free energy of adsorption are not significant.

6.5 Results and Discussion

We first analyze the interactions of the Au/TiO_2 model system with the environment which is either pure oxygen or oxygen and CO. This analysis allows us to propose a mechanism for low temperature CO oxidation on supported Au nano–structures. This is followed by an analysis of the same Au/TiO_2 model system under an external environment which is characterized by the presence of Cl and oxygen. We focus on Cl, because Cl salts are often used in the synthesis of Au catalysts, and we believe that this has led to a large number of confusing interpretations of experimental findings. We will use this analysis to suggest an explanation for contradictory literature reports on the role of cationic Au in oxidation reactions.

6.6 Thermodynamics of Oxygen and CO Adsorption

6.6.1 Pure oxygen reservoir

In Figure 8.2 we show calculated Gibb's free energies of adsorption with respect to molecular oxygen for various structures with atomic oxygen adsorbed on the Au/TiO_2 model system. In these calculations, all accessible sites on the Au/TiO_2 system were probed, including the sites at the Au/TiO_2 interface and on the Au(111) facets of the nano–rod away from the interface. Oxygen coverage is quoted in mono–layers so that 1ML O is equal to the complete coverage of Au atoms in the Au(111) surface.

Figure 8.2 shows that the sites that bind oxygen the strongest are at the interface of the Au nano–structure and TiO_2. These sites are populated at low oxygen chemical potentials. The adsorption sites are characterized by oxygen atoms interacting with Au atoms and the coordinately unsaturated 'cus' Ti^{+4} site on TiO_2. Our calculations showed that the oxygen adsorption at the Au/oxide interface sites was more favorable than adsorption away from the interface by approximately 0.75 eV. Depending on the exact location of the Au nano–structure with respect to the oxide

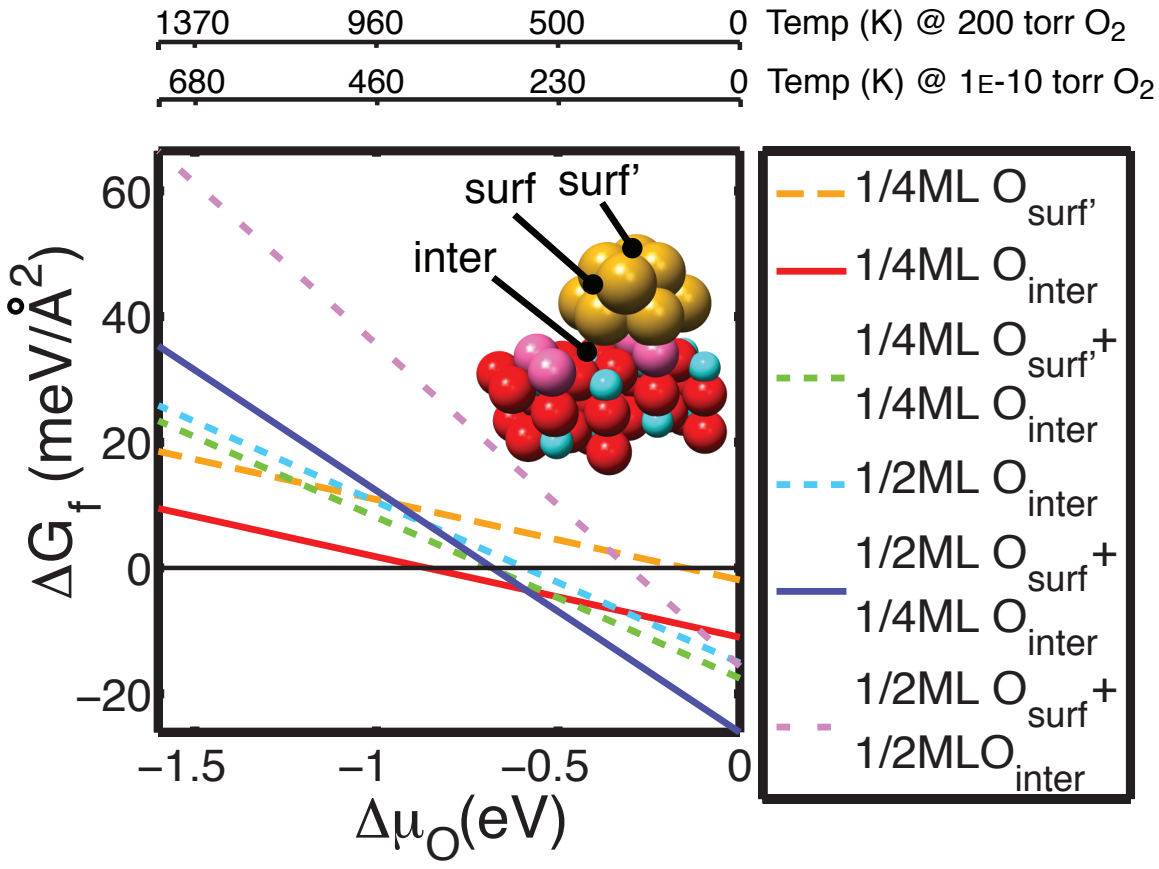

Figure 6.2: Gibb's free energy of adsorption for atomic O adsorbed on the Au nano-rod/TiO_2. The oxygen adsorption sites are labeled with black dots and are grouped into surface (Au–only) and interface (Au/oxide interface) sites. Oxygen at the interface site is bound between a coordinatively unsaturated 'cus' titanium Ti^{+4} atom and the perimeter of the Au nano–rod. ΔG_f is referenced to an adsorbate free Au/TiO_2 surface and gas phase molecular oxygen O_2. $\Delta\mu_O$ at 200 torr O_2 and 300K is approximately –0.27 eV.

surface and the location of oxygen atoms at the interface, the adsorption energy with respect to gas phase O_2 at the interfacial sites was calculated to be –1.0 eV/O and –0.9 eV/O at the nano–rod perimeter and directly beneath the nano–rod respectively. Figure 8.2 also shows that as the chemical potential of oxygen is increased, in addition to the sites at the interface, the sites on the Au nano–structure away from the interfaces are also occupied by oxygen. Our calculations show that the oxygen atoms at the Au/TiO_2 interface stabilize the oxygen atoms at the surface of the Au nano–structure, i.e., on the Au nano–structure in the neighborhood of the interface. For example, oxygen adsorption on the upper Au(111) facet of the 2–layer nano–rod without interfacial oxygen was calculated to be –0.15 eV/O whereas in the presence of a the interfacial oxygen atoms, the oxygen atoms at the upper Au(111) facet were stabilized by an additional 0.4 eV/O. This effect has been previously reported and attributed to an increased chemical activity of the Au nano–structures strongly bound to off–stoichiometric defects on oxide surfaces [46]. These results show that, unlike clean Au surfaces which do not bind oxygen, Au/TiO_2 systems can accommodate oxygen atoms at the Au/oxide interface and at the sites on the Au nano–structure in the neighborhood of the interface. We believe that these sites play a critical role in catalytic oxidation reaction on Au/TiO_2. It is also important to stress that these results show that oxygen atoms bind exothermically even to Au nano–structures which are not anchored on the oxygen vacancies on oxide surfaces [39, 44].

6.6.2 CO and Oxygen Reservoirs

Since we are interested in the behavior of Au/TiO_2 systems in CO oxidation, in Figure 6.3 we show an *ab initio* thermodynamic plot describing the most stable structures for CO and O adsorbates on the Au/TiO_2 model system. We obtained these structures by applying the so called constrained *ab initio* thermodynamics formalism where adsorbates (CO and O) were allowed to adsorb on the substrate without re-

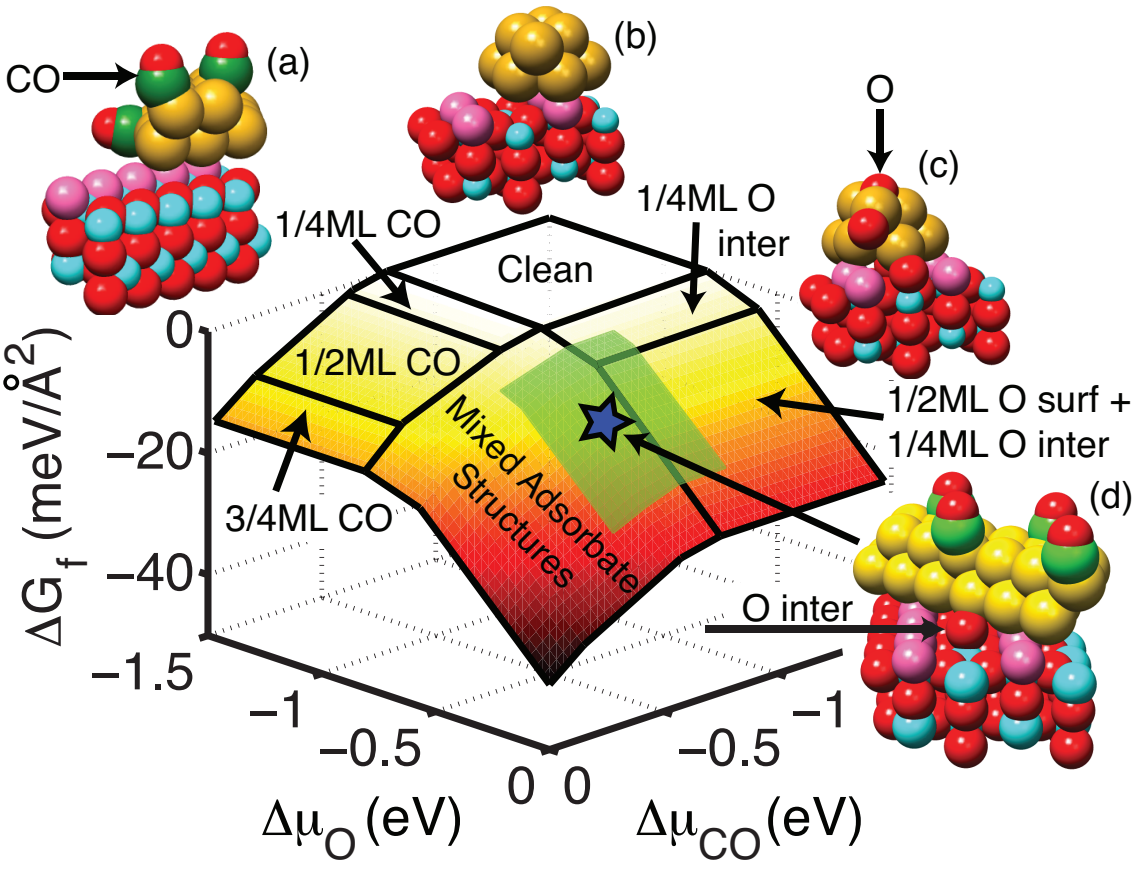

Figure 6.3: Constrained *ab initio* thermodynamics of the Au/TiO_2 surface in contact with O_2 and CO gas phase reservoirs. (a) Geometry of 3/4 ML CO adsorbate over–layer, (b) the adsorbate–free Au/TiO_2 surface, (c) 3/4 ML O adsorbate over–layer, and (d) model of surface under reactions conditions marked by green area and star. ΔG_f is referenced to the adsorbate free surface and gas phase O_2 and CO.

acting to form CO_2. We will comment on this assumption below when we discuss the overall mechanism. Our analysis shows that at realistic chemical potentials of oxygen and CO the adsorption of the adsorbates on the model system is characterized by the Au/oxide interface occupied with O atoms and other sites on the Au nano–structure occupied with CO. This arrangement is not surprising considering that the adsorption of CO on Au only sites is more exothermic than the process of dissociative adsorption of O_2. On the other hand, at the Au/TiO_2 interface there is preference for the adsorption of atomic oxygen.

6.7 Mechanism of CO Oxidation

Figure 6.3 allows us to postulate possible mechanism for CO oxidation on Au/TiO_2. The most stable structures, under realistic thermodynamically constrained conditions, contain the Au/TiO_2 interface rich in oxygen and CO adsorbates on the Au nano–structure away from the interface. Whether these structures are realized under operating conditions is governed by the rates of dissociation of O_2 and the rates of the reaction between O and CO on the catalyst surface to form CO_2. The rate of the formation of CO_2 is governed by the coverages of O and CO, the rates of their diffusion on the catalyst surface, and the rates of the elementary chemical reactions associated with the formation of O—CO chemical bonds. In this study we did not investigate the kinetics of these processes since it is almost impossible due to the complexity of the model, to identify the lowest energy pathways with a high degree of certainty. However, we can relate these results to previous experiment observations and formulate a likely mechanism.

Since most experimental studies have relied on measuring the charge state (electronic structure) of Au with x–ray absorption spectroscopy, it is important to understand how the critical adsorbates, CO and O, affect the electronic structure of Au. To quantify the local electronic structure of Au in the vicinity of O and CO

adsorbates, Bader charge analysis was performed on the systems that are the most stable under realistic constrained thermodynamics conditions. Bader charge analysis employs an algorithm which traces out localized volumes, around a particular atom in real space, bracketed by zero flux surfaces to divide atoms. A zero flux surface is a surface on which the charge density is a minimum perpendicular to the surface. This scheme effectively partitions electronic charge and allocates it to the particular atom centers [118]. The local Bader charges on Au atoms calculated for the most stable Au structures are presented in Table 6.1. It is clear that the effect of the O adsorbate on the electronic structure of Au is much more significant than the effect of the CO adsorbate; the formation of Au—O bonds leads to the formation of the positively charged cationic Au.

This observation is further supported by the analysis of the local density of states (LDOS) projected on Au atoms in the most stable systems (see Figure 6.4). The LDOS analysis shows that the electronic structure in the neighborhood of the Fermi level for Au in the adsorbate–free case was fairly similar to bulk Au with moderate shifts of electronic states toward the Fermi level due to the under coordinated Au environment. A similar electronic structure was found for the Au atoms which bind CO. In contrast to the clean Au and Au covered with CO, the Au/TiO_2 structures which are characterized by the presence of oxygen atoms at the Au/TiO_2 interface have significantly different electronic structure. The electronic structure of the interfacial Au atoms bonded to the O atoms is characterized by the appearance of unpopulated d–states above the Fermi level. It is interesting that this change in the electronic structure manifests itself in the appearance of intense white lines in x–ray absorption near edge spectroscopy (XANES) measurements. We note that XANES measures electronic transitions from core electron levels to unoccupied states, localized on the particular atom. For example, the Au L_{III}–edge is produced by an excitation of $2p_{\frac{3}{2}}$ electrons to s– or d–states above the Fermi level, and is commonly used to track the

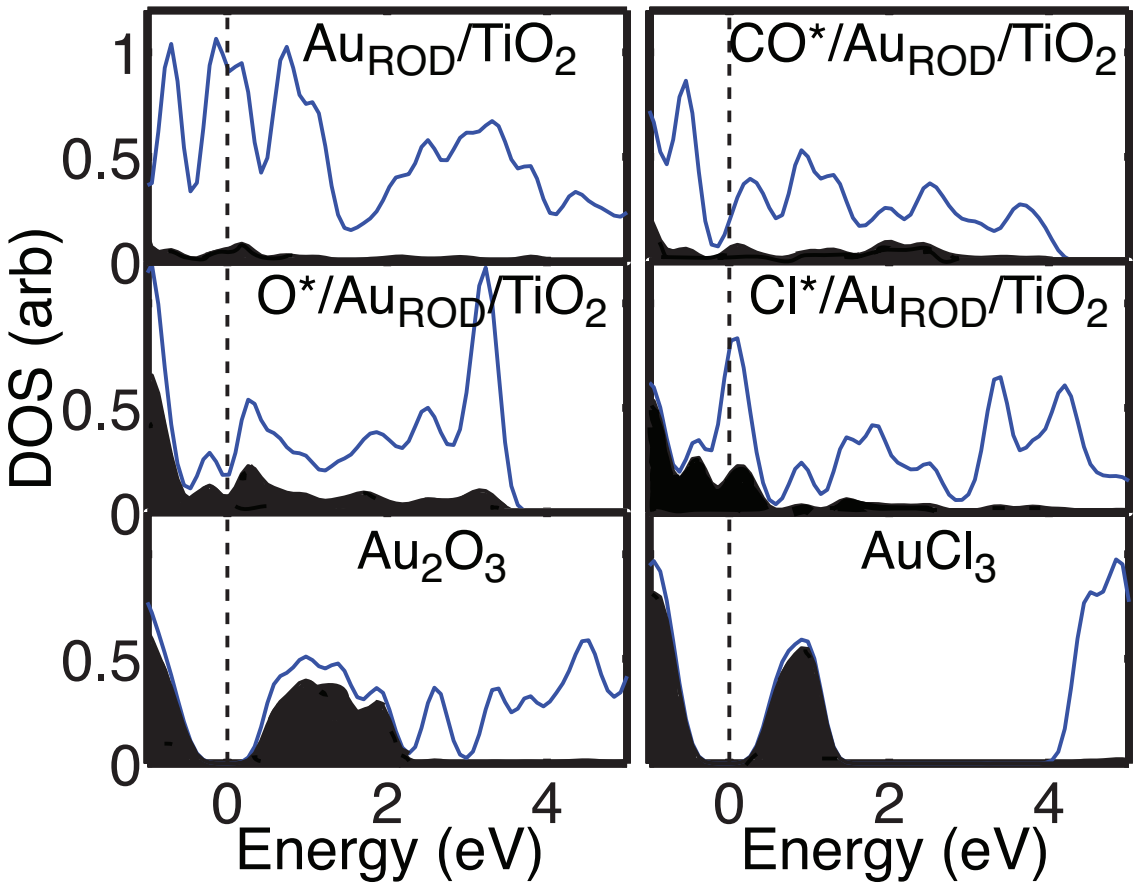

Figure 6.4: Total density of states (blue) and d–symmetry states (filled black) projected on Au atoms for the clean Au/TiO_2, and Au atoms bonded to CO*, O*, and Cl*. The Fermi level is set to zero and indicated by a black dashed vertical line. The available d–states above the Fermi level can be seen for the Au atoms bonded to oxygen and chlorine. This indicates that either species would produce a similar whiteline intensity increase in XANES.

oxidation state of Au. When Au is in a given oxidation state, such as Au(III), the Au d–states are under populated which leads to a sizable increase in the whiteline intensity (the feature directly above x–ray absorption onset) due to the availability of the unoccupied Au d–states above the Fermi level.

Based on this analysis it can be concluded that the Au electronic structure is affected only for those Au atoms that form a chemical bond with oxygen. The Au atoms that bind CO have an electronic structure which is very similar to metallic Au. Since as shown in Figure 6.3 the most stable structures contain oxygen adsorbates at the interface and CO on Au, depending on external steady state conditions (temperature and partial pressures of CO and O_2) the Au atoms will have either metallic (neutral) or electron deficient (cationic) electronic signature. The cationic signature is mainly associated with the Au atoms at the Au/TiO_2 interface which bind oxygen atoms strongly. These oxygen atoms are not expected to be moving on the Au nano–structure at low temperatures since their adsorption energy on the interfacial sites is much more exothermic than on the Au sites away from the interfaces, so there is no thermodynamic driving force to move these atoms from the interface. On the other hand CO molecules adsorb on the sites away from the interface will diffuse on the surface of the Au nano–structure. This process of CO diffusion will lead to surface collisions between CO and O at the interface resulting in the exothermic formation of CO_2.

This analysis clearly shows that depending on the experimental conditions, an *in situ* steady–state measurements will yield cationic or metallic Au fingerprint. It is important to realize that this does not mean that for the case on cationic Au the entire Au nano–structure is covered by oxygen, it rather means that there are O atoms at the Au/TiO_2 interface which are chemically bonded to Au. These Au atoms will be observable in a XANES measurement since they are characterized with high–intensity white lines which dominate the Au XANES spectrum.

Table 6.1: Calculated Bader charge for Au atoms bonded directly to CO, oxygen, or chlorine adsorbates or present in bulk oxide or chloride materials.

System	clean	CO*	O*	Cl*	Au_2O_3	$AuCl_3$
Charge	0.0	0.0	+0.5	+0.2	+1.2	+0.8

We note that the above postulated mechanism is consistent with previous contributions of Hammer and coworkers who showed based on DFT calculations that there are low energy pathways for bimolecular reactions of O_2 with CO to from CO_2 and adsorbed oxygen atoms at the Au/TiO_2 interface [57]. The calculated activation barriers were ~ 0.15 eV. It was also shown that adsorbed oxygen atoms reacts with adsorbed CO to form CO_2 in a barrier–less process. It is important to note the activation barrier for the diffusion of CO on Au is between 0.1 and 0.2 eV. These results indicate that it is plausible that under steady–state conditions, the functioning catalyst will have small concentration of oxygen atoms at Au/TiO_2 interface and CO adsorbates away from the interface. These conclusions are also consistent with the results of recent pulsed reactor studies by Behm and coworkers which showed oxygen can be stored on the catalyst surface in the absence of CO and then reacted away with CO to form CO_2. Furthermore, it was also found that a clear connection between the particle perimeter length and the rate of CO_2 formation [68].

6.8 Impact of Cl Precursors and Catalyst Pretreatment

The analysis above suggests that cationic and/or metallic Au atoms could be observed under reaction conditions and that these structures should be catalytically active. The results suggest that a red–ox cycle on Au atoms at the Au/TiO_2 interface is associated with the dominant reaction pathway. However, the results also contradict a number of experimental studies which showed that cationic Au is not active [52, 65]. Two common features among these experimental studies are that the Au/oxide catalysts were prepared using gold chloride precursors under low pH con-

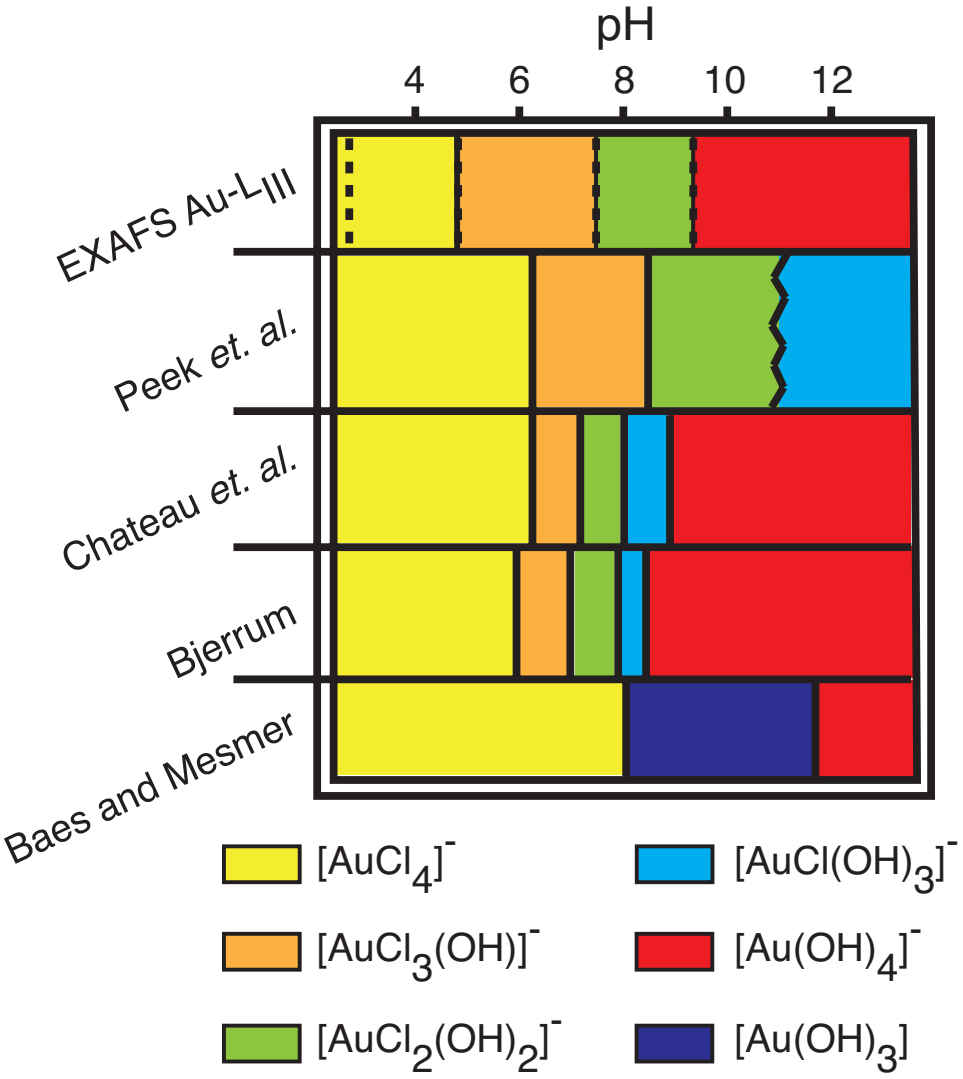

Figure 6.5: The Au species present under various values of pH in aqueous solution. At low values of pH $AuCl_4^-$ persists. As pH is increased chlorine ligands are replaced by hydroxyls forming a mixed Au (chloro)hydroxide i.e., $AuCl_{4-x}(OH)_x^-$. At pH above ~8 the solution is dominated by $Au(OH)_4^-$. The figure is adapted from ref. Farges *et al.*

ditions (dry impregnation, incipient wetness, or low pH deposition precipitation) and that the experimental measurements that lead to the conclusion that cationic Au is not involved in the process of CO oxidation were performed on as–prepared catalysts, i.e., no catalyst pretreatment (calcination or reduction) was performed. It has been shown previously that under low pH conditions, the gold is deposited on a support in the form of $AuCl_x$ [119].

To understand how Cl affects the Au/TiO_2 system, we have performed *ab initio* thermodynamic analysis for chlorine adsorption on the Au/TiO_2 model systems. We found that chlorine atoms preferentially adsorb on the same sites as oxygen atoms, i.e., if Cl is present in the system, the Cl and O adsorbates will compete for identical adsorption sites. This is illustrated in Figure 8.4 where we show *ab initio* thermodynamic plots for the Au/TiO_2 surface in contact with oxygen (gas phase O_2) and chlorine (gas phase Cl_2) reservoirs. We found that for all explored structures it was more energetically favorable to populate the available sites on Au/TiO_2 surface with chlorine than oxygen. This is a consequence of a stronger interaction between Cl and Au.

From Figure 8.4 it can be seen that chlorine adsorption dominates most of the (μ_O, μ_{Cl}) phase space. Furthermore, it is clear that very high chemical potentials of oxygen are required to displace chlorine from the Au/TiO_2 system. In addition, most likely there are high activation barriers associated with the formation of Cl_2 by reacting interfacial Cl atoms, and it would be difficult to overcome these barriers under low temperature operating conditions. This would indicate that as–prepared Au nano–structures, which are not pretreated in any way, might have interfacial sites occupied by Cl and these interfacial sites would be inaccessible to oxygen atoms. These catalysts would have low catalytic activity since the dissociation of O_2 could not be activated by the Au/oxide interface. Furthermore, it is very interesting that the electronic structure of Au atoms bonded to Cl is very similar to the electronic

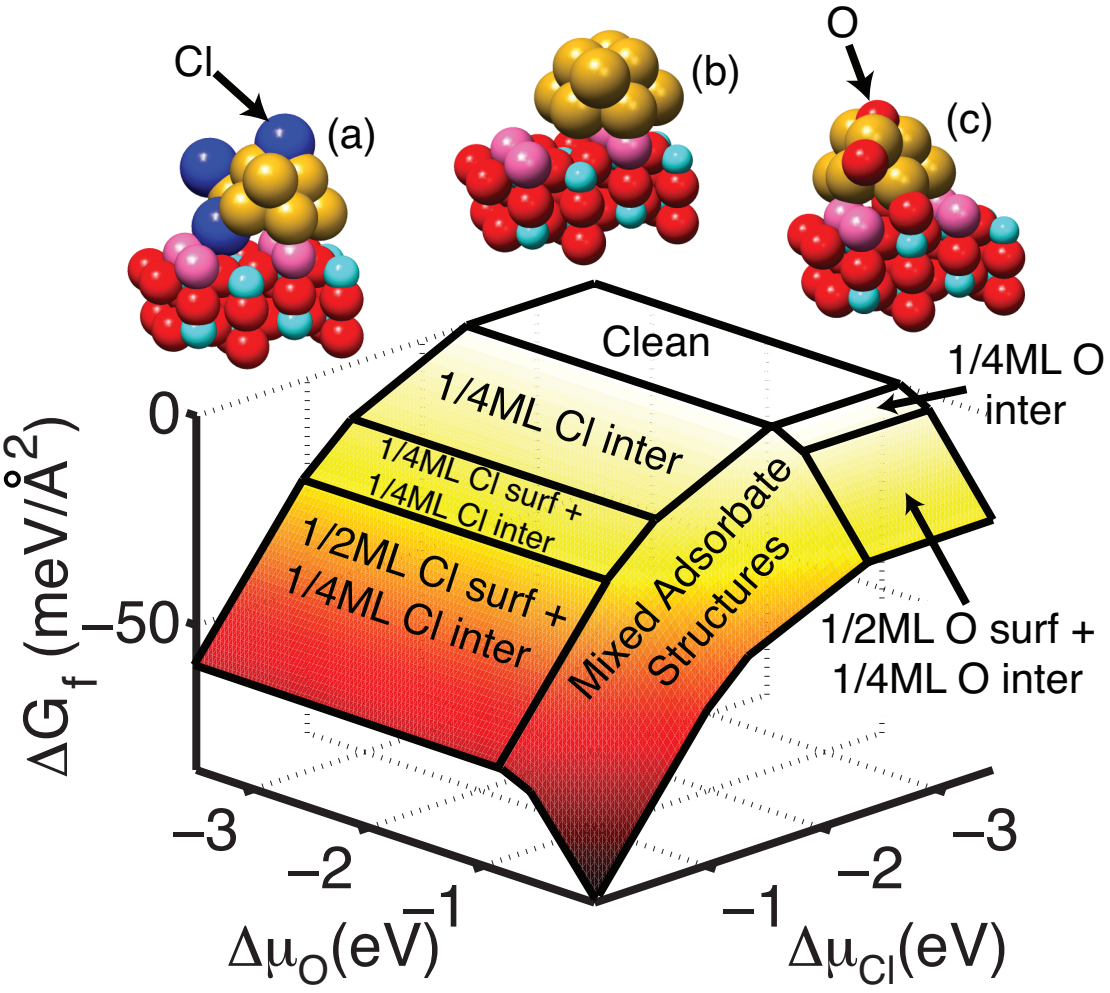

Figure 6.6: Constrained *ab initio* thermodynamics of the Au/TiO_2 surface in contact with O_2 and Cl_2 gas phase reservoirs. (a) Geometry of 3/4 ML Cl adsorbate over–layer, (b) the adsorbate–free Au/TiO_2 surface, (c) 3/4 ML O adsorbate over–layer. The power of chlorine to poison the interface sites is clear since only a small portion of the $\Delta\mu_O$ and $\Delta\mu_{Cl}$ produces a surface that may perform catalytic CO oxidation i.e., a oxygen rich Au/oxide interface region. ΔG_f is reference to an adsorbate free surface and gas phase O_2 and Cl_2.

structure of Au bonded to oxygen. This is shown in Figure 6.4 which depicts the electronic structure of Au bonded to Cl. This electronic structure is characterized by depletion in the filling of d–orbitals due to the shift of electron density from Au to Cl. Even a small amount of Cl would populate the interfacial sites and the electronic structure of Au would be consistent with cationic Au.

6.9 Summary and Conclusions

Quantum chemical and *ab initio* thermodynamic calculations have been used to investigate the mechanism of CO oxidation on Au/TiO_2 and the geometric and electronic character of active Au atoms. Our results show that CO oxidation over Au/TiO_2 may proceed via a two site mechanism with oxygen adsorbing and dissociating at the Au/oxide interface or the perimeter of Au particles and CO adsorbing on Au sites away from the interface. The electronic fingerprint of active Au is a function of external conditions and it is likely that most Au atoms will be populated by CO and electronically neutral with a small minority at metal/oxide interface having cationic fingerprint due to their interaction with oxygen adsorbates. The Au/oxide interface site is highly susceptible to chlorine poisoning and thus the presence of chlorine influences the availability of these sites to incoming oxygen. Therefore, the catalytic activity of supported Au nano–structures will depend highly on the choice of catalyst preparation procedure (preparation conditions and the choice of precursors) and catalyst pretreatment.

CHAPTER VII

Connection Between the Oxide's Electronic Structure and the Chemistry of Oxide Supported Au

7.1 Overview

In this section we attempt to connect the electronic structure of an oxide to the chemical activity present at the Au/oxide interface perimeter. We utilized *ab initio* quantum chemical and thermodynamic calculations to show that the activity of Au/oxide interface sites is directly affected by the type of oxide support in contact with the Au nano–structure. Our calculations suggest that the activity of the Au/oxide interface perimeter site increases as more metallic oxides, as opposed to semi–conductors or insulators, are used to support the Au nano–structure. For example, a fairly inert interface site may be produced when Au is supported by an insulator such as SiO_2. On the other hand, supporting Au by a metallic oxide such as IrO_2 produces an interface site that binds oxygen very strongly. When investigating the thermodynamic driving force for O_2 dissociation at the interface site for the four oxide supports considered we find that there exists a maximum in the driving force situated in the vicinity of the semi–conductor supports. This indicates that optimal Au–oxide couples may exist that result in low activation barriers for O_2 dissociation

and high activity in low–temperature oxidation reactions. Serendipitously, the peak in O_2 thermodynamic driving force lies close to Au/TiO_2 which is the most active Au catalyst for low–temperature CO oxidation.

7.2 Introduction

Oxide supported gold (Au) exhibits low–temperature catalytic chemical activity in many chemical reactions such as CO oxidation, water–gas shift, NO_x reduction, and partial oxidation [12–14, 101, 107]. The catalytic activity of Au at low temperature can even surpass that of Pt–group metal–based catalysts when compared at low temperatures. Therefore, Au–based catalysts may be viable replacements or supplements for costly Pt–based catalysts. However, several key issues, dealing with catalyst activity and stability, must be addressed before Au can be widely implemented as a catalyst. Most notably, it has been found that the type of oxide used to disperse Au drastically affects the activity and stability of the final Au/oxide catalyst [72]. The interactions that govern these effects are not well understood, however, it has been postulated that the chemistry occurring at the Au/oxide interface is directly affected by the oxide support [32, 44, 47, 72, 73, 75, 76, 81, 102, 120]. Our aim in this section is to use *ab initio* calculations on well–defined model systems to determine the dominant interactions present at the Au/oxide interface and make connections between these interactions and the chemical activity present near the interface.

7.3 Background

The studies of the Au/oxide interface, in connection with Au catalytic activity and stability, have leaned heavily towards a partially reduced interface [34, 36, 40, 42, 95, 96, 99, 112]. When considering the partially reduced Au/oxide interface, oxide surface oxygen vacancies (oxide surface defects) are present and have been shown to anchor Au structures to the oxide surface [36]. It has been suggested that these oxygen vacancies, being electron rich, may also impart additional chemical activity to Au, facilitating O_2 binding and dissociation [34, 39, 42, 44, 121, 122]. The mechanism driving O_2 dissociation being an electronic charge transfer from the oxygen vacancy

to Au and then from Au to O_2 weakening the O—O bond facilitating dissociation [34, 37–39, 44, 102]. However, the view that oxide surface oxygen vacancies play a crucial role in Au catalysis may be challenged because of the large amount of energy required to form the vacancies (∼2.5–5.0 eV) [95, 114, 123–125]. It is this energetic unfavorability, combined with evidence from well–defined UHV STM experiments indicating H_2O and O_2 quickly heal oxide surface oxygen vacancies even under well–baked UHV conditions, that makes it difficult to envision how oxygen vacancies play a significant role in the overall catalytic activity of Au [58, 126].

An alternate view of the Au/oxide interface involves an oxygen–rich interface and possibly portions of cationic oxidized Au. For example, many *in situ* or *in operando* x–ray absorption spectroscopy experiments indicate the presence of cationic Au under reaction conditions of low–temperature CO oxidation and water–gas shift reactions [47, 92, 93, 127]. Furthermore, secondary–ion mass spectroscopy of non–model Au/TiO_2 and Au/Al_2O_3 catalysts active in CO oxidation, prepared via the deposition–precipitation method (pH 7), also indicated that Au was bound to oxygen even after high temperature calcination (350 °C) [93]. In a study by Besenbacher and co–workers, these Au–O interactions at the Au/oxide interface were directly probed using atomically resolved STM. The studies pointed towards strong Au—O bonds present at the Au/oxide interface, which prevented sintering at elevated temperatures when when compared to Au on oxygen vacancy rich or hydroxylated TiO_2 surfaces [55]. Further, many theoretical quantum chemical calculations also indicate that the Au/oxide interface or Au particle perimeter can be a highly active site for binding and dissociating oxygen without evoking oxygen vacancies [39, 40, 46].

In this contribution we present results that indicate sites at or near the Au/oxide interface may be highly active in binding and dissociating atomic and molecular oxygen respectively. We show that the Au/oxide interface perimeter site is highly active, and is dramatically affected by the type of oxide support present under the

Au nano–structure. We find that the effect of the oxide can be traced to electrostatic and electronic interactions between the adsorbates, Au, and the oxide support. We present concepts grounded in physically transparent mechanisms to rationalize the chemistry taking place at this special location on the Au/oxide surface. We find that a key step to oxygen adsorption is charge transfer from Au or the oxide to the oxygen adsorbate leading to favorable electrostatic interaction with the oxide surface cation. The relative amount of interaction between atomic or molecular oxygen and the oxide surface follows the trend of oxide reducibility. The metallic oxide (IrO_2) is found to stabilize oxygen at the Au/oxide interface greatly, semi–conducting oxides (TiO_2 and SnO_2) moderately, and the insulating oxide (SiO_2) only marginally. Interestingly, the stabilization of atomic and molecular oxygen follow different trends as the oxide reducibility is increased. This results in a volcano shaped curve in the thermodynamic driving force for O_2 dissociation indicating optimal Au–oxide couples that may result in low O_2 dissociation activation barriers.

7.4 Model Motivation

To investigate the effect of the oxide support on the activity of the Au/oxide interface/perimeter site we employed quantum chemical and *ab initio* thermodynamic calculations. The model Au structures were motivated closely by many experimental findings that indicate nanometer or sub-nanometer sized Au particles were the highly active Au geometry [36, 91, 96, 103, 128]. For example, it has been found that 2–3 atomic layer thick sub-nanometer sized Au particles on FeO_x were highly active in room temperature CO oxidation [103]. Furthermore, similar geometries were also produced in STM studies on Au/TiO_2 and determined to be highly active in room temperature CO oxidation [91, 96, 111]. Further examples of two dimensional Au nano–structures on the oxides of interest were independently discovered using atomically resolved STM and high resolution medium energy ion scattering [55, 128].

Driven by these findings we chose a two atomic layer Au nano–rod geometry to model Au deposited on different oxides. This model is representative of the perimeter edge of a larger flat nano–particle (2–3 nm diameter) and exhibits fully developed metallic electronic structure. Since our investigation will involve a range of oxides that have markedly different Au/oxide interface interaction energies, which would dictate Au particle geometry, i.e., spherical or hemi–spherical particle shape, we focused on two nano–rod systems: one with a low contact angle at the Au/oxide perimeter and another with a high angle of contact representing weak and strong Au/oxide interface interactions respectively. Furthermore, we also investigated a platinum (Pt) nano–rod of the same geometry to test whether the calculated support effect was special for Au or was a general phenomena.

As oxide models we choose the rutile crystal structure of oxides of varying reducibility i.e., insulator, semi–conductor, or metallic. Four oxides were chosen, two p–block and two d–block, an insulator SiO_2, two semi-conductors TiO_2 and SnO_2, and a metallic oxide IrO_2. The oxides were chosen because of their respective intra–block reducibility. The rutile crystal structure was used as it is the most thermodynamically favorable crystal structure at room temperature and pressure for TiO_2, SnO_2, and IrO_2 [129, 130]. Rutile SiO_2 is a higher energy polymorph of SiO_2 thus is marginally activated with respect to the quartz crystal structure. Therefore, utilizing rutile SiO_2 will indicate an upper bound for the activity of the Au/SiO_2 interface. By constraining calculations to the same crystal structure for all oxide supports, similar adsorption geometries could be calculated while only changing the type of oxide present. This effectively allows the conclusions to be based upon the oxide's electronic structure and minimally on the local adsorption site geometry. The (110) oxide surface termination was used as this is the most most thermodynamically favorable facet of the rutile crystal structure. The stoichiometry of the oxide surfaces was determined by *ab initio* thermodynamic calculations with the stoichiometric termination found to

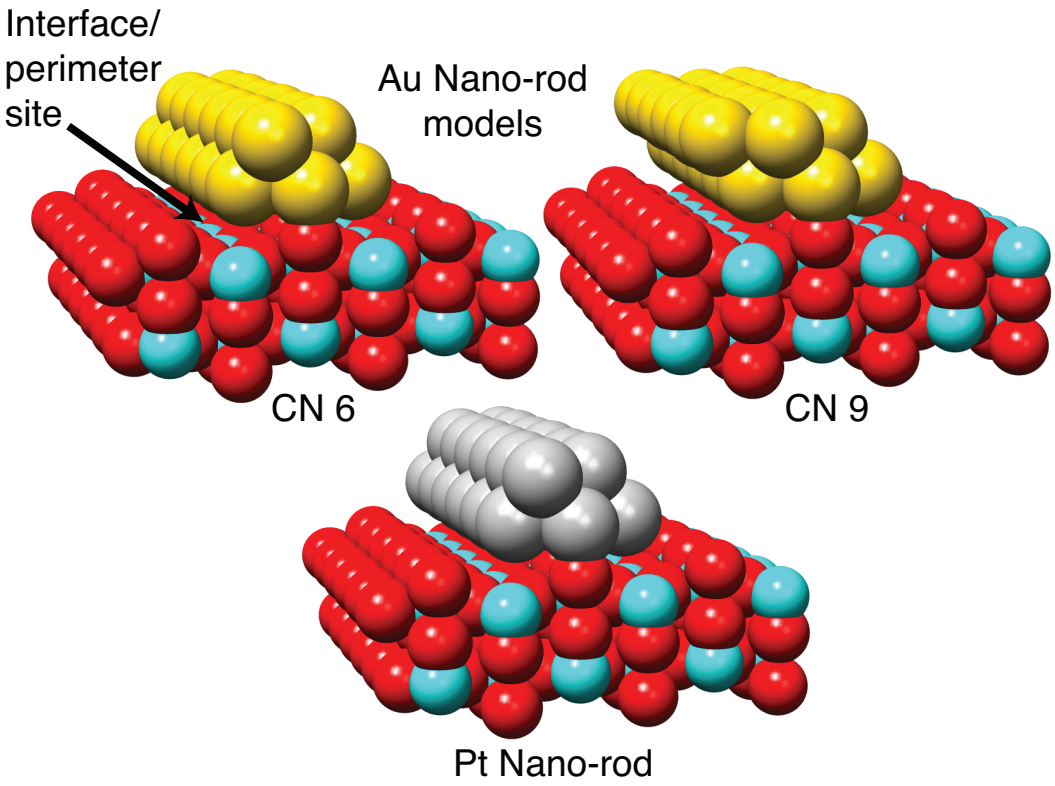

Figure 7.1: Au and Pt nano–rod models supported by rutile crystal structure oxide support. The two atomic layer thick nano–rod geometry is motivated by high resolution scanning tunneling microscopy and aberration corrected scanning transmission electron microscopy (see model motivation text). Molecular and atomic oxygen adsorption was tested directly at the Au/oxide interface site in contact with an oxide surface cation. Four oxides (SiO_2, TiO_2, SnO_2, and IrO_2) were chosen with varying electronic structure to investigate the effect of the oxide support on the activity of the Au/oxide interface site.

be the most favorable for all oxides considered except for IrO_2 where an over oxidized surface was favorable at higher oxygen chemical potentials.

7.5 Model and Calculation Specifics

The nano–rod model system consisted of two atomic layers of the metal. The models used are presented in Figure 7.1. The geometry of the metal, either Au or Pt, was fixed in the xy-plane and relaxed in the z–direction. The (111) facet of the nano–rod was in contact with the oxide surface [131]. The stoichiometric termination was used for all calculations. The oxide was modeled by two tri–layers of the oxide or six atomic layers. Due to the lattice mismatch between the oxides and Au, larger supercells were required to minimize the Au lattice stretch. The Au—Au bond stretch for each model system was 0.2, 0.9, 5.4, and 1.8% expansion for SiO_2, TiO_2, SnO_2, and IrO_2 respectively. Either 2x2 or 5x1 oxide supercells were used to accommodate the Au and Pt nano–rods. This allowed a distance of 5.5 $\AA$ or greater between periodic nano–rod structures. Molecular and atomic oxygen were adsorbed at the metal/oxide interface in direct contact with both the nano–rod and the coordinatively unsaturated oxide surface cation. Oxygen adsorption above the oxide surface anions (oxygens) was always found to be unfavorable on the stoichiometrically terminated oxide. It should be noted that all oxygen adsorption energies presented are with respect to gas phase molecular oxygen.

The calculations were performed with the DACAPO total energy code [85]. Atomic cores were described by Vanderbilt ultra–soft pseudo–potentials [116]. Plane–waves were utilized as the basis set for the total wave–function. Plane–waves with energy below 350 eV were included in the description of the total wave–function. The electronic k–space was sampled by a (2x2x1) or (1x2x1) Monkhorst–Pack k–point sampling mesh for the 2x2 and 5x1 oxide supercells respectively, which, due to the large supercell, lead to convergence of the adsorbate adsorption energies. The maximum

force present on the atoms allowed to move in the geometry optimization calculations was minimized below 0.05 eV/Angstrom. The vacuum space was kept at or larger than 10 Angstroms and a dipole correction was applied to cancel the dipole produced by adsorbate over–layers.

7.6 Oxygen Adsorption and Dissociation at the Au/oxide Interface: The effect of the support

First, we aimed to understand how different oxide supports can affect the chemistry of the Au/oxide interface adsorption site. We start by calculating the adsorption of molecular and atomic oxygen on clean stoichiometric oxide surfaces. Molecular and atomic oxygen adsorption on the clean stoichiometric oxide surfaces was found to be endothermic with respect to molecular oxygen for all configurations tested except on the metallic oxide, IrO_2. The adsorption of atomic oxygen on IrO_2 was –0.57 eV/O. These trends are in line with the conventional view that oxide surfaces terminate stoichiometrically and without surface dipoles [98, 114, 125, 132].

We also tested adsorption of molecular and atomic oxygen in the presence of the Au nano–rod. We found that, in the presence of Au, O_2 and O adsorption was promoted markedly. When compared to adsorption of atomic oxygen at similar sites of the unsupported Au nano–rod, the presence of the oxide enhanced binding by as little as 0.1 eV/O for SiO_2 and as much as 0.8 for TiO_2 and SnO_2. When calculating the thermodynamic driving force for O_2 dissociation, which can be correlated to the activation barrier for dissociation [133–135], it was found that there exists a volcano–shaped correlation between the reducibility of the oxide support and the driving force for O_2 dissociation. A maximum in the driving force was calculated in the vicinity of semi–conducting oxide supported Au systems, TiO_2 and SnO_2. The results are summarized in Figure 7.2 with adsorption and thermodynamic driving force plotted

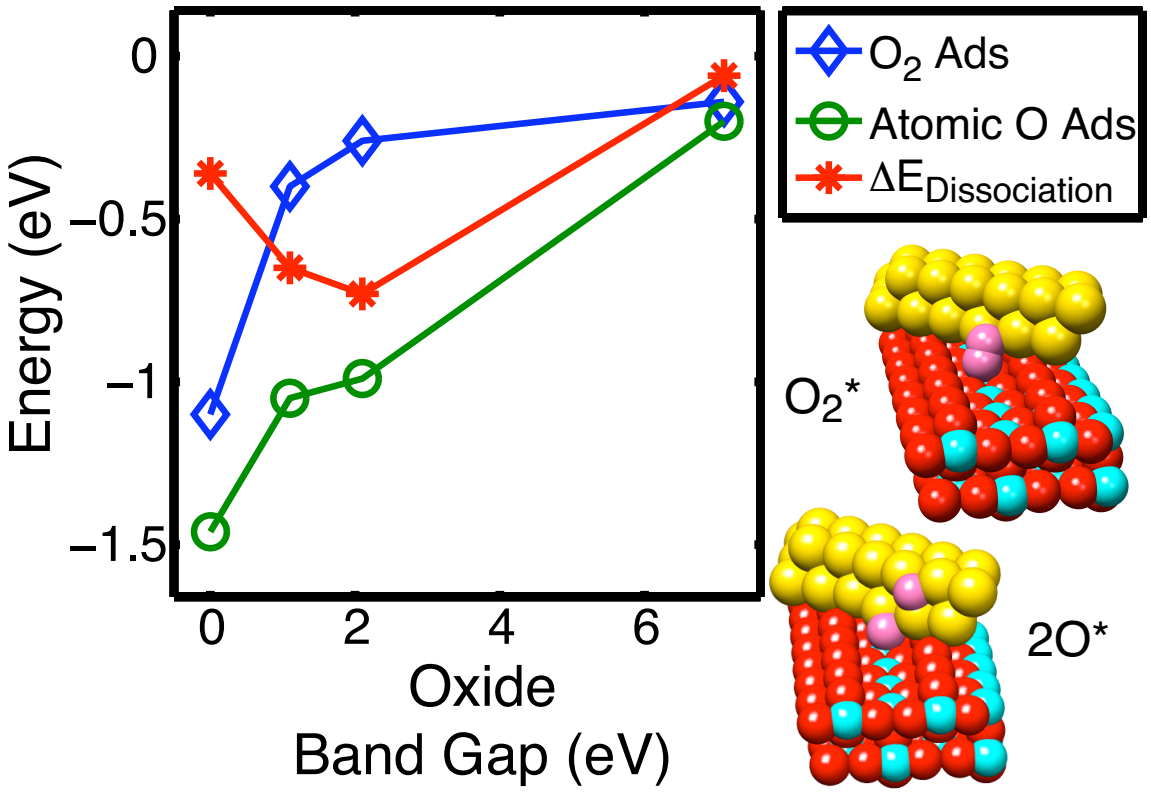

Figure 7.2: The adsorption of molecular and atomic oxygen at the Au/oxide interface were calculated for the four oxide support cases. Here the adsorption energies are plotted against the oxide band gap, which is used as a measure of oxide surface reducibility. The thermodynamic driving force for O_2 dissociation is also presented to illustrate the tunability of the Au/oxide interface site. The fundamental physical mechanisms which govern the Au/oxide interface site are discussed in section 7.8.

against the band gap of the oxide. The dominant physical mechanisms which govern the adsorption at the Au/oxide interface are discussed later.

When considering the effect of the oxide support, the equilibrium metal particle shape may also play a significant role in the activity of the metal/oxide interface sites. To test this effect we contrast oxygen adsorption on Au nano–rod model systems which mimic Au nano–particles that either wet or don't wet the oxide surface (see Figure 7.1 (a) and (b)). The results are shown in Figure 7.3. Interestingly, when testing this effect we found that the interface sites of Au/SiO_2 and Au/IrO_2 were affected marginally by the change in Au nano–rod shape. Whereas, the case of TiO_2 and SnO_2 were affected significantly. This indicates that in the two latter cases, the shape of the Au nano–particle could significantly affect the overall measured catalytic chemistry. This result is directly in line with previous results presented by Haruta and coworkers indicating the contact angle of the Au particle can affect both activity and selectivity in CO oxidation and the epoxidation of propylene [107]. Furthermore, is in line with theoretical calculations by Norskov and co-workers showing that under coordinated sites may play a crucial role in Au catalytic chemistry [21].

7.7 Contrasting Au/oxide with Pt/oxide interface

The effect of the oxide support on Au catalyst activity has usually been attributed to geometric effects [72, 75]. For example, the support effect in catalysis by Pt–group metals was attributed to metal particle encapsulation by the support material (Strong Metal Support Interaction) and the spill–over mechanism [15]. However, in oxide supported Au catalysis, the activity and stability of Au catalysts exhibit pronounced support effects that do not adhere to either of these mechanisms. To investigate whether there are different mechanisms that dominate the Au/oxide systems we calculate atomic oxygen adsorption at the Pt/oxide interface for comparison. When calculating the adsorption energy of atomic oxygen at the Pt/oxide interface

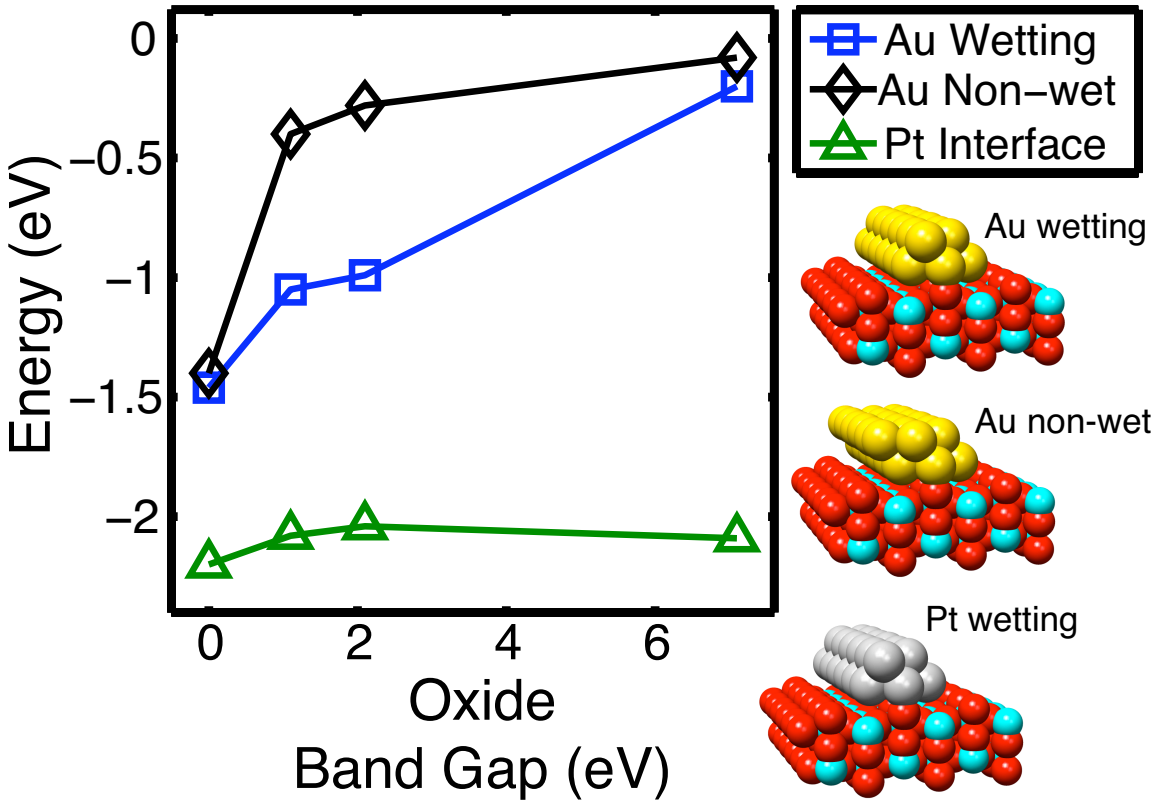

Figure 7.3: The effect of particle perimeter geometry was tested for the four Au/oxide systems. The 'wetting' (squares) and 'non-wetting' (diamonds) models are used to approximate small flat and large rounded particles respectively. The effect of Au coordination at the interface is as expected with oxygen adsorption energy being reduced. However, the support induced stabilization of the adsorbate persists. With oxygen adsorption becoming more exothermic as the oxide is more reducible. Oxygen adsorption at the Pt/oxide interface was also tested to illustrate how Au is special with respect to the support effect. Furthermore, the adsorption at the Pt/oxide interface may be too strong and these sites may be catalytically inactive.

we found that there was little effect of the oxide, unlike the Au/oxide interface. See Figure 7.3.

The difference between the Au/oxide and Pt/oxide interface may be rationalized by considering the nobility of Au in comparison to Pt. Unsupported uncharged Au does not interact strongly with oxygen adsorbates. This nobility of Au is attributed to its fully populated d–states and electronegativity relative to oxygen [100]. Upon oxygen adsorption, on bulk–like Au, charge is transfered from Au to O, depopulating Au—Au bonding s– and p–states, resulting in endothermic adsorption. In the presence of an oxide, the oxide cation at the interface presents a binding site that electrostatically stabilizes the Au—O charge sharing by forming coupled dipoles, i.e., favorable cation–anion–cation interactions. The resulting oxygen stabilization is oxide electronic structure specific, and dependent upon the ability of the oxide to interact electronically with the adsorbate. Unlike Au, oxygen adsorption on the Pt nano–rod is exothermic by ∼1.2 eV/O even in the absence of the oxide support. In the presence of the oxide, there is an electrostatic stabilization (∼0.8 eV/O) that does not depend upon electronic interactions thus is general for the four oxides tested. The contrast of Au/oxide and Pt/oxide interface chemistry indicates the balance of electronic structure and electrostatic interactions between the metal, oxide, and adsorbate dictate the chemistry at these special sites. It should also be noted that the oxygen adsorbed at the Pt/oxide interface (∼2.0 eV/O) is likely bound too strongly to be active in low-temperature oxidation catalysis. On the other hand, it has been shown in similar calculations that atomic oxygen bound at the Au/oxide interface with and energy of ∼1.0 eV/O can be removed by CO with minimal activation barrier [57].

7.8 Fundamental Mechanisms that Govern Adsorption at the Au/oxide Interface

We find that the energetics of oxygen adsorption at the Au/oxide interface are governed by a balance of electrostatic and electronic interactions. The dominant interactions between the adsorbate, Au, and the oxide surface are: *i*) charge transfer to the oxygen adsorbate from the Au nano–structure, *ii*) electrostatic interaction between the oxide surface cation, oxygen adsorbate, and Au, in the form of coupled dipoles ($M^{\delta+}O^{\delta-}Au^{\delta+}$), and *iii*) Au promoted electronic interaction between the adsorbate and the oxide surface. First, we discuss the charge transfer steps present at the interface in the absence and presence of Au, and then, the electronic interaction between the adsorbate and the oxide surface.

7.8.1 Electrostatic Effects at the Au/oxide Interface

We investigate the role electrostatics plays in oxygen adsorption at the interface site by tracking the changes in surface dipole upon adsorption with and without the Au nano–structure present, see Table 7.1. We start by investigating the change in clean oxide surface dipole caused by oxygen adsorption. Before oxygen adsorption, the oxides exhibit no surface dipoles, which is inline with non–polar oxide terminations being energetically favorable [114, 125, 132, 136]. Upon adsorption of oxygen, a surface dipole develops pointing in the negative z–direction, from negative to positive charge, indicating charge transfer to the adsorbate (column 2 in Table 7.1). Interestingly, the resultant dipole is almost identical for all four oxides, however, the energy associated with adsorption roughly tracks with oxide reducibility (column 5 Table 7.1), with endothermic binding for all oxides except for IrO_2, the metallic oxide. These results indicate that charge transfer and electronic interaction with the clean oxide surface does not account for the improved stability of oxygen at the Au/oxide

Table 7.1: The surface dipole for the model surfaces is presented along with the adsorption energy of oxygen with and without the Au nano–rod present. The dipoles presented are the clean stoichiometrically terminated oxide, the oxide with and oxygen atom adsorbed atop the surface cation, the oxide in the presence of the Au nano–rod, and the oxygen adsorbed at the surface cation in the presence of the Au nano–rod. The values are in units of Debye (esu·a_0). The adsorption energies are in electron volts per adsorbate (eV/O).

System	oxide	O/oxide	Au/oxide	O/Au/oxide	$E^{ads}_{O/oxide}$	$E^{ads}_{O/Au/oxide}$
SiO_2	0.00	-0.23	+0.16	+0.41	3.17	-0.20
TiO_2	+0.07	-0.20	+0.16	+0.43	3.24	-0.99
SnO_2	-0.03	-0.20	+0.38	+0.42	1.90	-1.05
IrO_2	0.00	-0.18	+0.38	+0.41	-0.57	-1.46

interface.

A very different case is found when Au is introduced to the oxide surface. Upon adsorption of the Au nano–structure on the clean oxides, charge is transfered to the oxide terminating oxygens, producing positive dipoles. Upon adsorption of oxygen at the Au/oxide interface, the magnitude of the positive dipoles increases to much the same value for all four oxides. Comparing these dipoles to the dipoles of oxygen adsorption on clean oxides, the magnitude of charge transfer from Au to O is greater than from the oxide to O, i.e., the direction of the overall measured dipole flips from negative to positive. Considering the calculated adsorption energy of oxygen at the interface, which contains both electrostatic, charge transfer, and electronic energy contributions, we see that the charge transfer from Au is by far more favorable than charge transfer from the clean oxides. It should also be noted that the increased charging of the adsorbate likewise increases the favorable electrostatic interaction with the oxide surface cation. This synergic effect of Au donating charge to O, and O interacting with the oxide surface cation appears to explain the oxygen adsorption promotion. However, because the oxygen adsorption at the interface is affected by the type of oxide present, electronic interactions between the oxide surface and the oxygen adsorbate must play a role as well.

7.8.2 Electronic Structure at the Au/oxide Interface

All of the oxides tested have cation and anion formal charges of +4 and –2 respectively. Therefore, if the effect of the oxide was solely electrostatic every oxide should bring about the same stabilization of oxygen, however, this is not the case. In light of this, we investigate the changes in electronic structure of the oxides in the presence and absence of Au and adsorbed atomic oxygen to better understand how the electronic structure of the oxides dictates the stability of the adsorbate. For clarity and space conservation we present data for the Au/TiO_2 system, but it should be noted that the other three systems behave similar.

First we investigated changes in the electronic structure of the oxides upon adsorption of atomic oxygen. For SiO_2 and TiO_2 it was found that the electronic structure of the extra atom of oxygen was highly localized near or at the Fermi level indicating very little interaction with the oxide surface cation. In the case of the more reducible oxides, SnO_2 and IrO_2, the electronic structure was more dispersed and clearly hybridized with the oxide surface states. However, the oxygen states were situated much lower in energy when adsorbed on IrO_2 than SnO_2 indicating a more energetically favorable charge sharing/transfer from the cation. Interpretation of these electronic structures are in line with the adsorption energy of the oxygen on the oxides, +3.2, +3.2, +1.9, and –0.6 eV for SiO_2, TiO_2, SnO_2, and IrO_2 respectively.

Interestingly, when the Au nano–rod is introduced to the system the electronic interaction between the oxygen adsorbate and the oxide appears to be greatly increased. Exhibited by wide spread adsorbate LDOS which clearly hybridizes with portions of the oxide's electronic states, see Figure 7.5. It is also a clear that as the oxide becomes more reducible there is more electronic density shared/transfered to the oxygen adsorbate. This is seen through a lowering in energy of the adsorbate LDOS states as the more reducible oxide support is tested. This indicates that Au may act as an electron reservoir from which oxygen can gain electronic charge, but

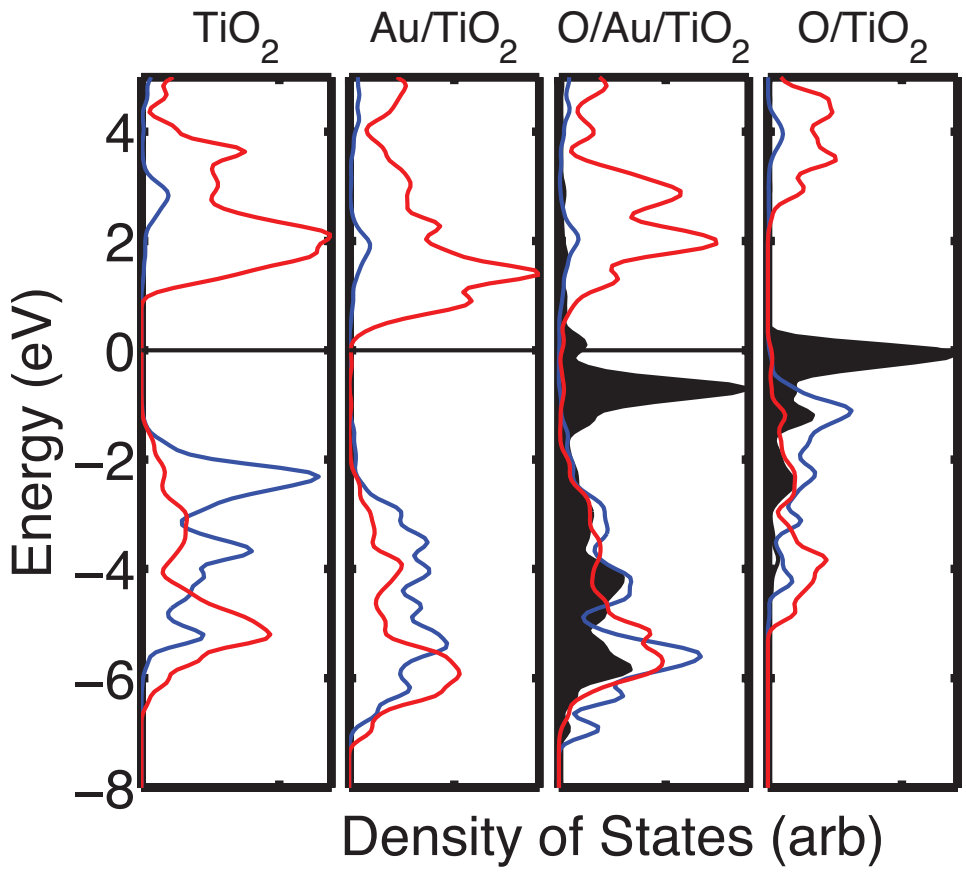

Figure 7.4: As example, the changes in electronic structure upon adsorption of atomic oxygen at the Au/TiO_2 interface are presented. From left to right, panel (a) stoichiometric TiO_2, (b) TiO_2 with the Au nano–rod adsorbed, (c) case (b) with oxygen adsorbed the interface site, and (d) oxygen adsorbed in the absence of the Au nano–rod. The oxide cation and anion states are plotted in red and blue respectively and the adsorbate oxygen in under–shaded black. In the absence of Au, the adsorbate oxygen states are highly localized indicating little interaction with the surface. In the presence of Au, interaction between the oxide surface and the adsorbate is apparent exhibited by the more energetically dispersed states appearing at similar energy levels as the oxide states. This Au facilitated interaction, coupled with electrostatics, leads to the greatly stabilized oxygen adsorption.

may also facilitate the electronic interaction between the adsorbate and the oxide surface. The trend found here falls nicely in line with what is found experimentally with irreducible oxide supported Au being much less active than reducible oxide supported Au in CO oxidation or water–gas shift.

7.9 Conclusion

In many experimental and theoretical studies the catalytic activity of Au–based catalysts has been associated with the Au/oxide interface perimeter site. Based upon these insights, we performed a theoretical study investigating the effect of oxide support electronic structure on the activity of the Au/oxide interface perimeter site. We used four oxides (SiO_2, TiO_2, SnO_2, and IrO_2) with differing electronic character, i.e., insulator, semi–conductor, and metallic. The calculations suggest that the aggressiveness of the the Au/oxide interface site towards binding and dissociating O_2 was proportional to the inertness of the oxide. We found that mechanisms governing the chemistry of the interface site were a balance of one electron energies and electrostatic interactions. When the oxygen species adsorbs at the interface site it picks up charge from either Au or the oxide cation it favorably interacts with. This partially negative charge interacts favorably with the cation of the oxide surface greatly increasing the adsorbates stability. Interestingly, the electrostatic stabilization appeared to drive further charge transfer from Au indicating that it may be favorable to oxidize Au in the presence of the electrostatic field presented by an oxide surface. These results are directly in line with the catalytic performance measured for the Au/oxide couples tested and may help to understand how the active site in Au catalysis is inextricably connected to the oxide used to disperse Au.

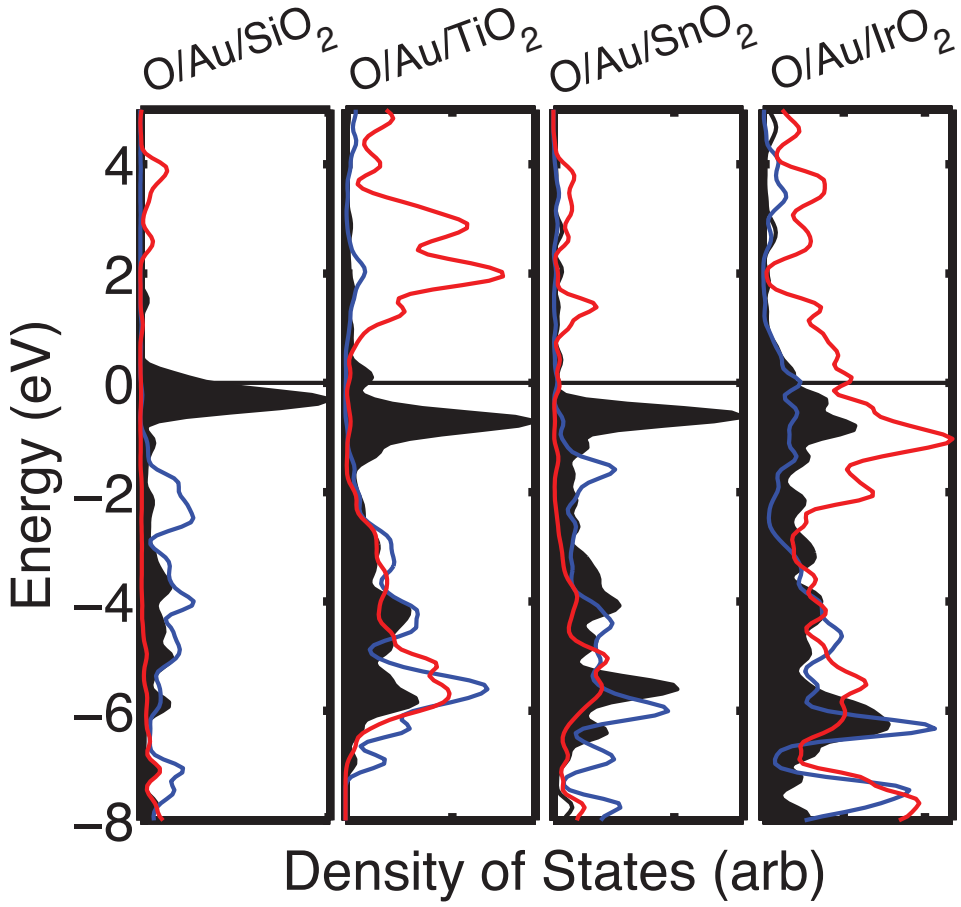

Figure 7.5: To illustrate how the oxide's electronic structure plays a direct role in the oxygen binding we present the changes in electronic structure of the atomic oxygen adsorbed at the Au/oxide interfaces. From left to right the oxide support is SiO_2, TiO_2, SnO_2, and IrO_2. Firstly, it should be noticed that the magnitude of interaction between the adsorbed oxygen and the oxide surfaces increases as the support reducibility increases (left to right increasing). Secondly, the energy at which the adsorbate electronic states reside lowers in energy indicating a larger amount of electronic charge is transfered as the reducibility of the oxide increases. Clearly a trend exists for this interface site with respect to oxide electronic structure.

CHAPTER VIII

Theoretical/Experimental Analysis of Active Sites in Low–Temperature CO Oxidation

8.1 Overview

In this chapter we combined theoretical insights from quantum chemical calculations with bench–top reactor studies to further isolate the active species of Au in low–temperature CO oxidation. As shown in the previous chapters, our calculations indicated that appreciable concentrations of oxygen and chlorine could be stabilized near the Au/TiO_2 interface. In these calculations we showed that Cl competes with O adsorbates for the interfacial sites poisoning the active sites. These theoretical studies led us to develop procedures for catalyst synthesis which allow us to control the amount of Cl, and therefore the performance of the catalyst. In this chapter we test these synthesis procedures experimentally. We found the catalysts containing $Au(OH)_y/AuO_y$ were highly active in room temperature CO oxidation, whereas, those containing $AuCl_x$ or $AuCl_x(OH)_y$ were less active or inactive at room temperature.

8.2 Introduction

Bulk gold (Au) is historically used to craft items of value because of its inherent resistance to oxidation and corrosion. For example, molecular oxygen and water (O_2 and H_2O) do not adsorb or dissociate on the surface of bulk–like Au crystals near ambient temperatures [17, 18, 25]. However, when Au is constrained to the nanometer scale (<5 nm), its chemical activity changes dramatically. Nano–particles of Au are active in many different catalytic reactions [72, 106]. Possibly of most interest is Au's ability to catalyze CO oxidation at temperatures below 300 K. This unprecedented low–temperature activity indicates that the chemistry of surfaces can change markedly simply by constraining the physical geometry of the material. Interestingly, the mechanisms that govern this nano–size effect are still not well understood.

One critical aspect of Au catalysis, that has yet to be unequivocally determined, is the chemical nature of the catalytically active Au site. Many studies have shed light on the active form of Au in low–temperature catalytic CO oxidation, however, due to variations in catalyst preparation, pretreatment, characterization, and experimental approach, a consensus has not been reached [137]. Evidence has been presented implicating all available oxidation states of Au ($Au^{\delta-}$, Au^0, and $Au^{\delta+}$). It has generally been postulated that anionic Au is active under UHV conditions, and metallic and cationic Au is active under steady–state reaction conditions at atmospheric pressure [46, 59]. In this chapter we focus on metallic and cationic Au. For example, Au/TiO_2 catalysts prepared via deposition–precipitation at pH 8, exhibited cationic Au signal in XANES, and were found to be active in low–temperature CO oxidation ($\sim$1.4 mol CO/mole Au/s) [47]. On the other hand, Au/Al_2O_3 catalysts produced by a similar preparation procedure, exhibited a catalytic rate two orders of magnitude lower than Au/TiO_2 (<0.02 mol CO/mol Au/s), yet contained cationic Au measured by XANES [48]. In a more extreme example, Au/Al_2O_3 was found to be completely inactive at room temperature even though cationic Au was present [52]. Upon treating the cata-

lyst with reductive pretreatments, catalytic activity increased, indicating metallic Au was the active form of Au in low–temperature CO oxidation. Au/TiO_2 catalysts prepared via an incipient–wetness procedure with subsequent pH adjustment to 7, were inactive at room temperature CO oxidation "as–prepared", and exhibited a cationic Au fingerprint in XANES [65]. From this collection of results it can be seen that the active form of Au is still uncertain, and that unaccounted for aspects of the catalyst preparation procedure may be responsible for the wide range catalytic activities encountered.

8.3 Approach

We use first principles calculations to investigate the energetic stability (ΔG_f) of cationic Au, formed by either oxidation (AuO_y) or chlorination ($AuCl_x$). Both AuO_y and $AuCl_x$ are possible products of common catalyst preparation procedures. The thermodynamic calculations are used to asses how easily these Au complexes would form and how stable they are under a range of external conditions. Using a multicomponent thermodynamic calculations with oxygen and chlorine present, we postulate the role AuO_y and $AuCl_x$ plays in catalytic CO oxidation. Directed by these results, we developed catalyst preparation procedures that allowed the deposition of $AuCl_x$, $AuCl_xO_y$, or AuO_y on TiO_2. The catalytic activity of the catalysts was investigated using temperature programmed reaction and steady–state studies. The activity of the catalysts at low temperatures was found to be directly inline with the predictions formulated from the first principles calculations.

8.4 Model System

Our quantum chemical model systems consisted of rutile TiO_2 (110) oxide supported two atomic layer Au nano–rods, see Figure 8.1. This primary model system was

motivated closely by experimentally observed Au nano–structures [14, 36, 91, 103]. For example, Ultra–high Vacuum (UHV) Scanning Tunneling Microscopy studies on model Au/TiO_2 system indicated that 2-3 atomic layer Au nano–structures exhibited the highest catalytic activity towards low–temperature CO oxidation [36, 91]. Similar Au structures were found to be highly active in non–model FeO_x supported Au catalysts characterized by aberration corrected high angle annular dark field scanning transmission electron microscopy (HAADF–STEM) [103]. Similar quantum chemical atomic model systems have been employed previously by our research group, and the groups of others [39, 40, 46, 59, 102, 138]. The oxide support was modeled by a rutile TiO_2 surface oriented to expose the (110) surface. The rutile crystal structure was chosen as it is the most thermodynamically stable, and the most well characterized experimentally [114, 129, 130]. The surface was stoichiometrically terminated (i.e., oxygen vacancy free). This termination was motivated by a recent high resolution UHV STM study that showed oxygen vacancy rich TiO_2 surfaces were healed rapidly by O_2 or H_2O, even under well–baked UHV conditions [126]. Furthermore, from our previous results, we showed that oxygen vacancies are highly energetically unfavorable, even in the presence of Au, and that they would be healed quickly by O_2 if not kinetically trapped [46].

Models for cationic Au were produced by adsorbing oxygen or chlorine on the surface of our base model system in increasing coverages. O and Cl coverages were entertained to produce a surface Au:X ratio, were X is either O or Cl, of $\sim$2:1, which resulted in appreciable cationic character in the Au–rod calculated via Bader and Mulliken charge and electronic structure analyses [59, 118, 139]. This approach was motivated by experimental preparation procedures that utilize $HAuCl_4{\cdot}3H_2O$ as the Au metal precursor [14, 77, 87, 137, 140]. In dry–impregnation and incipient–wetness this precursor is deposited directly onto the oxide surface, whereas, in deposition–precipitation the precursor is reacted with NaOH or Na_2CO_3 to form $Au(OH)_y$, which

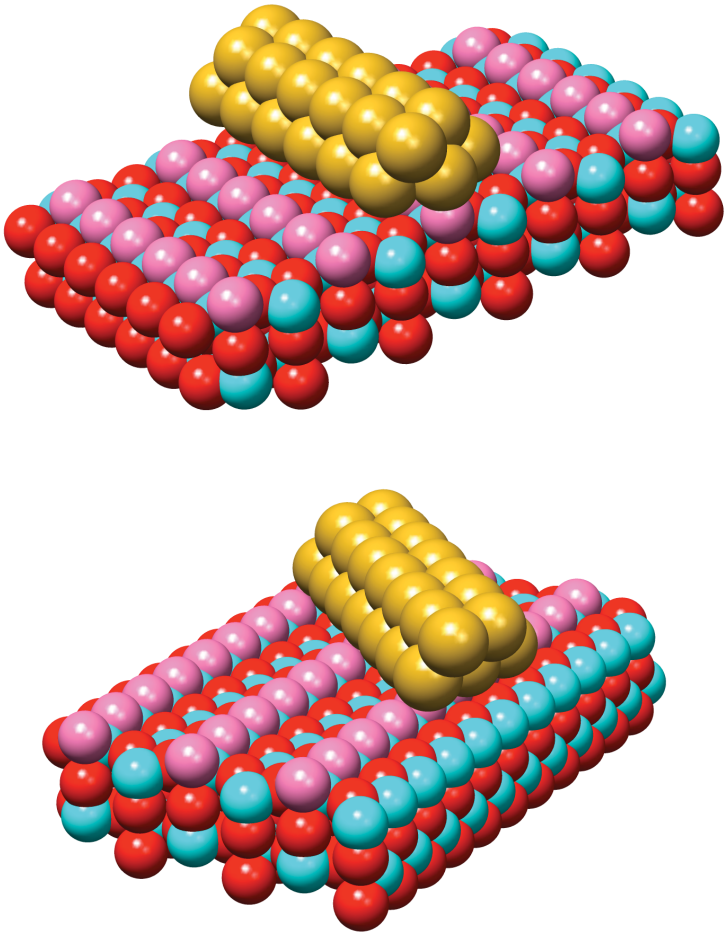

Figure 8.1: Au nano–rods supported by stoichiometric TiO_2 were utilized in our quantum chemical and *ab initio* thermodynamic study. These model systems allow both the Au surface and the Au/oxide interface to be probed. Geometries and supercell sizes were chosen so that the lattice stretch in the Au structure was less than 1%. Gold, red, and light blue spheres correspond to gold, oxygen, and titanium atoms. Light red spheres indicate bridging oxygen atoms in the stoichiometric TiO_2 surface.

deposits onto the oxide.

8.5 *Ab Initio* Calculations

Our *ab initio* calculations consisted of quantum chemical calculations to quantify the internal energy, or electronic energy, of atoms, molecules, and surfaces. Entropic energy contributions were added to the calculated internal energy to investigate changes in Gibb's free energy of formation (ΔG_f) as a function of external conditions ($\Delta\mu_X$). These calculations allowed us to identify energetically the most stable structure as a function of external conditions.

8.5.1 Quantum Chemical Calculation Parameters

The internal energy, i.e., electronic energy, of atoms, molecules, and surfaces was calculated using the DACAPO total energy code with periodic boundary conditions [85]. Atomic cores were described by Vanderbilt ultra–soft pseudo–potentials [116]. The total wave–function was described by a plane–wave basis set, with all waves with energy below 350 eV included. The electronic k–space was sampled by a (2x2x1) or (1x2x1) Monkhorst–Pack k–point sampling mesh for the 2x2 and 5x1 TiO_2 supercells respectively. Because such large supercells were employed, a small number of Brillouin zone sampling points (k–points) were required to achieve convergence of adsorption energies. The maximum force on the atoms in the geometry optimization calculations was below 0.05 eV/Angstrom. The vacuum space was kept at or larger than 10 Angstroms and a dipole correction was applied to cancel the dipole produced by adsorbate over–layers.

8.5.2 *Ab Initio* Thermodynamics

The effect of external conditions on the model system formation energy was calculated by including entropic and internal energy contributions to the change in Gibb's

free energy. These calculations allow us to asses the relative stability of a model system under a range of external gas phase conditions, i.e., temperatures, pressures, and compositions. The calculated change in Gibb's free energy, if negative, indicates that the system calculated is more thermodynamically favorable than the reference state, Au/TiO_2. If the change in Gibb's free energy is positive then the system would return to the reference state if not kinetically limited. The general equation used to calculated the change in Gibb's free energy is Eqn. 8.1.

$$\Delta G_f\left(T, P_i\right) \approx \frac{1}{A}(E_{O,Cl}^{ads} - N_O \Delta\mu_O\left(T, P_O\right) - N_{Cl}\Delta\mu_{Cl}\left(T, P_{Cl}\right)) + \Delta E_{ads}^{vib} \qquad (8.1)$$

Where $\Delta G_f(T,P_i)$ is the temperature and pressure dependent change in Gibb's free energy of formation for the adsorbate over–layer. A, $E_{O,Cl}^{ads}$, N_X, and $\Delta\mu_X$ are the supercell area, adsorption energy of O and Cl, number of adsorbates in the supercell, and the external chemical potential of O or Cl respectively. ΔE_{ads}^{vib} is the change in surface vibrations upon adsorbate over–layer formation. Upon an order of magnitude estimation, the contribution from surface vibrations is minimal and would contribute less than 5 meV, therefore, is neglected.

8.6 Experimental

All catalysts contain 1.0 wt% of Au on TiO_2. They were produced by three methods: dry–impregnation (IMP), modified incipient–wetness (Mod–IW), and deposition–precipitation (DP). Au chloride, $HAuCl_4{\cdot}3H_2O$, was used as the Au source in all preparation methods. The Au salt was deposited on Evonic (Degussa) P25 TiO_2, which had a measured surface area of $\sim$50 m^2/gram. Prior to Au deposition, the oxide was calcined under flowing ultra–high purity air (250 SCCM) at 500 °C for 12 hours. The Au was deposited either as a solid (IMP) or mixed with 5 wt% HCl/H_2O (DP and Mod–IW) prior to deposition.

The catalyst preparation methods were described in detail in chapter 3, however, will be recounted here briefly. In the dry–impregnation catalyst preparation procedure, the Au salt was mechanically mixed with dry TiO_2 for 10 minutes, and then dried. To produce the Au/TiO_2 catalyst via the modified incipient–wetness method, the Au salt was mixed with the proper volume of 5 wt% HCl/H_2O such that incipient–wetness may be achieved once mixed with the oxide powder. This mixture was then suspended in 25 °C H_2O and the pH adjusted to 7 using 0.1 molar NaOH, centrifuged, washed, and dried. In the deposition–precipitation method, an appropriate amount of 30 wt% $HAuCl_4 \cdot 3H_2O$ in 5 wt% HCl/H_2O was added with 250 mg support to 250 mL of deionized H_2O at 70 °C. The pH of the solution was adjusted to the desired value (2–11) by 0.1 molar NaOH in H_2O. This mixture was aged for one hour, centrifuged, washed, and dried. All catalysts prepared were subject to the same drying procedure: 120 °C under flowing ultra–high purity (UHP) air (250 SCCM) for 12 hours. No pretreatments were employed after the drying procedure.

The Au chemical complex present in the deposition–precipitation method solutions was characterized by UV–Vis absorption. In UV–Vis absorption spectroscopy, electronic transitions within a material are excited by ultra–violet and visible light. The excitations are accompanied by the absorption of light radiation of corresponding energy. This spectroscopy may be used to identify chemical species in solution at relatively low concentrations. In our experiments Deuterium/hydrogen and xenon lamps were used as the radiation source and the spectra was collected in transmission mode. The results obtained were compared to literature concerning similar systems [90, 113, 141, 142].

The oxide supported Au particle size were imaged using a JEOL 2010-F transmission electron microscope operating in high angle annular dark field scanning mode (HAADF–STEM). This imaging mode yields Z–contrast images, with higher atomic number atoms imaging with higher contrast. The powdered samples were dispersed

on holey carbon supported on a copper grid. Many particle agglomerates were investigated, however, no Au particles were found in the as–prepared catalyst samples, indicating that the Au was present as a low density species, i.e., $AuCl_x$, $Au(OH)_y$, AuO_y, or small Au clusters, which were undetectable by the non–aberration corrected microscope. After temperature programmed reaction, particles were observed of size ranging from <2–10 nm.

X–ray photoelectron spectroscopy was used to measure the oxidation state of Au and quantify the presence of chlorine in the catalyst samples. The instrument used was a Kratos Axis Ultra XPS with a monochromatic aluminum source (1486.7 eV). The sample transfer and analysis chamber pressures were ∼5E–7 and ∼5E–9 torr respectively. The samples were pressed onto copper tape and allowed to degas for ∼12 hours before being transfered to the analysis chamber.

The activity of the catalyst samples was tested in a custom built temperature controlled u–tube reactor, with the effluent characterized by gas chromatography. Samples of the effluent were taken every 5.75 minutes. The catalyst bed consisted of 1.0 mg catalyst dispersed in 250 mg low surface area SiO_2 suspended between two quartz wool plugs. The reactant gas flow was 30 SCCM CO, 200 SCCM O_2, and 50 SCCM N_2, all UHP gases. To determine the activity of the catalysts as a function of temperature, temperature programmed reaction experiments were employed. The temperature was ramped from 30 °C to 300 °C at a rate of 2.25 °C/minute. A more complete description of the reactor setup is presented in chapter 3.

8.7 Theoretical Results

8.7.1 Thermodynamics of TiO_2 supported AuO_y

We start by investigating the formation of cationic Au by probing the adsorption of oxygen on the Au/TiO_2 model system. The *ab initio* thermodynamic plots for

oxygen adsorption are presented in Figure 8.2. We find that not all adsorption sites are equally active on the model surface. Au–only adsorption sites, not in contact with the oxide support, were probed away from the Au/oxide interface on the surface of the Au nano–rod, and adsorption was found to be endothermic or rather weak (<–0.15 eV/O). Adsorption sites at the perimeter of the Au structure, in contact with the oxide surface, were much more favorable with adsorption energies of –0.9 to –1.0 eV/O depending on the adsorption site. These calculations indicate that the Au sites away from the Au/oxide interface may not play a significant role in Au/TiO_2 catalytic chemistry as they do not interact appreciably with oxygen. Furthermore, the calculations suggest that the Au/oxide interface may contain sites of high activity.

Our thermodynamic calculations also show that the improved adsorbate stability at the Au/oxide interface propagates away form the interface. The effect of the interface resulted in exothermic oxygen binding, even at relatively high coverages, promoting the oxidation of Au. Exothermic binding per oxygen atom was found for oxygen coverages of four O per ten Au in the supercell used. This equates to an Au:O surface stoichiometry of Au_6O_4, close to that of Au_2O and approximately half that of the natural oxide of Au (Au_2O_3). It should be noted that in these calculations, oxygen adsorption was only calculated on the Au(111) facets of the rod and directly at the interface

8.7.2 Thermodynamics of TiO_2 supported $AuCl_x$

Next, we investigated the formation of cationic Au by populating the Au/TiO_2 surface with atomic chlorine. The thermodynamic plots are presented in Figure 8.3. Similar to oxygen adsorption, we probed Au–only sites and sites at the Au/oxide interface perimeter. We find that adsorption of chlorine follows identically the trend of oxygen. Chlorine adsorption away from the interface was found to be thermoneutral or endothermic, whereas, adsorption at the interface was highly exothermic, –2.43

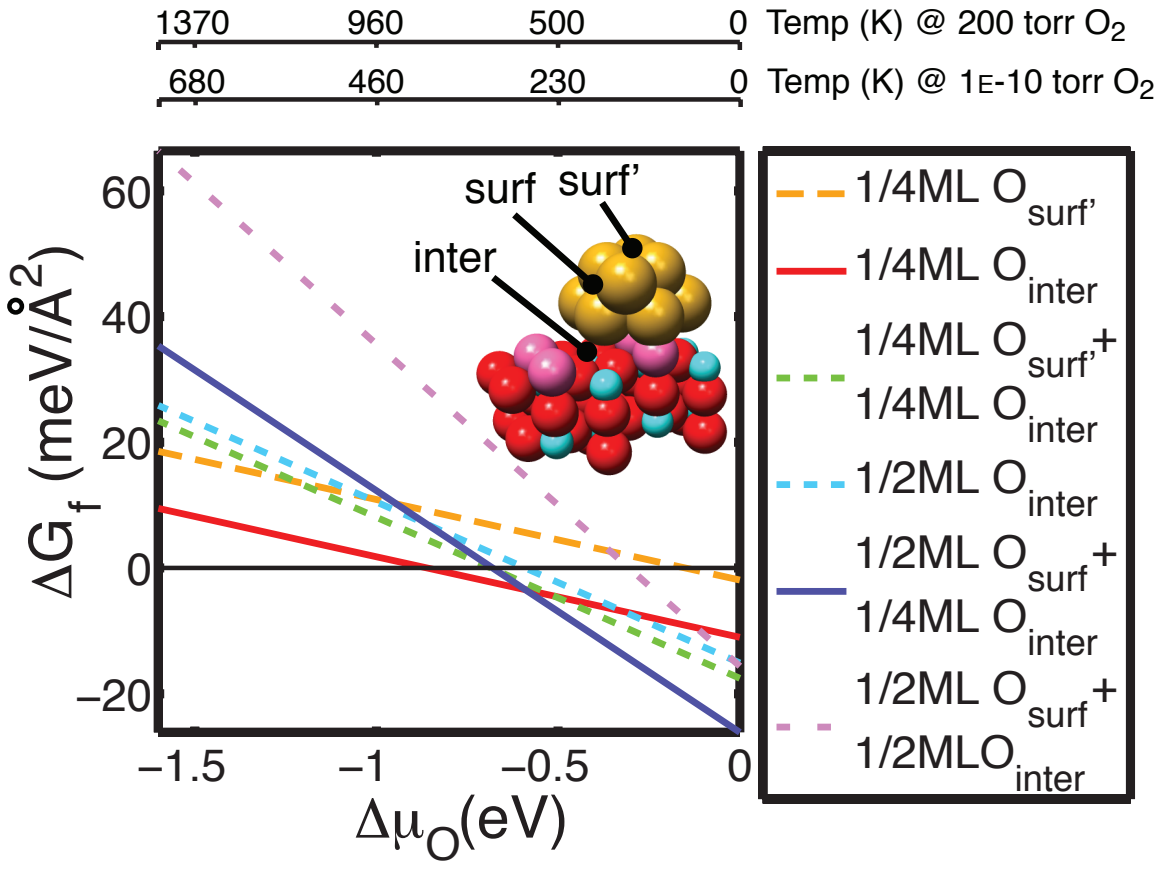

Figure 8.2: Gibb's free energy of adsorption for atomic O adsorbed on the Au nano–rod/TiO_2. The oxygen adsorption sites are labeled with black dots and are grouped into surface (Au–only) and interface (Au/oxide interface) sites. Oxygen at the interface site is bound between a coordinatively unsaturated 'cus' titanium Ti^{+4} atom and the perimeter of the Au nano–rod. ΔG_f is referenced to an adsorbate free Au/TiO_2 surface and gas phase molecular oxygen O_2. $\Delta\mu_O$ at 200 torr O_2 and 300K is approximately –0.27 eV.

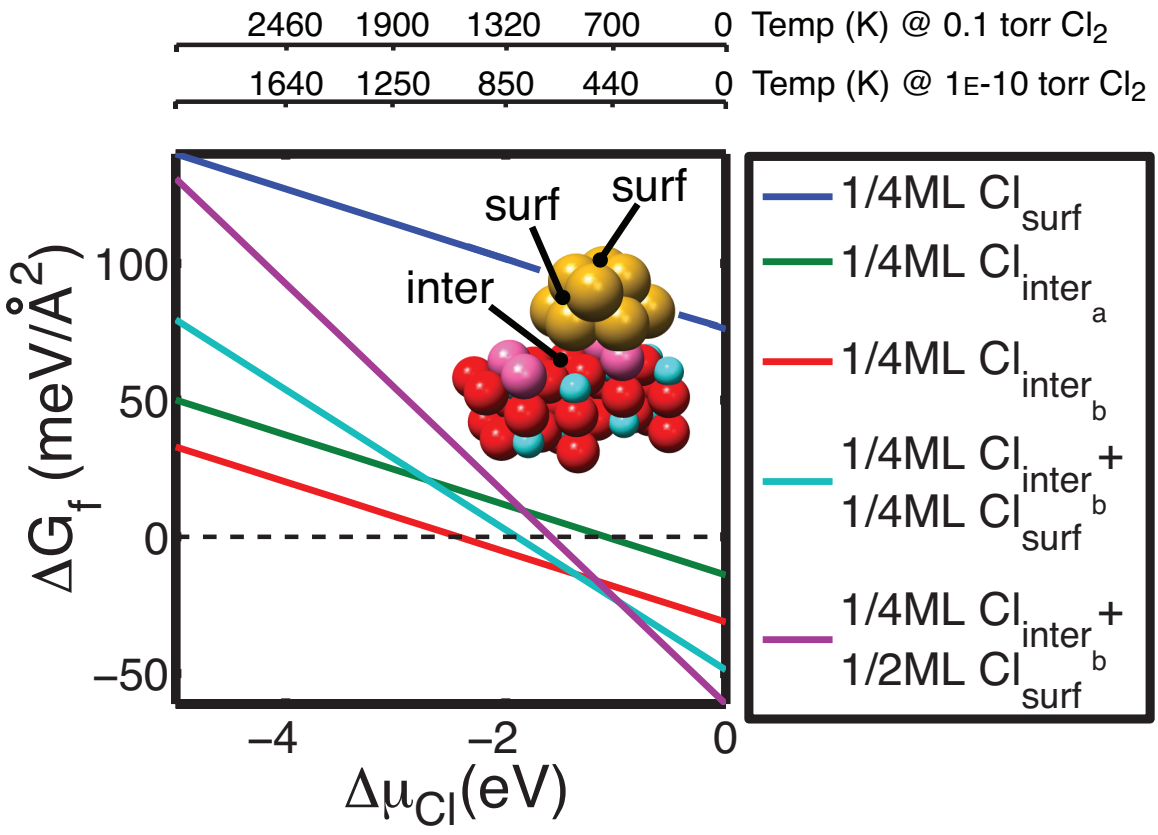

Figure 8.3: Gibbs free energy of adsorption for atomic Cl adsorbed on the Au nano–rod/TiO_2. The chlorine adsorption sites are labeled with black dots and are grouped into surface (Au–only) and interface (Au/oxide interface) sites. Chlorine at the interface site is bound between a coordinatively unsaturated 'cus' titanium Ti^{+4} atom and the perimeter of the Au nano–rod. ΔG_f is referenced to an adsorbate free Au/TiO_2 surface and gas phase molecular oxygen O_2. $\Delta\mu_O$ at 200 torr O_2 and 300 K is approximately –0.27 eV

eV/Cl, with respect to gas phase Cl_2. As with oxygen adsorption, this indicated that the Au/oxide interface perimeter may be a highly active site on the catalyst surface, and that the site was not only active for binding oxygen, but also bound chlorine very strongly.

Higher concentrations of chlorine were calculated to simulate deposition of an $AuCl_x$ precursor under acidic catalyst preparation conditions. It was found that subsequent addition of chlorine near the Au/oxide interface perimeter was highly exothermic even up to the highest surface concentration of chlorine entertained, Au_6Cl_4. As with oxygen, we found that the Au/oxide interface promoted the oxidation of Au approximately two atomic lengths away from the interface. From the chlorine adsorption studies we conclude that $AuCl_x$ could easily persist on the oxide surface under a wide range of external conditions. This may help to understand why high temperature reduction in H_2 is required to activate some catalysts [52, 65].

8.7.3 The role of AuO_y and $AuCl_x$ in Catalytic Oxidation

The relative scale of thermodynamic stability may be seen by plotting the thermodynamics of oxygen and chlorine together without allowing the two species to react (Constrained *ab initio* thermodynamics), see Figure 8.4. From Figure 8.4 it can be seen that chlorine dominates much of the ($\Delta\mu_{Cl}$, $\Delta\mu_O$) phase space illustrating the strength at which the chlorine interacts with the Au/TiO_2 surface. If we consider a model system that starts with a high concentration of oxygen on the surface, it can be seen that chlorine would easily displace these oxygens even at very low $\Delta\mu_{Cl}$. On the other hand, if we start with a chlorine laden surface, very high chemical potentials of oxygen would be needed to displace the adsorbed chlorine. These results indicate that catalyst preparation procedures that result in chlorine laden surfaces would require high temperatures or reactive reducing environments to free active sites of chlorine. Conversely, if the preparation procedure resulted in oxygen laden Au/TiO_x surfaces,

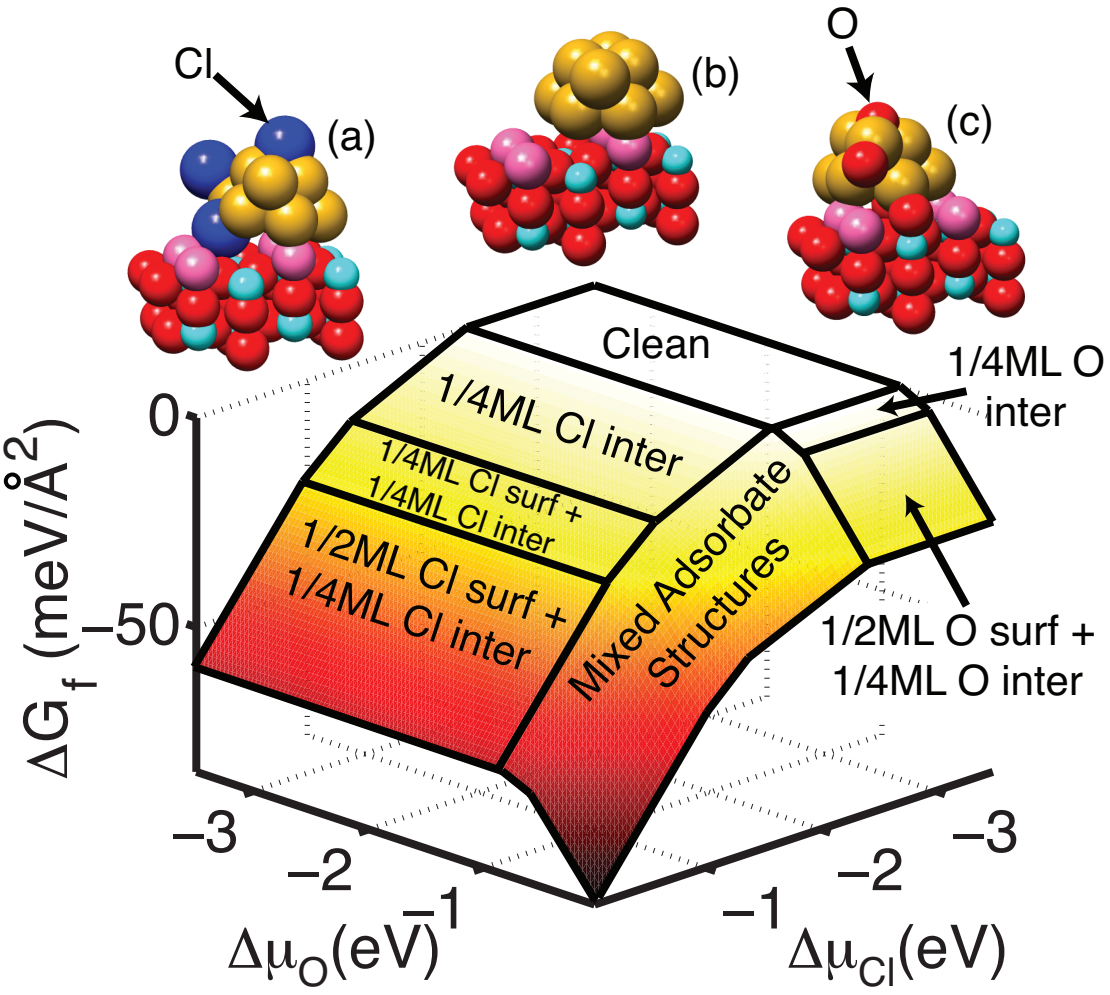

Figure 8.4: Constrained *ab initio* thermodynamics of the Au/TiO_2 surface in contact with O_2 and Cl_2. Here both O and Cl are allowed to interact with the model surface, constrained such that O does not react with Cl. Chlorine clearly dominates the ($\Delta\mu_{Cl}$, $\Delta\mu_O$) phase space, indicating the strength at which the chlorine adsorbs to the Au/TiO_2 surface.

catalytic oxidation would likely occur at many sites close to the Au/oxide interface. We tested these predictions in a number of experimental studies.

8.8 Experimental Results

8.8.1 Characterization of the Au Deposition

Using the insights obtained from the *ab initio* calculations, we attempted to produce Au/TiO_2 catalysts with different Au species present on the surface, namely, $AuCl_x$, $AuCl_x(OH)_y$, and $Au(OH)_y$. We employed UV–Vis absorption spectroscopy to investigate the Au species in solution prior to deposition, and connect this with what is measured on the surface via XPS. From published literature it was found that UV–Vis absorption spectroscopy may be used to track AuX_z species present in acidic and basic solutions similar to those used in the deposition–precipitation method [113, 141, 142].

Aqueous Au chloride solutions were prepared, identical to those used to produce Au/TiO_2 catalysts via the deposition–precipitation method, with a range of pH from 2–11. Aliquots of the catalyst preparation solutions were tested via UV–Vis absorbance 20 minutes after heating to 70 °C, see Figure 8.5. Under acidic conditions (the pH of 40 mg $HAuCl_4{\cdot}H_2O$ dissolved in 250 mL H_2O is ∼2.3) there was a clear absorption peak at ∼310 nm. This may be attributed to Au chloride species present in solution [113, 141, 142]. As the pH was increased with 0.1 molar NaOH the absorption peak shifted to higher energy (lower wavelength) indicating a change in Au species. Visually, this was apparent as well since the solution changed from bright yellow to clear as the pH was increased. Contrasting our results with UV–Vis and x–ray absorption spectroscopy (XAS), the absorption peak progressing to higher energy i.e., lower wavelength, corresponds to gradual substitution of Cl with OH groups ($AuCl_4^-$ species at low pH, mixed (chloro)hydroxide species ($AuCl_x(OH)_y^-$) at interim

pH, and $Au(OH)_4^-$ at pH of 8 and higher) [113, 141, 142]. The Au species were stable at 70 °C for approximately 30 minutes before precursor decomposition became appreciable. Upon precursor decomposition very small collections of particles could be seen within the solution.

From previously published literature it can be concluded that almost complete deposition of Au from solution onto the oxide occurs at pHs below 10 [77, 119]. This indicates the Au chemical species, characterized in the UV–Vis experiments, are deposited on the TiO_2 surface. Under low pH (acidic) conditions $AuCl_x$ species are deposited, indicating that low pH deposition–precipitation, dry–impregnation, or incipient–wetness catalyst preparation procedures may have a high concentration of Au chloride or mixed Au (chloro)hydroxide species present on the surface. On the other hand, under basic conditions (high pH), $Au(OH)_y$ is deposited on the oxide surface. We show below that this has profound consequences on the catalytic activity of the catalysts.

8.8.2 Reactor Study of Powdered Au/TiO_2

The catalytic activity of the $AuCl_x$, $AuCl_x(OH)_y$, and $Au(OH)_y$ or AuO_y species were tested by producing six catalysts: four via the deposition–precipitation method at a pH of 3, 5, 7, and 9, one by dry–impregnation (low pH), and one via modified incipient–wetness (low pH). The nominal loading of Au was 1.0 wt%. The activity of the catalyst was measured by performing temperature programmed reaction experiments with no high temperature pre–treatment employed. Because all precursor species deposit readily at a pH below 10, the catalytic activity of the sample may be directly connected to Au species measured in the UV–Vis experiments. The light–off curves for the six catalysts are presented in Figure 8.6. It can be seen that the catalysts fall in three distinct categories. The first consisting of the catalyst prepared via the dry–impregnation method. This catalyst was not active at low temperatures, and

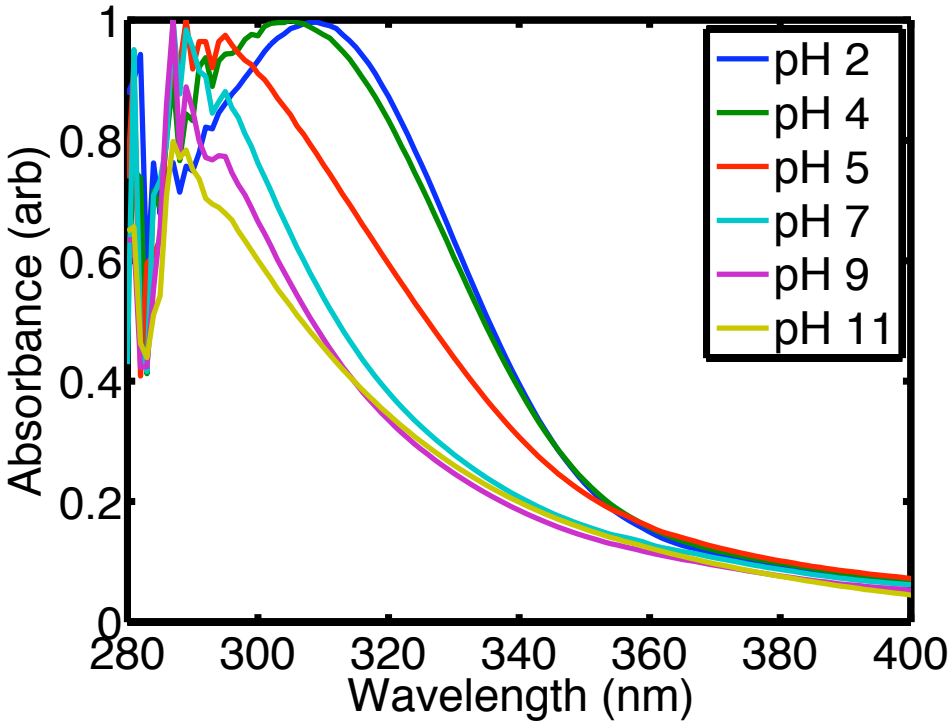

Figure 8.5: UV–Vis absorption spectra of an Au chloride precursor in H_2O under a range of acidic and alkali conditions. The solution conditions were identical to the deposition–precipitation catalyst preparation conditions without TiO_2 present. The Au species present under acidic conditions is likely $AuCl_4^-$, whereas under alkali conditions $Au(OH)_4^-$.

the catalytic activity increased at approximately 250 °C, very close to the decomposition temperature (254 °C) of Au_2Cl_6. The second group appeared to have similar light–off temperatures of 150–175 °C, yet exhibited two different initial low temperature activities. With the modified incipient–wetness and the pH 3 sample exhibiting very low reaction rates at low temperatures and the pH 5 sample having measurable activity at low temperatures. The catalysts synthesized at pH 7 and 9 exhibited high catalytic activity at room temperature and upon heating quickly consumed the maximum amount of CO present leading to 100% conversion. Efforts to correlate catalyst activity to Au particle size failed as no particles were found using HAADF–STEM before the reaction. Au particles of similar size (2–10 nm) were found in all samples after reaction. This is most likely due to the thermal sintering of the as–deposited Au species.

8.9 Chlorine and Au Oxidation State

Depending on the preparation procedure very different Au species were deposited on the oxide surface. Since all Au species present below a pH of ~ 10 deposit on TiO_2 with approximately equal affinity, it may be assumed that the species detected via UV–Vis are present on the oxide surface and may be connected to catalytic activity. In an attempt to further verify the nature of the Au site we utilized XPS to verify the presence of chlorine and quantify the oxidation state of Au.

The chlorine x–ray photoelectron spectra for the samples is presented in the Figure 8.7 (a). The presence of chlorine was clearly measured in the samples produced via dry–impregnation and the catalysts produced at a pH of 3, 5, and 7. On the other hand, the catalyst prepared at a pH of 9 exhibited no chlorine signal. It should be noted that all catalysts, except for the dry–impregnation catalyst, were washed with copious amounts of H_2O and were subjected to the same drying procedure. As no Au nano–particles were measured it may be hypothesized that the presence or absence

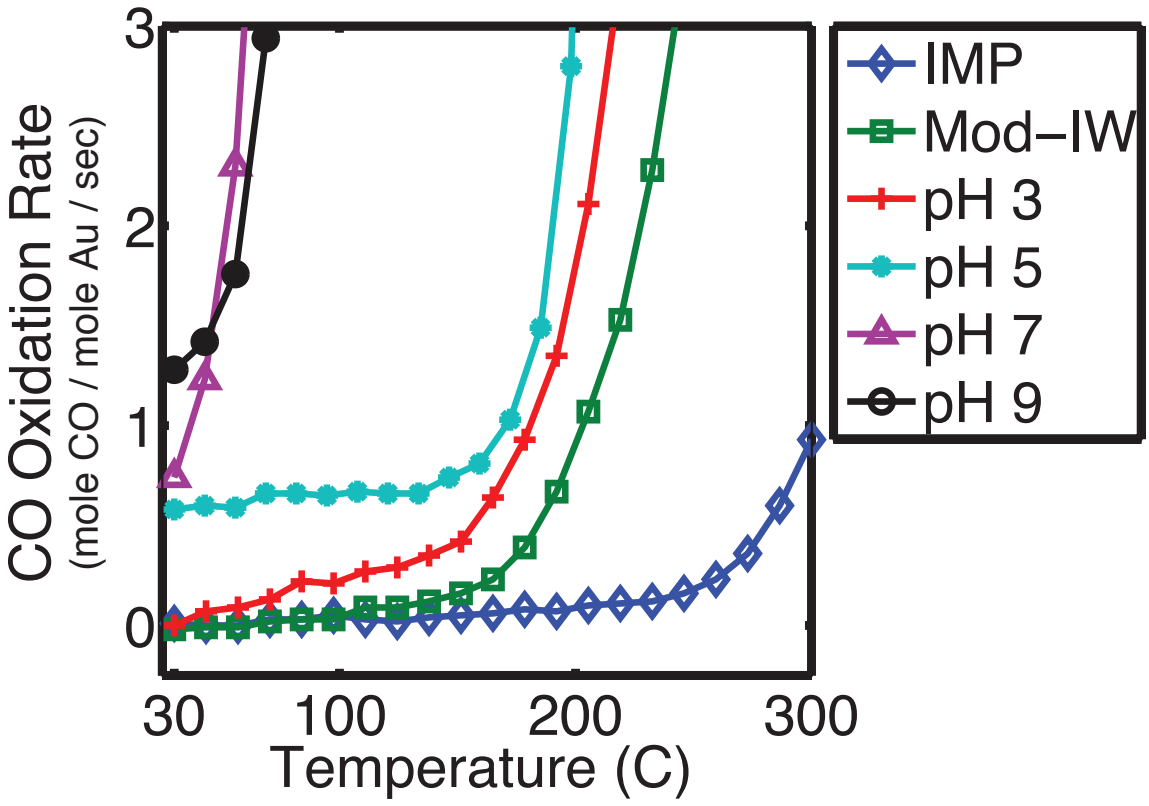

Figure 8.6: Au/TiO_2 light–off curves for the six catalysts tested. A mass of 1.0 mg catalyst diluted by ∼250–300 mg low surface area SiO_2 was tested for activity in CO oxidation. The catalysts underwent no pretreatments thus the species deposited via the preparation procedure was assumed to be present at the time of reaction.

of chlorine coincides with the presence of $AuCl_x$ or $Au(OH)_y/AuO_y$ on the oxide surface. The measured presence of chlorine on the catalyst surface correlates well with the measured catalytic activity.

The x–ray photoelectron spectra of Au 4f states were measured as well to quantify the oxidation state of the deposited Au species. The Au 4f XPS of the samples is presented in Figure 8.7 (b). It was found that only metallic Au was present on the oxide surface with no shift in the Au 4f binding energy to higher binding energy. This indicates that most if not all of the deposited Au species was reduced at sometime during the the experiment. From the UV–Vis data it can be concluded that the Au species was present in non–metallic form since absorption peaks at lower energy corresponding to metal nano–particle formation were not detected. Similarly, after the drying procedure no Au nano–particles were detected via HAADF–STEM indicating that the Au was not reduced by the drying procedure.

Therefore, to test the possibility that the UHV environment was directly affecting the chemistry of the catalyst surface, we allowed the samples to stay under UHV at room temperature for an additional 12 hours. Upon measuring the chlorine spectra we found the signal had dropped by an order of magnitude. This indicated that the UHV environment was rapidly reducing the samples. Contrasting the relative stability of the Au chloride and hydroxide/oxide species, the former more stable than the latter, it may be possible that the Au hydroxide/oxide was rapidly reduced upon introduction to the UHV atmosphere ($\sim$ 12 hours before initial spectra collection) explaining the metallic Au signal measured for all samples.

8.10 Discussion

Insights from our *ab initio* calculations and well–defined experiments indicate that $Au(OH)_x$ and AuO_x exhibit high catalytic activity in low–temperature CO oxidation. Furthermore, specific catalyst preparation procedures may be used to directly

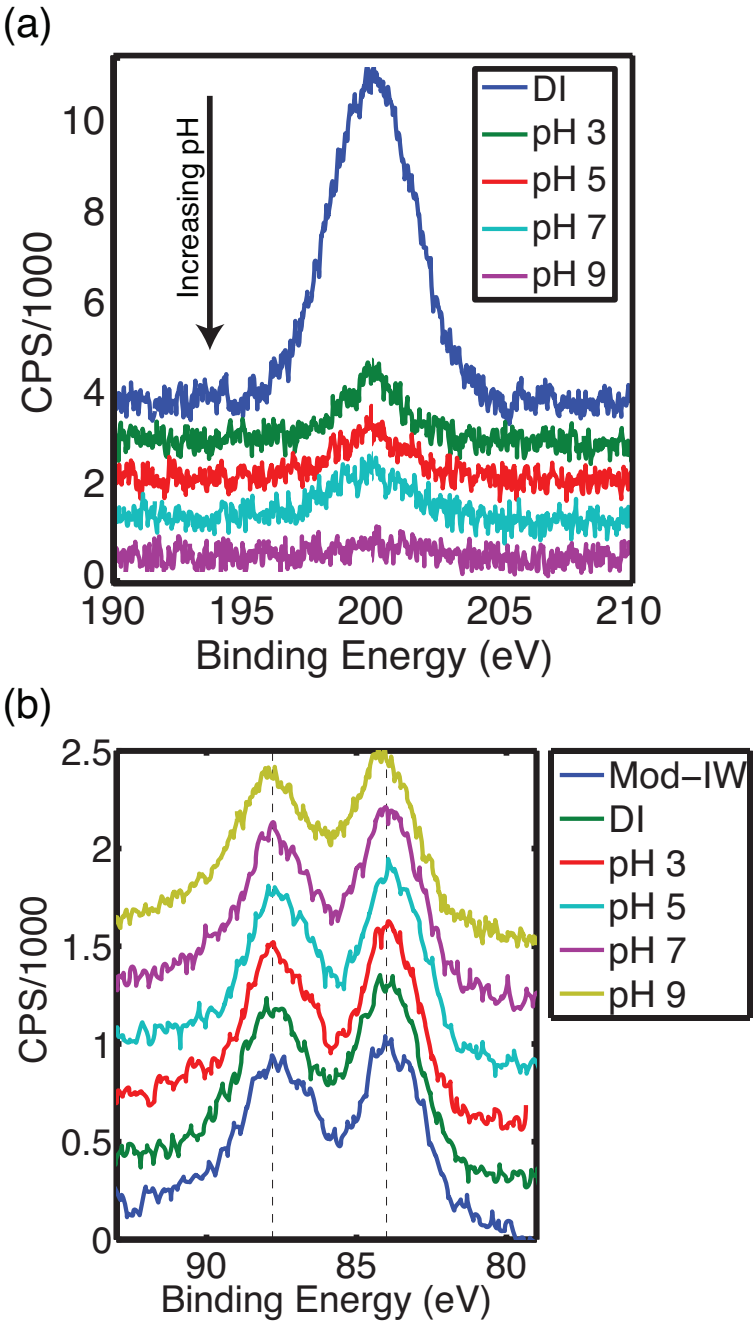

Figure 8.7: X–ray photoelectron spectroscopy of selected catalyst samples. The presence of chlorine in the samples clearly correlates with the overall catalytic CO oxidation activity. Metallic Au was the only Au species present. It should be noted that the Au species quickly reduce under the UHV environment. This is exemplified by an order of magnitude decrease in the chlorine counts per second if the samples are left under UHV for an additional 12 hours. As Au chloride is more stable than Au oxide or hydroxide it is possible that the latter species may be exceedingly difficult to measure in UHV XPS experiments.

produce this active species without high temperature pretreatments that reduce the concentration of catalytically active sites. Here we contrast our results with previously published literature and previously presented concepts that govern precursor adsorption and the structure of catalytically active Au.

Undoubtedly, highly active Au can be produced without high–temperature calcination or reduction pretreatments. Moreover, by not employing high temperature pretreatment the overall catalytic activity of the catalyst on a per mole Au basis is greatly increased. From our results and the results of others it is apparent that Au can deposit in the TiO_2 surface in any of the following forms: $AuCl_x$, $AuCl_x(OH)_y$, or $Au(OH)_y$ [113, 141, 142], with the decisive factor being the chemical environment at which the Au is deposited. Incipient–wetness or dry–impregnation yield $AuCl_x$, which is inactive in low–temperature CO oxidation. Other methods such as the modified incipient–wetness or low to neutral pH deposition–precipitation methods may produce Au species with a mixture of chlorine and hydroxyl groups, which may exhibit measurable activity. On the other hand, at high pH, $Au(OH)_y$ is deposited, possibly decomposing to AuO_y, and is the highly active form of Au. These results are corroborated by similar experiments performed by Park and Lee showing similar reaction rates with high pH deposited Au [47]. Moreover, a similar effect of pH was noted in separate investigations by Bond and co–workers and Wolf and Schuth, however, the reported reaction rates on a mol per mol basis were much lower [77, 119].

The prominence of contradictory results in literature relating cationic Au signals measured in x–ray absorption spectroscopy to catalyst activity again most likely stem from depositing the chloride or (chloro)hydroxide form of Au instead of the highly active Au hydroxide or support specific affinities for chloride species. As shown by Park and Lee extremely active Au can be produced via high pH deposition and exhibit cationic whiteline intensity in XAS [47]. Whereas, catalysts produced by similar methods or modified incipient–wetness can exhibit cationic Au in XAS, yet have no

catalytic activity or activity orders of magnitude lower [63, 65]. These differences likely stem directly from the catalyst preparation procedure resulting in chlorine rich Au or Au/oxide interface perimeters. In our experiments it was found that the transformation of Au chloride to Au hydroxide was almost instantaneous when solid $HAuCl_x$ was dissolved in 5 wt% HCl, yet when the solid was used directly the transformation was slow and sometimes incomplete. Furthermore, continual adjustment of the solution pH is required during the preparation as the solution pH continually drops as the Au chloride is converted to Au hydroxide over time, sometimes tens of minutes. Many reported preparation techniques labeled deposition–precipitation involved changing the Au solution pH before adding the oxide powder with no subsequent pH adjustment after oxide addition. From our studies we find that the presence of the oxide powder facilitates the Au chloride/hydroxide transformation exhibited by stable pH without oxide and continual pH after the addition of the oxide over several minutes. Unfortunately, the exact dynamics of the precursor chemistry were not determined as that was not the aim of our study.

Our results indicate a direct connecting between $Au(OH)_y/AuO_y$ and the active form of Au in low–temperature CO oxidation. From the calculations presented herein and calculations published previously we conclude that an area at the Au/oxide interface stays oxidized even at relatively high temperature [46, 59]. Even when the surface of the Au particles is completely reduced calculations suggest highly active sites present at the Au/oxide interface perimeter that may re–oxidize readily under reaction conditions or upon exposure to air. The persistence of an over oxidized Au/oxide interface has been corroborated by many experiments. For example, well defined UHV scanning tunneling microscopy studies showed that Au deposited on over oxidized i.e., extra atomic oxygen on a stoichiometric $TiO_2(110)$ surface, stabilized Au nano–particles against sintering [55]. Additionally, Au/TiO_2 catalysts prepared by deposition–precipitation under basic conditions calcined at 350 °C exhibited AuO^-,

$Au(OH)^-$, and AuO_2^- fragments in time–of–flight secondary ion mass spectroscopy [93]. However, the reported molar rate was an order of magnitude less than our and Park and Lee's catalysts [47]. The activity of the Au/oxide interface undoubtedly is present for metallic Au–based catalysts yet by simple comparison of the global molar rates it can be seen that many of the Au atoms are not available to perform catalytic reactions. Therefore, it may be concluded that the Au/oxide interface not only is a highly active site but also may help to stabilize oxidic Au at a short distance.

The final point of discussion is the directed at connecting our results with published results concerning chlorine poisoning. From our calculations, we find that sites highly active in binding and possibly dissociating oxygen are the same sites that favor chlorine adsorption. More pertinent is that the adsorption of chlorine at these sites is so thermodynamically favorable that if present, chlorine could not be displaced by oxygen. These calculations are verified directly by our reactor studies showing that the activity of Au towards low–temperature CO oxidation can be tuned simply by sequentially replacing chlorine ligands by hydroxyls or oxygens by rationally tuning catalyst preparation conditions. Similar conclusions were drawn by Kung and co–workers who studied the effect of halide poisons, where they postulated that the Au/oxide interface perimeter may be the active site for CO oxidation and the location of chlorine poisoning [143]. Many more indirect examples exist where Au catalysts were produced under conditions where $AuCl_x$ species persisted but the chlorine was unmeasurable via common solution based tests and likely reduced when tested via XPS. Even when investigated via XAS, Au chloride can easily be misidentified as Au oxide or hydroxide as all species have highly similar electronic structures directly above the Fermi level [59].

8.11 Conclusion

In summary, *ab initio* calculations were performed to gain insight into the active form of Au in low–temperature CO oxidation. These insights were then used to design active Au/TiO_2 catalyst with one of the highest global molar CO oxidation rates reported. The success of the combined theoretical/experimental approach helped to determine that some form of oxidic Au may be the active form of Au in low–temperature CO oxidation. Further, the *ab initio* calculations also helped to understand how predominately metallic Au–based catalysts are able to successfully catalyze the reaction. Finally, it was determined that the Au/oxide interface region exhibits interesting chemistry and the ability to stabilize oxidic Au species at short range even at temperatures higher than the decomposition temperature of bulk Au oxide.

CHAPTER IX

Summary and Future Work

9.1 Overview

In this dissertation, we have investigated the fundamental physical mechanisms that govern chemical and catalytic activity of oxide supported Au. Using *ab intio* quantum chemical and thermodynamic calculations, in combination with with experimental studies, we have isolated the active form of Au in low-temperature CO oxidation and have determined several fundamental physical mechanisms which may directly govern catalytic activity of Au. The physical mechanisms found to affect Au/oxide chemistry are segregated into Au–only sites affected by the Au/oxide interface and Au sites directly at the perimeter of the Au particle where the oxide plays a direct role.

9.2 Au–Only Reaction Sites

Largely from theoretical calculation we determined that Au nano–particle surface site activity can be directly and significantly affected by chemical changes at the nearby Au/oxide interface. From the previous literature the promotional affect of oxide surface oxygen vacancies was known [144]. It was thought that these oxygen vacancies could transfer electronic charge up into the Au nano–particle leading to anionic Au and an increase in Au surface activity [144]. This effect was verified both experimentally and with quantum chemical calculation [144]. On the other hand, in non–model powdered catalysts prepared via common aqueous solution techniques metallic or cationic Au was measured under reaction conditions via XAS [144]. Gas phase Au cluster experiments and quantum calculations indicate that uncharged Au clusters, even very small clusters <2 nm, cannot bind atomic or molecular oxygen with energies that would produce a low kinetic barrier for O_2 dissociation [144]. Considering these results we found that the presence of the oxide support was crucial in promoting Au surface chemistry (Chap 4 and 5). Furthermore, not only the presence of the oxide support was necessary, but the presence of oxide surface perturbations such as oxygen vacancies, extra oxygens, steps, or edges, were needed to promote Au nano–particle surface chemistry. From careful inspection of the calculated Au/oxide geometries it was found that the oxide surface perturbations, either oxygen vacancies or extra oxygens, bound strongly to the base of the Au nano–structures and induced a reduction of Au—Au bonding. The destabilization of the Au—Au bonds within the Au structure enhanced the nano–particle surface chemistry and promoted CO, atomic oxygen, and molecular oxygen adsorption. Both oxygen vacancies and extra oxygen atoms have been directly visualized interacting strongly with Au nano–structures with the latter of the two possibly measured via XAS under reaction conditions on non–model powdered catalysts [47]. Therefore, the major conclusion that can be drawn here is that the surface activity of Au nano–structures may be directly affected by

oxide surface perturbations leading to enhanced CO, atomic oxygen, and molecular oxygen adsorption. This conclusion helps to understand how the oxide surface promotes Au nano–particle chemistry that is not present in unsupported uncharged particles of similar geometry.

9.3 Au/Oxide Interface Perimeter Sites

In Au catalyzed oxidation reactions the dissociation of O_2 is commonly determined to be the rate determining step. The activation barrier for dissociation reactions may be linearly correlated to the thermodynamic driving force for dissociation, where a larger thermodynamic driving force produces a smaller activation barrier [144]. When considering the adsorption energies of atomic and molecular oxygen at Au–only sites these energies are large enough to bind adsorbates but possibly too small for O_2 to dissociate at low temperatures. However, when focusing on Au/oxide interface perimeter sites the adsorption of O and O_2 produce a significant thermodynamic driving force of $\sim$1.6 eV/O_2, which would equate to an activation barrier of $\leq$0.3 eV [133]. These calculations along with the fact that CO has no preference for the interface site indicates that the Au/oxide interface perimeter site may be a highly active site for binding and dissociating O_2. Furthermore, it should be noted that even though atomic oxygen is bound at the Au/oxide interface with an energy of $\sim$1.0 eV that there is still a further thermodynamic driving force of $\sim$1.0–1.5 eV to oxidize CO to CO_2 ($CO + \frac{1}{2}O_2 \rightleftharpoons CO_2$ $E_{RXN} \approx 3.0$ eV) depending on the adsorption energy of CO.

When considering the Au/oxide interface perimeter as the active site for low temperature CO oxidation it was deemed instructive to investigate the effect of poisons on this reaction site. As Au chloride precursors are commonly employed to produce Au/oxide catalysts, the adsorption of chlorine at the interface perimeter site was investigated. Just as with oxygen, it was found that chlorine bound very strongly

to the interface site. So strongly in fact that removing chlorine in favor of atomic oxygen would be endothermic by ∼1.4 eV/Cl*. Therefore, calculation confirms that the Au/oxide interface site is both highly active for binding and dissociating O_2 and is susceptible to chlorine poisoning, findings that are in line with what is measured experimentally [143]. For further verification of this view, well–defined experiments were performed where AuO_x, AuO_xCl_y, and $AuCl_y$ was directly deposited on TiO_2 powder and it's catalytic activity tested. Measured activities of "as–prepared" i.e., no reductive pretreatment, catalysts indicated that a catalyst which was prepared from AuO_x deposition was highly active in room temperature CO oxidation whereas when the catalyst was prepared with $AuCl_y$ or AuO_xCl_y much lower or no activity was found.

To further investigate the possibility of the Au/oxide interface perimeter site as the active site for O_2 dissociation four oxide supports of differing electronic property i.e., insulator, semi–conductor, and metallic, were used to support the Au nano–rod. Again the theoretical calculations fell in line with experimentally observed phenomena. It was found that the Au/oxide interface perimeter site activity was highly dependent upon the type of oxide present with stronger adsorption of atomic and molecular oxygen occurring as the more metallic oxide was introduced. For example, the weakest binding of O and O_2 was calculated for SiO_2 (insulator oxide) supported Au and the strongest binding for IrO_2 (metallic oxide) supported Au. What is more interesting is that the thermodynamic driving force for O_2 dissociation was not a linear function of the oxide's electronic character. On the other hand, a volcano type curve with a peak at the semi-conductor oxides (TiO_2 and SnO_2) was found. This indicates that the oxygen species can be too weakly or too strongly bound to the interface site and produce a thermodynamic driving force that would result in a large barrier and correlate to minimal low temperature oxidation activity. Interestingly, this again correlates with the activity of at least three of the four (TiO_2, SiO_2, and

IrO_2) model systems calculated.

9.4 Insights into the Oxidation Mechanism

Coupling all of the aforementioned results a clear picture of the Au/oxide surface reactivity has been formed. It may be concluded that Au catalyzed low temperature CO oxidation may proceed via an approximate two site mechanism: *i*) Au–only sites populated by CO and possibly atomic oxygen via diffusion, and *ii*) Au/oxide interface perimeter sites binding and dissociating molecular oxygen. This view of the catalytic mechanism appears to be in line with many mechanisms proposed previously by Bond and Thompson, however, without the thermodynamically unfavorable oxide surface oxygen vacancies. The proposed oxidation mechanism is further supported by the calculations concerning chlorine poisoning and the support effect.

9.5 Suggestions for Future Work

Many questions remain to be answered in Au catalysis, catalysis in general, and rational design of materials. Much of the current understanding of heterogeneous catalysis stems from many decades of work studying the reactivity of bulk metal facets, steps, and edges. Unfortunately, little progress has been made in understanding the relative surface reactivates of metals within a group, row, or column of the periodic table. For example, until very recent progress by Norskov and coworkers, there were no predictive theories to explain the energetics of even a simple dissociation reaction such as $H_2 \rightleftharpoons 2H$ as one moves across the d–block of the periodic table [100, 145–147] . Such fundamental understandings are key not only to understanding catalytic phenomena, but also for rational design of materials in general. We present some possible future directions related to this work.

1. The effect of oxide surface hyrogen/hydroxyl groups on the stability and activ-

ity of catalytically active Au: The chemical termination of oxide surfaces under conditions relevant to catalysis are not well understood. Under aqueous catalyst preparation conditions, the oxide surface can split water and become hydroxylated. The concentration of hydroxyl species is oxide specific and appears to play a role in decomposing catalyst precursors and the thermal stability of metal nano–particles. In our studies, we employed hydroxyl free oxide surfaces and found that oxide surface defects played a direct role in Au stability and activity. If the oxide surface is naturally hydroxylated when in contact with H_2O, then hydroxyl defects may play a similar role as oxygen defects do on pristine oxide surfaces. It has also been postulated that direct chemical bonding between the metal atom and oxygens at the oxide surface is necessary to stabilize highly dispersed metal species. If dealing with a hydroxylated oxide surface, understanding the chemistry present at the Au/oxide interface may help to improve catalyst stability and activity or lead to novel catalyst discovery.

2. The effect of oxide steps and edges on Au chemical activity: From our study it appears that chemically activated locations, such as surface defects, steps, and edges, on the oxide surface can play a non–trivial role in metal adsorption and in some cases catalytic activity. The investigation presented herein could easily be extended from point defects to oxide surface steps and edges to facilitate a more thorough understanding of metal precursor decomposition, metal adhesion, and the activity of metal particles bound at these sites. Recent studies have shown that selected d–block metals have a tendency to adsorb strongly to oxide surface steps, whereas, other d–block metals preferred adsorption at the extended terraces. These experimental and theoretical results indicate that specific and possibly tunable interactions govern the adhesion of metal particles to oxide surface, and that the interactions between metal and oxide may be chemically different at oxide terraces and steps or edges.

3. Electrostatic stabilization of chemical species via Madelung field propagation: Our results indicate that oxide surfaces may stabilize the oxidation of Au at higher temperatures than the decomposition temperature of Au oxide. Investigating this effect we found that significant electrostatic interactions may be responsible for this improved stability and that these interactions were oxide specific. Interestingly, the stabilized oxidic Au species appeared to exhibit chemical reactivity dissimilar to the bulk oxide and the bulk metal. This indicates that the chemical activity of a material may be highly tunable when experiencing environments affected by electrostatic fields. With many oxide supported metal catalysts containing nano–sized metal particles, these types of interactions may be present, be highly tunable depending on the catalyst preparation procedure, and have gone unnoticed due to classic mix and bake catalyst preparation techniques. Understanding these types of unnatural chemical properties will help to expand the tool box available to scientists for the development of novel highly tunable materials.

4. General connections between oxide electronic structure and oxide surface reactivity: With photocatalysis gaining momentum in the research community developing a connection between the electronic structure of photocatalytically active oxides is required. With the current understanding of electronic structure it is possible to explain the photocatalytic dynamics of a well known oxide or semi–conductor material. However, it is all together another task to rationally design a material which exhibits a specific electronic structure. From our studies focused on oxides we propose that quantum calculation may help to further the understanding of electronic structures to the point of rational design. The benefit of using *ab initio* calculations is that many materials may be calculated, their energetic feasibility, and electronic structure determined with only moderate effort. Driven by these calculations materials may be synthe-

sized that exhibit electronic characters previously unseen when utilizing oxides or semi–conductors available today.

BIBLIOGRAPHY

BIBLIOGRAPHY

[1] North American Catalysis Society, 2009.
http://www.nacatsoc.org/what.asp.

[2] World Bank, 2009.
http://siteresources.worldbank.org/datastatistics/Resources/GDP.pdf.

[3] J.N. Galloway, F.J. Dentener, D.G. Capone, E.W. Boyer, R.W. Howarth, S.P. Seitzinger, G.P. Anser, C.C.Cleveland, P.A. Green, E.A. Holland, D.M. Karl, A.F. Michaels, J.H. Porter, A.R. Townsend, and C.J. Vorosmarty. Nitrogen cycles: past, present, and future. *Biogeochemistry*, 70:153–226, 2004.

[4] US Government Energy Information Administration, 2009.
http://www.eia.doe.gov

[5] J.G. Firth. Catalytic oxidation of methane on palladium–gold alloys. *Transactions of the Faraday Society*, 62:2566–2576, 1966.

[6] J.S. Campbell and P.H. Emmett. The catalytic hydrogenation of ethlyene on nickle–copper and nickle–gold alloys. *Journal of Catalysis*, 7(3):252–262, 1967.

[7] H.R. Gerberich, N.W. Cant, and W.K. Hall. Catalytic oxidation: I. the oxidation of ethylene over Pd and Pd–Au alloys. *Journal of Catalysis*, 16(2):204–219, 1970.

[8] G.C. Bond, P.A. Sermon, G. Webb, D.A. Buchanan, and P.B. Wells. Hydrogenation over supported gold catalysts. *Journal of the Chemical Society, Chemical Communications*, 13:444–445, 1973.

[9] S. Galvagno and G. Parravano. Supported Au–Pt catalysts: Characterization and hydrogen transfer activity between benzene and cyclohexane. *Journal of Catalysis*, 57:272–286, 1979.

[10] S. Galvagno, J. Schwank, and G. Parravano. Cyclopropane hydrogenation on Ru and Ru–Au catalysts. *Journal of Catalysis*, 61:223–231, 1980.

[11] J. Schwank, S. Galvagno, and G. Parravano. Isotopic oxygen exchange on supported Ru and Au catalysts. *Journal of Catalysis*, 63:415–424, 1980.

[12] M. Haruta, T. Kobayashi, H. Sano, and N. Yamada. Novel gold catalysts for the oxidation of carbon-monoxide at a temperature far below 0–degrees–C. *Chemistry Letters*, 2:405–408, 1987.

[13] M. Haruta, N. Yamada, T. Kobayashi, and S. Iijima. Gold catalysts prepared by coprecipitation for low–temperature oxidation of hydrogen and carbon monoxide. *Journal of Catalysis*, 115:301–309, 1989.

[14] M. Haruta, S. Tsubota, T. Kobayashi, H. Kageyama, M.J. Genet, and B. Delmon. Low temperature oxidation of CO over gold supported on TiO_2, α–Fe_2O_3, and Co_3O_4. *Journal of Catalysis*, 144:175–192, 1993.

[15] W.C. Conner and J.L. Falconer. Spillover in heterogeneous catalysis. *Chemical Reviews*, 95:759–788, 1995.

[16] M.A. Chesters and G.A. Somorjai. The chemisorption of oxygen, water, and selected hydrocarbons on the (111) and stepped gold surfaces. *Surface Science*, 52:21–28, 1975.

[17] A.G. Sault, R.J. Madix, and C.T. Campbell. Adsorption of oxygen and hydrogen on Au(110)–(1x2). *Surface Science*, 169:347–356, 1986.

[18] N. Saliba, D.H. Parker, and B.E. Koel. Adsorption of oxygen on Au(111) by exposure to ozone. *Surface Science*, 410:270–282, 1998.

[19] D.A. Outka and R.J. Madix. The oxidation of carbon monoxide on the Au(110) surface. *Surface Science*, 179:351–360, 1987.

[20] M. Mavrikakis, P. Stoltze, and J.K. Norskov. Making gold less noble. *Catalysis Letters*, 64:101–106, 2000.

[21] N. Lopez and J.K. Norskov. Catalytic CO oxidation by a gold nanoparticle: A density functional study. *Journal of American Chemical Society*, 124(38):11262–11263, 2002.

[22] Y. Xu and M. Mavrikakis. Adsorption and dissociation of O_2 on gold surfaces. *Journal of Physical Chemistry B*, 107:9298–9307, 2003.

[23] N. Lopez, T.V.W. Janssens, B.S. Clausen, Y. Xu, M. Mavrikakis, T. Bligaard, and J.K. Norskov. On the origin of the catalytic activity of gold nanoparticles for low–temperature CO oxidation. *Journal of Catalysis*, 223:232–235, 2004.

[24] S. Giorgio, C.R. Henry, B. Pauwels, and G. Van Tendeloo. Au particles supported on (110) anatase–TiO_2. *Materials Science and Engineering A*, 297:197–202, 2000.

[25] L.W. Anders and R.S. Hansen. Mixed adsorption of carbon monoxide and oxygen on tungsten (100), (110), and (111) single crystal faces. *The Journal of Chemical Physics*, 62(12):4652–4660, 1975.

[26] A. Winkler, G. Pozgainer, and K.D. Redulic. Desorption kinetics of H_2 from Al(100), Al(110), and Al(111). *Surface Science*, 251/252:886–890, 1991.

[27] S.R. Bare, K. Griffiths, W.N. Lennard, and H.T. Tang. Generation of atomic oxygen on Ag(111) and Ag(110) using NO_2: a TPD, LEED, HREELS, XPS, NRA study. *Surface Science*, 342:185–198, 1995.

[28] J. Kim, E. Samano, and B.E. Koel. Oxygen adsorption and oxidation reactions on Au(211) surfaces: Exposures using O_2 at high pressures and ozone (O_3) in UHV. *Surface Science*, 600:4622–4632, 2066.

[29] B.E. Salisbury, W.T. Wallace, and R.L. Whetten. Low temperature activation of molecular oxygen by gold clusters: a stoichoimetric process correlated to electron affinity. *Chemical Physics*, 262:131–141, 2000.

[30] W.T. Wallace and R.L. Whetten. Coadsorption of CO and O_2 on selected gold clusters. *Journal of American Chemical Society*, 124:7499–7505, 2002.

[31] X. Ding, Z. Li, J. Yang, J.G. Hou, and Q. Zhu. Adsorption energies of molecular oxygen on Au clusters. *Journal of Chemical Physics*, 120(20):9594, 2004.

[32] S. Arrii, F. Morfin, A.J. Renouprez, and J.L. Rousset. Oxidation of CO on gold supported catalysts prepared by laser vaporization: Direct evidence of support contribution. *Journal of American Chemical Society*, 126(4):1199–1205, 2004.

[33] G.M. Veith, A.R. Lupini, S. Rashkevv, S.J. Pennycook, D.R. Mullins, V. Schwartz, C.A. Bridges, and N.J. Dudney. Thermal stability and catalytic activity of gold nanoparticles supported on silica. *Journal of Catalysis*, tbd(tbd):tbd, 2009.

[34] A. Sanchez, S. Abbet, U. Heiz, W.-D. Schneider, H. Hakkinen, R.N. Barnett, and U. Landman. When gold is not noble: Nanoscale gold catalysts. *Journal of Physical Chemistry A*, 103:9573–9578, 1999.

[35] U. Heiz, A. Sanchez, S. Abbet, and W.D. Schneider. Tuning the oxidation of carbon monoxide using nanoassembled model systems. *Chemical Physics*, 262:189–200, 2000.

[36] E. Wahlstrom, N. Lopez, R. Schaub, P. Thostrup, A. Ronnau, C. Africh, E. Laegsgaard, J.K. Norskov, and F. Besenbacher. Bonding of gold nano–clusters to oxygen vacancies on rutile TiO_2(110). *Physical Review Letters*, 90:026101, 2003.

[37] T. Minato, R. Susaki, S. Shiraki, H.S. Kato, M. Kawai, and K. Aika. Investigation of the electronic interaction between TiO_2(110) surfaces and Au clusters by PES and STM. *Surface Science*, 566-568:1012–1017, 2004.

[38] M. Chen and D.W. Goodman. Catalytically active gold: From nanoparticles to ultrathin films. *Accounts of Chemical Research*, 39:739–746, 2006.

[39] Z. Liu, X. Gong, J. Kohanoff, C. Sanchez, and P. Hu. Catalytic role of metal oxides in gold-based catalysts: A first principles study of CO oxidation on TiO_2 supported Au. *Physical Review Letters*, 91(26):266102, 2003.

[40] L.M. Molina, M.D. Rasmussen, and B. Hammer. Adsorption of O_2 and oxidation of CO at Au nanoparticles supported by TiO_2(110). *Journal of Chemical Physics*, 120(16):7673, 2004.

[41] I.N. Remediakis, N. Lopez, and J.K. Norskov. CO oxidation on gold nanoparticles: Theoretical studies. *Applied Catalysis A*, 291:13–20, 2005.

[42] B. Yoon, H. Hakkinen, U. Landman, A.S. Worz, J. Antonietti, S. Abbet, K. Judai, and U. Heiz. Charging effects on bonding and catalyzed oxidation of CO on Au_8 clusters on MgO. *Science*, 307(403):403, 2005.

[43] A. S. Worz, U. Heiz, F. Cinquini, and G. Pacchioni. Charging of Au atoms on TiO_2 thin films from CO vibrational spectroscopy and DFT calculations. *The Journal of Physical Chemistry B*, 109(39):18418–18426, 2005.

[44] S. Laursen and S. Linic. Oxidation catalysis by oxide–supported Au nanostructures: The role of supports and the effect of external conditions. *Physical Review Letters*, 97:026101, 2006.

[45] Steeve Chretien and Horia Metiu. Density functional study of the charge on Au_n clusters n=1 to 7 supported on a partially reduced rutile TiO_2(110): Are all clusters negatively charged. *The Journal of Chemical Physics*, 126:104701, 2007.

[46] S. Laursen and S. Linic. Strong chemical interactions between Au and off–stoichiometric defects on oxides as a possible source of chemical activity of nano–sized Au supported on the oxide. *Journal of Physical Chemistry C*, 113(16):6689–6693, 2009.

[47] E.D. Park and J.S. Lee. Effects of pretreatment conditions on CO oxidation over supported Au catalysts. *Journal of Catalysis*, 186:1–11, 1999.

[48] C.H. Lin, S.H. Hsu, M.Y. Lee, and S.D. Lin. Active morphology of Au/γ–Al_2O_3–a model by EXAFS. *Journal of Catalysis*, 209:62–68, 2002.

[49] J. Guzman and B.C. Gates. Simultaneous presence of cationic and reduced gold in functioning mgo-supported CO oxidatoin catalysts: Evidence from x–ray absorption spectroscopy. *Journal of Physical Chemistry B*, 106(31):7659–7665, 2002.

[50] H.H. Kung, M.C. Kung, and C.K. Costello. Supported Au catalysis for low temperature CO oxidation. *Journal of Catalysis*, 216:425–432, 2003.

[51] J. Guzman and B.C. Gates. Oxidation states of gold in MgO–supported complexes and clusters: Characterization by x–ray absorption spectroscopy and temperature–programmed oxidation and reduction. *The Journal of Physical Chemistry B*, 107(10):2242–2248, 2003.

[52] C.K. Costello, J. Guzman, J.H. Yang, Y.M. Wang, M.C. Kung, B.C. Gates, and H.H. Kung. Activation of Au/γ–Al_2O_3 catalysts for CO oxidation: Characterization by x–ray absorption near edge structure and temperature programmed reduction. *The Journal of Physical Chemistry B*, 108(33):12529–12536, 2004.

[53] J.C. Gonzalez and B.C. Gates. Mononuclear Au(III) and Au(I) complexes bonded to zeolite NaY: Catalysis for CO oxidation at 298 K. *Journal of Physical Chemistry B*, 108(44):16999–17002, 2004.

[54] X. Deng, B.K. Min, A. Guloy, and C.M. Friend. Enhancment of O_2 dissociation on Au(111) by adsorbed oxygen: Implications for oxidation catalysis. *Journal of American Chemical Society*, 127(25):9267–9270, 2005.

[55] D. Matthey, J.G. Wang, S. Wendt, J. Matthiesen, R. Schaub, E. Laegsgaard, B. Hammer, and F. Besenbacher. Enhanced bonding of gold nanoparticles on oxidized $TiO_2(110)$. *Science*, 315(1692):1682, 2007.

[56] D. Pillay, Y. Wang, and G.S. Hwang. Nucleation and growth of 1B metal clusters on rutile $TiO_2(110)$: Atomic level understanding from first principles studies. *Catalysis Today*, 105:78–84, 2005.

[57] J.G. Wang and B. Hammer. Role of Au^+ in supporting and activating Au_7 on TiO_2 (110). *Physical Review Letters*, 97:136107, 2006.

[58] J.G. Wang and B. Hammer. Oxidation state of oxide supported nanometric gold. *Topics in Catalysis*, 44(1-2):49–56, 2007.

[59] S. Laursen and S. Linic. Geometric and electronic characteristics of active sites on TiO_2–supported Au nano–catalysts: Insights from first principles. *Physical Chemistry Chemical Physics*, xx:xxx–xxx, 2009.

[60] C. Burgel, N.M. Reilly, G.E. Johnson, R. Mitric, M.L. Kimble, A.W. Castleman, and V.B. Koutecky. Influence of charge state on the mechanism of CO oxidation on gold clusters. *Journal of American Chemical Society*, 130:1694–1698, 2008.

[61] V. Schwartz, D.R. Mullins, W. Yan, B. Chen, S. Dai, and S.H. Overbury. XAS study of Au supported on TiO_2: Influence of oxidation state and particle size on catalytic activity. *The Journal of Physical Chemistry B*, 108(40):15782–15790, 2004.

[62] J.T. Calla and R.J. Davis. Investigation of alumina–supported Au catalyst for CO oxidation by isotopic transient analysis and x–ray absorption spectroscopy. *The Journal of Physical Chemistry B*, 109(6):2307–2314, 2005.

[63] J.T. Calla and R.J. Davis. X–ray absorption spectroscopy and CO oxidation activity of Au/Al_2O_3 treated with NaCN. *Catalysis Letters*, 99(1-2):21–26, 2005.

[64] J.A. van Bokhoven, C. Louis, J.T. Miller, M. Tromp, O.V. Safonova, and P. Glatzel. Activation of oxygen on gold/alumina catalysts: In situ high–energy–resolution fluorescence and time–resolved x–ray spectroscopy. *Angewandte Chemie International Edition*, 45:4651–4654, 2006.

[65] N. Weiher, E. Bus, L. Delannoy, C. Louis, D.E. Ramaker, J.T. Miller, and J.A. van Bokhoven. Structure and oxidation state of gold on different supports under various CO oxidation conditions. *Journal of Catalysis*, 240:100–107, 2006.

[66] J.T. Miller, A.J. Kropf, Y. Zha, J.R. Regalbuto, L. Delannoy, C. Louis, E. Bus, and J.A. van Bokhoven. The effect of gold particle size on Au—Au bond length and reactivity toward oxygen in supported catalysts. *Journal of Catalysis*, 240:222–234, 2006.

[67] N. Weiher, A.M. Beesley, N. Tsapatsaris, L. Delannoy, C. Louis, J.A. van Bokhoven, and S.L.M Schroeder. Activation of oxygen by metallic gold in Au/TiO_2 catalysts. *Journal of American Chemical Society*, 129(8):2240–2241, 2007.

[68] M. Kotobuki, R. Leppelt, D.A. Hansgen, D. Widmann, and R.J. Behm. Reactive oxygen on a Au/TiO_2 supported catalyst. *Journal of Catalysis*, 264:67–76, 2009.

[69] S. Galvagno, J. Schwank, and G. Parravano. Bimetallic Ru–Au catalysts: Effect of the support. *Journal of Catalysis*, 69:283–291, 1981.

[70] S.D. Lin, M. Bollinger, and M.A. Vannice. Low temperature CO oxidation over Au/TiO_2 and Au/SiO_2 catalysts. *Catalysis Letters*, 17:245–262, 1993.

[71] M.A. Bollinger and M.A. Vannice. A kinetic and DRIFTS study of low temperature carbon monoxide oxidation over Au-TiO_2 catalysts. *Applied Catalysis B*, 8:417–443, 1996.

[72] M. Haruta. Size– and support–dependency in the catalysis of gold. *Catalysis Today*, 36:153–166, 1997.

[73] J. Grunwaldt, M. Maciejewski, O.S. Becker, P. Fabrizioli, and A. Baiker. Comparative study of Au/TiO_2 and Au/ZrO_2 catalysts for low temperature CO oxidation. *Journal of Catalysis*, 186:458–469, 1999.

[74] J. Grunwaldt, C. Kiener, C. Wogerbauer, and A. Baiker. Preparation of supported gold catalysts for low temperature co oxidation via size controlled gold colloids. *Journal of Catalysis*, 181:223–232, 1999.

[75] M.M. Schubert, S. Hackenberg, A.C. van Veen, M. Muhler, V. Plzak, and R.J. Behm. CO oxidation over supported gold catalysts – "inert" and "active" support materials and their role for the oxygen supply durring reaction. *Journal of Catalysis*, 197:113–122, 2001.

[76] M. Schubert, V. Plzak, J. Garche, and R.J. Behm. Activity,selectivity, and long–term stability of different metal oxide support gold catalysts for the preferential CO oxidation in H_2–rich gas. *Catalysis Letters*, 76(3-4):143–150, 2001.

[77] A. Wolf and F. Schuth. A systematic study of the synthesis conditions for the preparation of highly active gold catalysts. *Applied Catalysis A*, 226:1–13, 2002.

[78] Cecile Rossignol, Sandrine Arrii, Franck Morfin, Laurent Piccolo, Valerie Caps, and Jean-Luc Rousset. Selective oxidation of CO over model gold–based catalysts in the presence of H_2. *Journal of Catalysis*, 230:476–483, 2005.

[79] Zhen Ma, Steven H. Overbury, and Sheng Dai. $Au/M_xO_y/TiO_2$ catalysts for CO oxidation: Promotional effect of main group, transition, and rare earth metal oxide additive. *Journal of Molecular Catalysis*, 273:186–197, 2007.

[80] J.A. Rodriguez, J. Evans, J. Graciani, J. Park, P. Liu, J. Hrbek, and J.F. Sanz. High water-gas shift activity in $TiO_2(110)$ supported cu and au nanoparticles: Role of the oxide and metal particle size. *Journal of Physical Chemistry C*, 113:7364–7370, 2009.

[81] J.A. Rodriguez, S. Ma, P. Liu, J. Hrbek, J. Evans, and M. Perez. Activity of CeO_x and TiO_x nanoparticles grown on Au(111) in the water–gas shift reaction. *Science*, 318(1757):1757, 2007.

[82] E. Schrodinger. Quantisation as an eigen value problem. *Annalen der Physik*, 79(4):361–U8, 1926.

[83] J.P. Perdew, K. Burke, and Y. Wang. Generlized gradient approximation for the exchange–correlation hole of a many–electron system. *Physical Review B*, 54(23):16533–16539, 1996.

[84] J.P. Perdew, J.A. Chevary, S.H. Vosko, K.A. Jackson, M.R. Pederson, D.J. Singh, and C. Fiolhais. Atoms, molecules, solids, and surfaces: Applications of the generalized gradient approximation for exchange and correlation. *Physical Review B*, 46(11):6671–6687, 1992.

[85] Center for Atomic scale Materials Design, DACAPO, 2009.
https://wiki.fysik.dtu.dk/dacapo

[86] US Government National Institute of Standards and Technology, Webbook, 2009.
http://webbook.nist.gov

[87] J.A. Schwarz, C. Contescu, and A. Contescu. Methods for preparation of catalytic materials. *Chemical Reviews*, 93(3):477–510, 1995.

[88] J.P. Brunelle. Preparation of catalysts by metallic complex adsorption on mineral oxides. *Pure and Applied Chemistry*, 50:1211–1229, 1978.

[89] K.J. Laidler. *Chemical Kinetics*. Benjamin-Cummings, 1997.

[90] P.J. Murphy, G. Stevens, and M.S. LaGrange. The effect of temperature and pressure on gold–chloride speciation in hydrothermal fluids: A raman spectroscopy study. *Geochemica et Cosmochimica Acta*, 64(3):479–494, 2000.

[91] M. Valden, X. Lai, and D.W. Goodman. Onset of catalytic activity of gold clusters on titania with appearance of nonmetallic properties. *Science*, 281:1647–1650, 1998.

[92] J. Guzman and B.C. Gates. Catalysis by supported gold: Correlation between catalytic activity for CO oxidation and oxidation states of gold. *Journal of American Chemical Society*, 126(9):2672–2673, 2004.

[93] L. Fu, N.Q. Wu, J.H. Yang, F. Qu, D.L. Johnson, M.C. Kung, H.H. Kung, and V.P. Dravid. Direct evidence of oxidized gold on supported gold catalysts. *The Journal of Physical Chemistry B*, 109:3704–3706, 2005.

[94] L.M. Molina and B. Hammer. Theoretical study of CO oxidation on Au nanoparticles supported by MgO(100). *Physical Review B*, 69:155424, 2004.

[95] P. Liu, S.J. Jenkins, and D.A. King. Role of nanostructured dual–oxide supported in enhanced catalytic activity: theory of CO oxidation over $Au/IrO_2/TiO_2$. *Physical Review Letters*, 93:15, 2004.

[96] M.S. Chen and D.W. Goodman. The structure of catalytically active gold on titania. *Science*, 306:252, 2004.

[97] W. Li, C. Stampfl, and M. Scheffler. Why is a noble metal catalytically active? the rold of the O–Ag interaction in the function of silver as an oxidation catalyst. *Physical Review Letters*, 90(25):256102, 2003.

[98] K. Reuter and M. Scheffler. Composition, structure, and stability of $RuO_2(110)$ as a function of oxygen pressure. *Physical Review B*, 65:035406, 2001.

[99] Z. Liu, S.J. Jenkins, and D.A. King. Origin and activity of oxidized gold in water–gas shift catalysis. *Physical Review Letters*, 94:196102, 2005.

[100] B. Hammer and J.K. Norskov. Why gold is the noblest of all the metals. *Nature*, 376:238–240, 1995.

[101] M. Haruta, B.S. Uphade, S. Tsubota, and A. Miyamoto. Selective oxidation of propylene over gold deposited on titanium–based oxides. *Research on Chemical Intermediates*, 24(3):329–336, 1998.

[102] L.M. Molina and B. Hammer. Some recent theoretical advances in the understanding of the catalytic activity of Au. *Applied Catalysis A*, 291:21–31, 2005.

[103] A.A. Herzing, C.J. Kiely, A.F. Carley, P. Landon, and G.J. Hutchings. Identification of active gold nanoclusters on iron oxide supported for CO oxidation. *Science*, 321(1331):1331, 2008.

[104] G. Mills and H. Jonsson. Quantum and thermal effects in H_2 dissociative adsorption: Evalulation of free energy barriers in multidimensional quantum systems. *Physical Review Letters*, 72(7):1124, 1994.

[105] N.C. Hernandez, J.F. Sanz, and J.A. Rodriguez. Unravelling the origin of the high–catalytic activity of supported Au: A density–functional theory–based interpretation. *Journal of American Chemical Society*, 128:15600–15601, 2006.

[106] M. Haruta and M. Date. Advances in the catalysis of Au nanoparticles. *Applied Catalysis*, 222:427–437, 2001.

[107] M. Haruta. Catalysis of gold nanoparticles deposited on metal oxides. *CATTECH*, 6(3):102–115, 2002.

[108] G.C. Bond and D.T. Thompson. Gold catalysed oxidation of carbon monoxide. *Gold Bulletin*, 33:41–50, 2000.

[109] A.S.K. Hashmi and G.J. Hutchings. Gold catalysis. *Angewandte Chemie International Edition*, 45:7896–7936, 2006.

[110] R. Coquet, K.L. Howard, and D.J. Willock. Theory and simulation in heterogeneous gold catalysis. *Chemical Society Reviews*, 37(2046):2046, 2008.

[111] M. Chen and D.W. Goodman. Catalytically active gold on ordered titania supports. *Chemical Society Reviews*, 37:1860–1870, 2008.

[112] I.N. Remediakis, N. Lopez, and J.K. Norskov. CO oxidation on rutile supported Au nanoparticles. *Angewandte Chemie International Edition*, 44:1824–1826, 2005.

[113] F. Farges, J.A. Sharps, and G.E. Brown. Local environment around gold(iii) in aqueous chloride solutions – an EXAFS spectroscopy study. *Geochemica et Cosmochimica Acta*, 57(6):1243–1252, 1993.

[114] U. Diebold. The surface science of titanium dioxide. *Surface Science Reports*, 48:53–229, 2003.

[115] W. Yan, B. Chen, S.M. Mahurin, V. Schwartz, D.R. Mullins, A.R. Lupini, S.J. Pennycook, S. Dai, and S.H. Overbury. Preparation and comparison of supported gold nanocatalysts on anatase, brookite, rutile, and P25 polymorphs of TiO_2 for catalytic oxidation of CO. *Journal of Physical Chemistry B*, 109(21):10676–10685, 2005.

[116] D. Vanderbilt. Soft self–consistent pseudopotentials in a generalized eigenvalue formalism. *Physical Review B*, 41(11):7892–7895, 1990.

[117] J. Rogal, K. Reuter, and M. Scheffler. CO oxidation at Pd(100): A first–principles constrained thermodynamics study. *Physical Review B*, 75:205433, 2007.

[118] Richard F. W. Bader. A quantum theory of molecular structure and its applications. *Chemical Reviews*, 91(5):893–928, 1991.

[119] F. Moreau, G.C. Bond, and A.O. Taylor. Gold on titania catalysts for the oxidation of carbonmonoxide: control of pH during preparation with various gold contents. *Journal of Catalysis*, 231:105–114, 2005.

[120] J. Grunwaldt and A. Baiker. Gold/titania interfaces and their role in carbon monoxide oxidation. *Journal of Physical Chemistry B*, 103:1002–1012, 1999.

[121] H. Hakkinen, S. Abbet, A. Sanchez, U. Heiz, and U. Landman. Structural, electronic, and impurity–doping effects in nanoscale chemistry: Supported gold nanoclusters. *Angewandte Chemie International Edition*, 42(11):1297–1300, 2003.

[122] G. Pacchioni, L. Giordano, and M. Baistrocchi. Charging of metal atoms on ultrating MgO/Mo(100) films. *Physical Review Letters*, 94:226104, 2005.

[123] M. V. Ganduglia-Pirovano, A. Hofmann, and J. Sauer. Oxygen vacancies in transition metal and rare earth oxides: Current state of understanding and remaining challenges. *Surface Science Reports*, 62:219–270, 2007.

[124] G. Pacchioni. Modeling doped and defective oxides in catalysis with density functional theory methods: Room for improvments. *The Journal of Chemical Physics*, 128:182505, 2008.

[125] M. Batzill and U. Diebold. The surface and materials science of tin oxide. *Progress in Surface Science*, 79:47–154, 2005.

[126] S. Wendt, R. Schaub, J. Matthiesen, E.K. Vestergaard, E. Wahlstrom, M.D. Rasmussen, P. Thostrup, L.M. Molina, E. Laegsgaard, I. Stensgaard, B. Hammer, and F. Besenbacher. Oxygen vacancies on TiO_2(110) and their interaction with H_2O and O_2. *Surface Science*, 598:226–245, 2005.

[127] Q. Fu, H. Saltsburg, and M. Stephanopoulos. Active nonmetallic Au and Pt species on ceria–based water–gas shift catalysts. *Science*, 301:935, 2003.

[128] T. Okazawa, M. Fujiwara, T. Nishimura, T. Akita, M. Kohyama, and Y. Kido. Growth mode and electronic structure of Au nano–clusters on NiO(001) and TiO_2(110). *Surface Science*, 600:1331–1338, 2006.

[129] A.A. Bolzan, C. Fong, B.J. Kennedy, and C.J. Howard. Structural studies of rutile type metal dioxides. *Acta Crystolography*, B53:373–380, 1997.

[130] W.H. Baur and A.A. Khan. Rutile type compounds. *Acta Crystolography*, B27:2133, 1971.

[131] F. Cosandey, L. Zhang, and T.E. Madey. Effect of substrate temperature on the epitaxial growth of Au on TiO_2(110). *Surface Science*, 474:1–13, 2001.

[132] H. Freund, H. Kuhlenbeck, and V. Staemmler. Oxide surfaces. *Reports on Progress in Physics*, 59:283–347, 1996.

[133] T. Bligaard, J.K. Norskov, S. Dahl, J. Matthiesen, C.H. Christensen, and J. Sehested. The Bronsted–Evans–Polanyi relation and the volcano curve in heterogeneous catalysis. *Journal of Catalysis*, 224:206–217, 2004.

[134] A. Logadottir, T.H. Rod, J.K. Norskov, B. Hammer, S. Dahl, and C.J.H. Jacobsen. The Bronsted–Evans–Polanyi relation and the volcano plot for ammonia synthesis over transition metal catalysts. *Journal of Catalysis*, 197:229–231, 2001.

[135] B. Hammer. Special sites at noble and late transition metal catalysts. *Topics in Catalysis*, 37(1):3–16, 2006.

[136] C. Noguera. Polar oxide surfaces. *Journal of Physics: Condensed Matter*, 12:R367–R410, 2000.

[137] V. Aguilar-Guerrero and B.C. Gates. Kinetics of CO oxidation catalyzed by supported gold: A tabular summay of the literature. *Catalysis Letters*, 130:108–120, 2009.

[138] P. Broqvist, L.M. Molina, H. Gronbeck, and B. Hammer. Promoting and poisoning effects of Na and Cl adsorption on CO oxidation over MgO–supported Au nanoparticles. *Journal of Catalysis*, 227:217–226, 2004.

[139] R.S. Mulliken. Electronic population analysis on LCAO–MO molecular wave functions. *The Journal of Chemical Physics*, 23(10):1833–1840, 1955.

[140] G.C. Bond and D.T. Thompson. Catalysis by gold. *Catalysis Reviews*, 41(3-4):319–388, 1999.

[141] G.S. Pokrovski, B.R. Tagirov, J. Schott, E.F. Bazarkina, J. Hazemann, and O. Proux. An in situ x–ray absorption spectroscopy study of gold–chloride complexing in hydrothermal fluids. *Chemical Geology*, xxx(xxxx):xxxx, 2008.

[142] A. Usher, D.C. McPhail, and J. Brugger. A spectrophotometric study of aqueous Au(III) halide–hydroxide complexes at 25–80 C. *Geochemica et Cosmochimica Acta*, 73:3359–3380, 2009.

[143] S.M. Oxford, J.D. Henao, J.H. Yang, M.C. Kung, and H.H. Kung. Understanding the effect of halide poisoning in CO oxidation over Au/TiO_2. *Applied Catalysis A*, 339:180–186, 2008.

[144] A. Pertinent Reference. Some well defined experimental or theoretical experiment. *Good Journal*, 1(1):1, 1978.

[145] B. Hammer, Y. Morikawa, and J.K. Norskov. CO chemisorption at metal surfaces and overlayers. *Physical Review Letters*, 76(12):2141–2144, 1996.

[146] J.K. Norskov, T. Bligaard, A. Logadottir, S. Bahn, L.B. Hansen, M. Bollinger, H. Bengaard, B. Hammer, Z. Sljivancanin, M. Mavrikakis, Y. Xu, S. Dahl, and C.J.H. Jacobsen. Universality in heterogeneous catalysis. *Journal of Catalysis*, 209:275–278, 2002.

[147] J.K. Norskov, T. Bligaard, B. Hvolbaek, F. Abild-Pedersen, I. Chorkendorff, and C.H. Christensen. The nature of the active site in heterogeneous metal catalysis. *Chemical Society Reviews*, 37:2163–2171, 2008.